RICE UNIVERSITY

MOLECULAR MODELING THE MICROSTRUCTURE AND THERMODYNAMIC PROPERTIES OF COMPLEX FLUIDS

by

CHRISTOPHER P. EMBORSKY

A THESIS SUBMITTED
IN PARTIAL FULFILLMENT OF THE
REQUIREMENTS FOR THE DEGREE

DOCTOR OF PHILOSOPHY

APPROVED, THESIS COMMITTEE

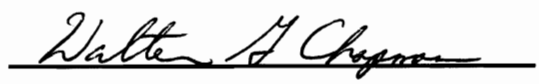

Dr. Walter G. Chapman, Chair
William W. Akers Professor
Chemical and Biomolecular Engineering

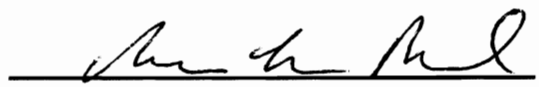

Dr. Sibani Lisa Biswal
Assistant Professor
Chemical and Biomolecular Engineering

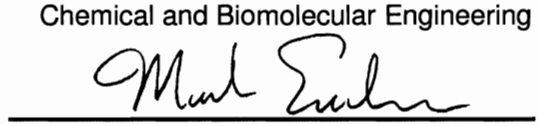

Dr. Mark Embree
Professor
Computational and Applied Mathematics

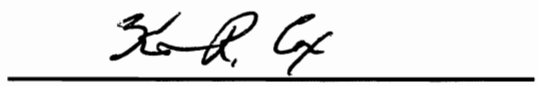

Dr. Kenneth R. Cox
Professor-in-the-Practice
Chemical and Biomolecular Engineering

HOUSTON, TEXAS
APRIL 2011

ABSTRACT

Molecular Modeling of the Microstructure and

Thermodynamic Properties of Complex Fluids

By

Christopher P. Emborsky

The accurate prediction of a complex fluid's equilibrium microstructure and corresponding thermodynamic properties relies on the capability to describe both the molecular level architecture and specific governing physics. This thesis makes key contributions to furthering the application and understanding of molecular models for complex bulk and inhomogeneous fluids with a specific interest in mixtures involving trace components. Such developments have potential for wide-ranging application to fields from consumer goods and medicine to energy and targeted specialized material design.

In the bulk, the perturbed-chain statistical associating fluid theory (PC-SAFT), an equation of state based on Wertheim's first order thermodynamic perturbation theory (TPT1) is used to demonstrate the robustness and performance of intrinsic molecular parameters determined for a complex fluid (water) with a new fitting strategy. Experimental solubility data at ambient conditions was used to find the PC-SAFT parameters for water which where capable of reproducing water content for binary mixtures with liquid and vapor n-alkanes under a myriad of physical conditions. The model gave excellent qualitative and very good quantitative agreement without the need of a binary interaction parameter.

For inhomogeneous fluids, the application of a density functional theory (DFT), also based on TPT1, is extended to model the self-assembly of amphiphilic molecules at a liquid-liquid interface. This DFT, interfacial SAFT (*i*SAFT), is validated against molecular simulation results for the microstructure and interfacial tension of a simple diatomic surfactant based on the continuum oil-water-surfactant model of Telo da Gama and Gubbins. A comprehensive systematic study is conducted for characterizing the affects of part of the vast parameter space governing the fluid microstructure and observed interfacial tension. The role of surfactant structure, oil structure, surfactant concentration, nonionic cosurfactant mixtures, and temperature play in altering molecular level phenomena such as surfactant aggregation, solvent depletion, and surfactant chain conformation as a result of the balance between enthalpic and entropic driving forces are described.

ACKNOWLEDGEMENTS

This research work was made possible by the support and contributions of many I would like to acknowledge. Through the personal struggles and tragedies of the past 15 years, my faith and belief in God has opened my life up to the many blessings his love brings. Despite my occasional doubts and uncertainty when times get difficult, he has shown me how we are never given anything we cannot handle and how those challenges in life often lead to personal growth.

I am forever grateful to my thesis advisor Professor Walter Chapman for his wisdom and insights throughout this work. He greatly expanded my interests in thermodynamics and molecular modeling by exposing me to many of the intricacies of statistical mechanics. In addition, his confidence in my ability and flexibility through my time at Rice has shown me how important individual relationships are in everything you do. He encourages these characteristics in his students as they continue in their professional careers. It was the personal recommendation and interaction with one of those former students, Professor Sharon Sauer, which brought me to Rice University. Given how that decision has shaped the direction of my life, I could never repay either of them for their generosity.

I also wish to thank Professor Ken Cox, Professor Sibani Lisa Biswal, and Professor Mark Embree for serving as my committee members and providing both their critical assessment of this work and interesting perspectives through their own interests. Specifically to Professor Ken Cox, the collaborations on this research from group meetings to individual conversations to assessments of

articles and presentations have been essential in my success. Your insights and experience always challenged my thinking which, while occasionally frustrating when there are more questions than I have answers for, provided excellent guidance and perspective.

A number of professional contacts also provided helpful discussion and support. I am thankful for the meetings and discussions with Dr. Laura Frink and Dr. Amalie Frischknecht which have provided great direction and understanding about the numerical complexities and difficulties within the many challenging systems studied using density functional theory. Specifically, the conference call with Dr. Frink which provided a detailed tutorial of Sandia National Laboratory's parallel TRAMONTO software package was invaluable. I appreciate the patience and exchange of ideas about code development and the use of fast Fourier transforms within the density functional theory with Professor Pawel Bryk. The code for the NIST equation of state for water was also graciously provided by Alan Harvey.

To the many characters of my research group, I am grateful for the friendships we have developed and the many memorable experiences we have shared. I am extremely grateful for Shekhar Jain and Adam Bymaster whose patience with my many questions about the theory and its implementation when I first joined the research group were invaluable. Shekhar was also a significant collaborator on my early studies with the density functional theory and experience with his own research greatly influenced some of this work. To Zhengzheng Feng, whose ideas and discussion have also had great impact on

this work, while we essentially progressed in understanding and grew in our expertise together, I am much more grateful for your friendship and many conversations we had over the years unrelated to research. To Charles Lena, Bennett Marshall, Deepti Ballal, and Kai Gong, I have thoroughly enjoyed the many conversations and questions as you all look to understand the central theory and its application so integral to the work of Professor Chapman's group. Being a conduit to the future success of this group is an exciting time and it has been crucial in the confidence I have in my own understanding. More specifically, I greatly appreciate the hard work of Charles during his summer of research which led to great visualization of my work and many improvements in computational efficiency. The continuation and extension of the main ideas in this research by Ben is also appreciated as it expands the impact of both the group's work in general and my studies specifically. I am also thankful for the comments and discussions with Fransisco Vargas, Aditya Agrawal, and Sai Panuganti during group meetings.

Lastly, and perhaps most importantly, I'd like to thank my family and loved ones for their encouragement and support throughout my education. All my love and appreciation goes out to my parents, Raymond and Gloria Emborsky. You have always been there giving the love and support I needed while also pushing and encouraging me to do great things. You are a tremendous influence on me, and it does my heart good to know I have made you proud. To my true love, Mika Baugh, you are my inspiration and my best friend. I have become a much

better person by having you in my life. You have sacrificed much so I could pursue this dream, and I hope we can share in its realization for a lifetime.

The financial support for this work was provided by The Petroleum Research Fund, the Robert A. Welch Foundation (Grant #C-1241), and the National Science Foundation (CBET-0756166). This work was also partially supported by the shared university parallel grid at Rice University which is funded by the National Science Foundation under grant EIA-0216467, and a partnership between Rice University, Sun Microsystems, and
Sigma Solutions, Inc.

TABLE OF CONTENTS

LIST OF FIGURES

LIST OF TABLES

CHAPTER 1 INTRODUCTION

This thesis serves as a review of the current state of theoretical molecular modeling through the use of thermodynamics and statistical mechanics. It advances the range of applicability and understanding for both real and model complex bulk and inhomogeneous fluid mixtures. Specifically, the emphasis is on non-ideal normal alkane-water mixtures and the partitioning effects of heteronuclear, amphiphilic molecules (surfactants) to a liquid-liquid interface. These developments have broad ranging impact on the understanding of molecular level physics in such fields as lubrication, enhanced oil recovery, drug delivery, and detergents to name a few. The rest of this chapter outlines the motivation, challenges, and theoretical basis for the remaining chapters.

1.1 Motivation and Challenges

The ability to accurately account for the molecular level physics of complex chemical systems has become a crucial part of process and material design as technology continues to move to smaller scales and become more specialized. Sophisticated predictive techniques allow us to gain an advanced understanding of the system microstructure and how it affects macroscopic properties to better guide future development. Over the past several decades, extensive work has been done to develop highly accurate models for systems of simple fluids. Simple molecules are characterized by their nearly spherical shape and weak attractive forces leading to the dense fluid structure being dominated by geometric packing constraints. With little contribution by the attractive forces, the

fluid structure is a function of the single length scale of molecular size. Some examples of simple fluids include argon and methane. Despite the depth of the work on simple fluids, many molecules do not fall within this classification. In stark contrast, much work still needs to be done to understand complex fluid behavior as these systems experience multiple length scale dependencies. In addition to molecular size and shape, the structure and properties can vary with molecular flexibility, thermal fluctuations, polar interactions, or other specific molecular interactions such as hydrogen bonding. Some of the many classes of complex molecules are polymers, surfactants, colloids, liquid crystals, gels, associating fluids, and biomolecules like lipids and proteins.

Physical experiments are often the first indication of any anomalous or interesting system behavior and remain essential in advancing the understanding of complex fluids. However, they can often be difficult to perform under certain conditions (e.g., high temperature and pressure or using trace components) and are often unable to provide mechanisms for separating the individual contributions to fluid behavior. Exhaustive studies can also be further hampered by the large parameter space involved in nearly all these systems. Molecular theories or simulations can be coupled with these experiments to accelerate such searches when seeking more complete understanding and performing material design. Developing such models is still a challenge due to the multiple length scales involved. Accurate prediction of the thermodynamics and microstructure is contingent upon the model's ability to appropriately capture the molecular architecture and specific intermolecular and intramolecular interactions that

govern the fluid behavior. The feasibility of applying such a model is directly connected to its thermodynamic consistency and computational tractability. Many of the most sophisticated and intricate theories are unable to meet such challenges. This research is motivated by a desire to demonstrate the capability to fill this void when predicting the equilibrium phase behavior, microstructure, thermodynamics, and macroscopic properties of complex fluids. The work here has two primary components — homogeneous (bulk) and inhomogeneous fluids.

1.1.1 Homogeneous Fluids

The van der Waals equation of state (EOS), proposed in 1873, was the first predictive model for calculating vapor-liquid bulk phase coexistence. Even today many of the conventional engineering equations of state are variants of the van der Waals equation. The premise of this approach is to account for the repulsive interactions through a hard sphere reference term and any additional attractions via a mean-field approximation term. The most common EOS in the van der Waals framework (e.g., Redlich-Kwong[1] and Peng-Robinson[2]) have implemented improvements to the accuracy to one or both of these terms. These equations have distinct advantages in their ease of implementation and ability to reproduce pressure, temperature, and phase composition relationships for multicomponent mixtures. However, these models are only accurate for mixtures of simple molecules (e.g., low molecular weight hydrocarbons or simple inorganic compounds). It is also well-known that these EOS are restricted to prediction of vapor pressure and suffer invariably in estimating saturated liquid densities.[3]

When considering more complicated polyatomic molecules, it is necessary to choose a more appropriate reference fluid that can account for molecular size and shape. Advances in statistical mechanics have led to the development of more sophisticated fundamental molecular based theoretical equations of state. In the mid 1980s, Wertheim[4-7] proposed a thermodynamic perturbation theory of first order (TPT1) to describe the phase behavior and thermodynamic properties of a fluid of hard spheres with multiple directional association sites. This work has served as the theoretical basis for a number of equations of state for chain molecules. Most notably, Chapman *et al.*[4-8] extended TPT1 to mixtures of associating atomic fluids and developed an EOS for hard chain fluids by taking the limit of complete association. This EOS, known as statistical associating fluid theory (SAFT), has the advantage of additional perturbations to the reference fluid being included to mimic the physics of more realistic fluid behavior. For example, the anisotropic polar effects are important contributions in ketones, alcohols, esters, and water where an imbalance in the electron density around the molecule induces a permanent directional dipole. Several SAFT versions are in regular use today, as it has become a standard EOS approach for engineering purposes – especially for those involving larger macromolecular fluids with complex intermolecular and intramolecular interactions. One of the more prominent versions, perturbed-chain SAFT (PC-SAFT)[4,5] is presented in Chapter 2 in the context of phase equilibrium calculations.

Despite years of work and development, even the more sophisticated and versatile equations of state still suffer from shortcomings. Some of these issues

include the inability to accurately predict thermodynamic properties in the critical region or capture the anomalous behavior of aqueous systems. Many of these problems are nontrivial and have been studied for some time. Improving the performance of PC-SAFT in the critical region using a renormalization group theory approach was investigated by this and other authors.[4] In addition, the significant nonlinearity of the SAFT family of EOS and the widely accepted parameter fitting strategy often leads to multiple equally effective pure component parameter sets for more complex species. Addressing the mechanism for fitting such pure component parameters in the specific context of modeling phase behavior of *n*-alkane-water binary mixtures is a specific focus of this research discussed in Chapter 2.

1.1.2 Inhomogeneous Fluids

Inhomogeneous fluids are characterized by a spatially dependent density profile with respect to at least one dimension. Figure 1.1 shows a simple example of the microstructure of a fluid near a solid surface. In this system, the inhomogeneity is in the dimension normal to the surface (z), which is scaled by the segment diameter (σ), where the surface is at $z < 0$. As is demonstrated with the figure, fluids at interfaces or confined within pores exhibit properties qualitatively different from their bulk counterparts. At higher densities, a density enhancement (wetting) behavior can be found near the surface often coupled with oscillatory convergence to the bulk density where the surface effects are no longer felt. However, there is typically a depletion region near the surface at lower densities with smoother convergence to the homogeneous region as

depicted in the figure. This type of inhomogeneous structuring is a consequence of interactions between the fluid molecules and the wall and/or within the fluid itself. Understanding this behavior is important as the fluid-fluid and fluid-wall interactions often compete, leading to the surface driven behavior of Figure 1.1, which is not present in bulk fluids.[5] These interesting structure-driven effects occur naturally in many systems including those with interfaces, within confined spaces, and involving self-assembling molecules. As the development of technology continues to move to smaller physical scales and become more specialized, the ability to understand system behavior on the molecular level has found interest in chemical, oil and gas, pharmaceutical, and biological industries, to name a few. Some processes and applications where such understanding is crucial and directly relevant include enhanced oil recovery; inks, paints and coatings; soaps, shampoos and detergents; food processing and preservation;

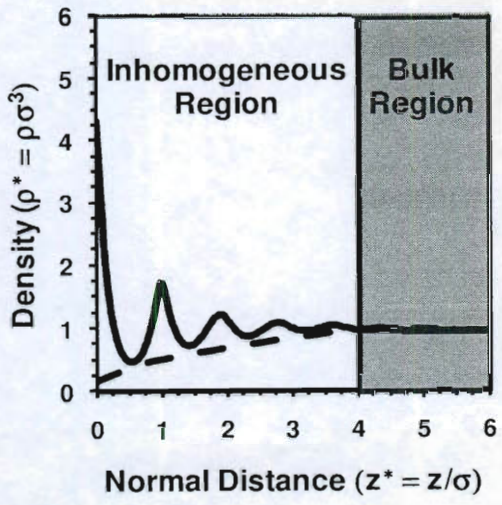

Figure 1.1 Qualitative features of fluid microstructure near a hard wall for high density (solid line) and low density (dashed line).

pharmaceutical suspensions, medical diagnostics and drug delivery; self-healing and performance/smart materials; affinity based separations; and chemically modified surfaces for sensors.

Understanding the molecular level physics (e.g., surface forces, interplay of multiple length scales, and varying dimensionality) that govern these systems is a very challenging problem. Experimental studies continue to provide many important insights into the behavior of such systems, including often providing us with the first observations of their interesting properties. However, as mentioned previously, they can become hampered by an inability to identify the governing physics on the molecular level and the inefficiency of performing sufficiently exhaustive searches of the large parameter spaces involved. Thus, theoretical models play an important role in furthering our understanding and aiding in the experimental design. The theories have limitations of their own, though, and one must choose carefully. Early scaling and mean-field theories do not provide detailed microstructure information accurately and are often limited to specific systems. Examples include the scaling theory of deGennes[6] for polymer brushes and the Asakura-Oosawa (AO) theory[7,8] for athermal polymer-colloid suspensions. More sophisticated approaches have been used extensively and with great success—most notably self-consistent field theory (SCFT)[9] and integral equation theory (IET)[10-12] These approaches suffer from limitations of their own, which will be covered in greater detail in Chapter 3. For example, SCFT is unsuitable for studying denser polymers near surfaces or in confined nanoslits[10,11] where local density fluctuations and liquid-like ordering become

important. Similarly, IET can be very sensitive to the particular closures employed within the theory often leading to inaccurate results.[12-15] Molecular simulations have also played an important role; however, due to the overwhelming amount of information retained in these computer-based experiments, they often quickly become computationally expensive. In fact, simulations can even sometimes become intractable when considering larger macromolecular polymer-like structures or dealing with mixtures with highly dilute solutes in explicit solvents.

Density functional theory (DFT) has emerged as a valuable tool that can be used to better understand the microstructure, thermodynamics, and phase behavior of inhomogeneous fluids. Rather than the highly coarse-grained representation of polymers used in mean-field theories, SCFT, and some simulations, DFT retains the microscopic details of a macroscopic system at a computational cost significantly lower than molecular simulation. In addition, density functional theory provides a single, self-consistent framework for modeling both bulk and interfacial properties. A thorough review of classical DFT was done by Evans,[5] while some of the range of applications was covered by Wu *et al.*[12,13] and Emborsky *et al.*[14] A more recent review of current applications to polyatomic and associating fluids, including the basic framework and a comprehensive literature review, is given in Chapter 3. Central to this review, as well as the work in this thesis, is Wertheim's TPT1. Given its importance in the work done with both bulk and inhomogeneous fluids, some of the key features of Wertheim's theory for association are presented in the following section.

1.2 Wertheim's TPT1 for Associating Fluids

Wertheim derived his first-order thermodynamic perturbation theory for describing the short-ranged, anisotropic attractions that govern the structure and phase behavior of associating fluids.[15-18] The theory has been used to study both homogeneous and inhomogeneous systems, leading to its use as an important basis and framework of a single modeling structure for bulk equations of state and density functional theories. Wertheim initially developed the theory for spheres with a single association site on the surface of the sphere and later generalized it for any number of association sites on a molecule. In later work, Chapman[19] extended Wertheim's TPT1 to mixtures of associating fluids. The key developments of the theory are outlined here using Chapman's notation.

Two associating molecules (represented as hard spheres with off-center, short-ranged and highly directional association sites on the surface as depicted in Figure 1.2) interact through a potential of interaction given as a summation of a hard core repulsion term, an anisotropic attraction term, and the contribution due to association according to

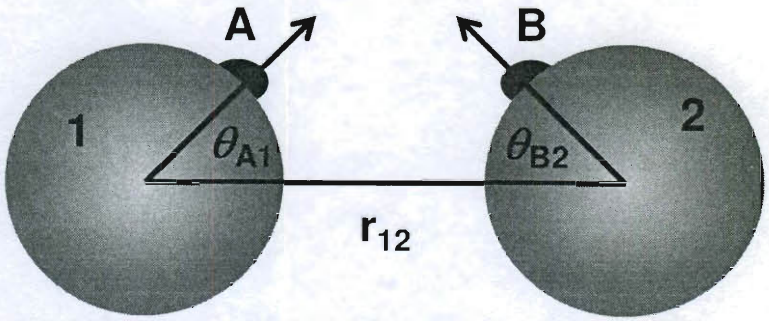

Figure 1.2 Schematic of Wertheim's TPT1 association mechanism.

$$u(\mathbf{r}_{12},\omega_1,\omega_2) = u^{ref}(\mathbf{r}_{12}) + \sum_A \sum_B u_{AB}^{assoc}(\mathbf{r}_{12},\omega_1,\omega_2) \tag{1.1}$$

where u^{ref} represents the reference fluid (hard core plus attractive) contributions u_{AB}^{assoc} is the directional contribution, $\mathbf{r}_{12}$ is the distance between the two segments, ω_1 and ω_2 are the orientations of the two segments, and the summations are over all association sites in the system. The association contribution is modeled as off-centered sites that interact through a short-ranged square-well potential. This potential of interaction between site A on one molecule and site B on a second molecule is written as

$$u_{AB}^{assoc}(\mathbf{r}_{12},\omega_1,\omega_2) = \begin{cases} -\varepsilon_{AB}^{assoc} & r_{12} < r_c; \theta_{A1} < \theta_c; \theta_{B2} < \theta_c \\ 0 & \text{otherwise} \end{cases} \tag{1.2}$$

where ε_{AB}^{assoc} is the square-well depth (association energy), θ_{A1} is the angle between the vector connecting the center of segment 1 to site A and the vector $\mathbf{r}_{12}$, θ_{B2} is the angle between the vector connecting the center of segment 2 to site B and the vector $\mathbf{r}_{12}$ as illustrated in Figure 1.2. The cutoff radius, r_c, and cutoff angle, θ_c, restrict association to occurring only when two segments have the correct orientation and separation as depicted in Figure 1.3.

Within the theory, only bonding between compatible sites is permitted (the bonding energy between incompatible sites A and B is zero, $\varepsilon_{AB}^{assoc} = 0$). Figure 1.3 also contains illustrations of additional constraints within the theory including: (1) once two molecules associate at compatible sites, those sites are no longer available for association with other molecules in the fluid, (2) any given site on a molecule can associate with only one site on another molecule, and (3) two sites

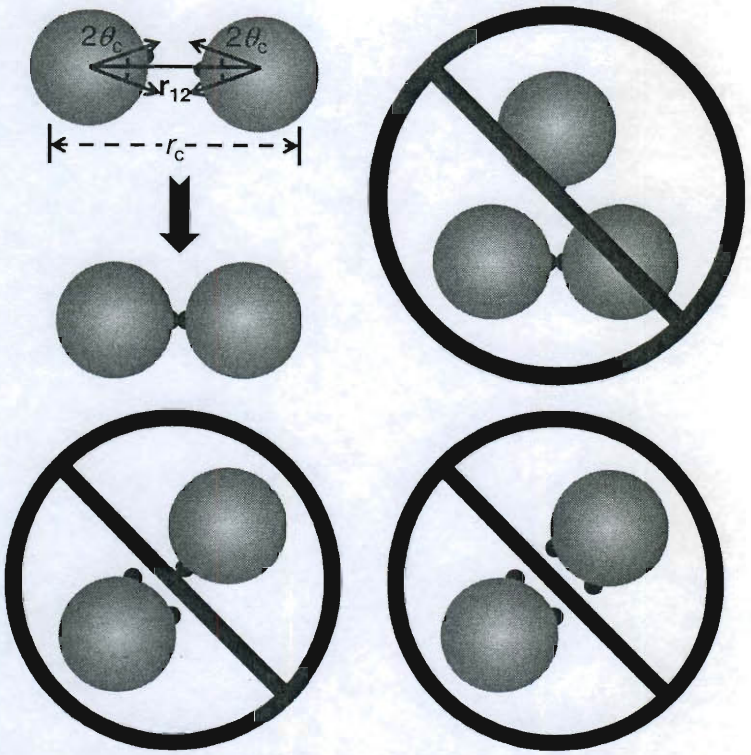

Figure 1.3 Bonding constraints between two molecules in Wertheim's TPT1.

on a molecule cannot simultaneously associate with two sites on another molecule in the fluid.

Using perturbation theory, the association Helmholtz free energy functional of m associating spheres can be written as

$$A = A^{ref} + A^{assoc} \tag{1.3}$$

where A^{ref} is the free energy functional of the reference fluid and A^{assoc} is the contribution due to association defined by

$$\beta A^{assoc} = \frac{\int d\mathbf{r} d\boldsymbol{\omega} \sum_{i=1}^{m} \rho_i(\mathbf{r}) \sum_{A \in \Gamma^{(i)}} \left(\ln \chi_A^{(i)}(\mathbf{r},\boldsymbol{\omega}) - \frac{\chi_A^{(i)}(\mathbf{r},\boldsymbol{\omega})}{2} + \frac{1}{2} \right)}{\int d\boldsymbol{\omega}} \tag{1.4}$$

where $\rho_i(\mathbf{r})$ is the density of segment i at position $\mathbf{r}$, $\beta = 1/k_b T$ is the Boltzmann factor, k_b is Boltzmann's constant, and T is the temperature. The summations are carried out over all the segments in the system and every association site in the set of association sites on each molecule, $\Gamma^{(i)}$. The fraction of type i segments not associated at site A is given by

$$\chi_A^{(i)}(\mathbf{r},\boldsymbol{\omega}) = \frac{1}{1 + \sum_{j=1}^{m} \sum_{B \in \Gamma^{(j)}} \frac{\int d\mathbf{r}' d\boldsymbol{\omega}' \chi_A^{(i)}(\mathbf{r}',\boldsymbol{\omega}') g^{ref}\left(|\mathbf{r} - \mathbf{r}'|\right) f_{AB}\left(|\mathbf{r} - \mathbf{r}'|, \boldsymbol{\omega}, \boldsymbol{\omega}'\right)}{\int d\boldsymbol{\omega}'}} . \tag{1.5}$$

Here, g^{ref} is the radial distribution function of the reference fluid and $f_{AB} = \exp\left(-\beta u_{AB}^{assoc}\right) - 1$ is the Mayer f-function for the association potential.

An ongoing challenge within the field of molecular thermodynamics is the development of a comprehensive model capable of predicting both interfacial and bulk properties within a single framework. As is evident with the above key expressions, and as initially noted by Chapman,[19] Wertheim's theory is formulated for inhomogeneous fluids. Thus, it serves as the basis for formulating both bulk equations of state and inhomogeneous density functional theories for associating fluids. In addition, as will be discussed in subsequent chapters, the theory can be extended to polyatomic chain-like molecules by imposing the limit of complete association between the individual spheres. To arrive at the homogeneous bulk equation of state (SAFT), one simply ignores the position and

orientation dependence of the density. As will be shown in Chapter 2, an equation of state of this form can be used to accurately describe the phase behavior and properties of real systems when an additional dispersion perturbation is included to account for long-range attraction. As mentioned previously, when the position and orientation dependence of all variables is retained, the free energy functional is suitable for describing inhomogeneous fluids. A small simplification can be made in equations (1.4) and (1.5) by relaxing the orientation dependence to reduce the expressions to functionals of position only. This was done by Segura *et al.*[20-23] to develop a DFT for associating spheres near a hydrophobic wall. The same approach was taken to extend this work to a DFT for fully flexible chain fluids known as interfacial SAFT (*i*SAFT).[24-26] A full review of both the history of DFT in general and recent applications of DFTs based on Wertheim's TPT1 (specifically *i*SAFT) are detailed in Chapter 3 and the work of Emborsky *et al.*,[14] which both serve as a detailed precursor to the remainder of this thesis.

1.3 Scope of Thesis

The research work documented within this thesis is focused on the development of molecular theories based in statistical mechanics. The goal is a single framework for the investigation and prediction of structural and thermodynamic properties of both bulk and interfacial complex fluids. Studies have been carried out for application to both real and model systems of theoretical, conceptual, and industrial importance. The basis of this work is Wertheim's first-order thermodynamic perturbation theory. Several equations of

state have been developed based on TPT1 in an effort to meet some of the challenges in accurately predicting the fluid phase equilibria and thermophysical properties of single and multicomponent systems involving complex molecular interactions. Despite these efforts, much work still remains to overcome the theoretical shortcomings to meet the challenges of real systems of complex mixtures and polymer solutions. Developing additional perturbation terms to account for increasingly more complex physics often leads to the addition of more pure component molecular parameters. The universally accepted fitting strategy does not allow for the separation of some or all of these parameters for complex molecules. This, coupled with the highly nonlinear nature of the model, can produce multiple equally effective parameter sets for reproducing pure component properties, but there is no mechanism for determining which set should be used when moving on to investigate mixtures. Chapter 2 provides an alternative technique for determining parameters for complex fluids by considering them in highly dilute mixtures where many of their anisotropic behaviors can be assumed negligible. This mechanism is demonstrated for predicting the water content in binary mixtures with normal alkanes (*n*-alkanes) exhibiting vapor-liquid, liquid-liquid, and vapor-liquid-liquid equilibrium where the hydrocarbon rich phase is modeled using the PC-SAFT equation of state and the pure component water parameters are determined using this technique. The resulting parameter set demonstrates a significant improvement in its ability to purely predict (no binary interaction parameter correction) experimental water content data across a wide range of pressure and temperature conditions. This

predictive model provides a tool for assessing the consistency of additional experimental measurements and allows for the extrapolation to conditions and hydrocarbons that have yet to be studied. Lastly, given the connections between statistical mechanics based models such as the SAFT family of EOS and molecular simulations, the logical reasoning used here allows for an assessment of the similar parameters needed in performing simulations.

The main focus of this thesis is the continued development and application of density functional theory. Chapter 3 provides a comprehensive background and review of density functional theory. It also outlines the basic formalism of constructing a DFT and presents many of the most recent applications of TPT1 based DFTs (*i*SAFT specifically) to a diverse set of challenging problems. These applications not only demonstrate the robust versatility of DFT, but accurate comparisons with simulation and experiments are made where possible. The power of DFT to answer many of the questions about the physics governing such interesting phenomena is also explored. Chapter 4 and Chapter 5 provide extensions of *i*SAFT to investigate the interfacial and structural properties of model inhomogeneous complex fluids where quantitative comparisons are made with molecular simulation, and qualitative behavior consistent with experiments is demonstrated. In these chapters, some of the more challenging problems involving amphiphilic molecules and their behavior at fluid-fluid interfaces are explored.

In Chapter 4, the polyatomic *i*SAFT density functional theory is used to study the effects of surface loading on the interfacial tension and corresponding

microstructure of a model oil-water-surfactant system. The results accurately demonstrate the partitioning of the diatomic amphiphilic surface active agent (surfactant) molecules to the interface as compared with molecular simulation. The advantage of a molecular theory capable of self-consistently modeling the entire system from the bulk to the interface despite only trace surfactant concentrations in the bulk is demonstrated through the equilibrium fluid structure. Some additional comparisons of interfacial tension predictions with simulation are also made for slightly different surfactant structures. The capability of accurately performing such fundamental calculations for simple model systems forms the basis for further extending the theory to unexplored regions of the vast parameter space.

Chapter 5 aims to further the understanding of the molecular level physics governing surfactant behavior and general structure-property relationships. Surfactants are ubiquitous in nearly every aspect of industry from consumer products such as shampoos and detergents to enhanced oil recovery to drug delivery to paints and coatings. However, many challenges still exist for experimentalists and theoreticians alike. The extremely broad parameter space, unique phase behavior, and complex interactions make such a system difficult to analyze and model. Here, *i*SAFT is used to characterize the effects of surfactant structure, oil structure, temperature, and bulk surfactant concentration on equilibrium properties such as the interfacial tension. The fluid structure is used to elucidate how these molecules work and how changing the parameters affect the system from the molecular level.

Finally, Chapter 6 summarizes the key achievements presented in this work. Some of the ideas for future development and areas of application for the density functional theory are also addressed.

CHAPTER 2 CORRELATION AND PREDICTION OF WATER CONTENT IN ALKANES USING A MOLECULAR THEORY

2.1 Introduction

Modeling the equilibrium water content of gas and/or liquid hydrocarbons and their mixtures has proven to be of vital importance to the gas and petroleum industries for inherently safe design, operation, and efficient performance of process equipment. Prediction of water content is important in preventing corrosion problems caused by moisture condensation in pipelines or process equipment and the dosage of chemical inhibitors designed to prevent hydrate crystal formation in subsea and terrestrial pipelines. Hydrates have been known to create blockages in fluid transmission lines, cause serious damage to plant equipment, and pose significant safety concerns.

Through the efforts of many experimentalists,[27-33] the mutual solubility of binary alkane-water mixtures has been measured across a wide range of conditions. These go from the extreme pressures and temperatures of deep sea reservoirs to the more modest platform conditions to cryogenic conditions necessary for gas processing.[34] A designation of "extensive" coverage of such conditions can strictly only be used for a few alkanes (e.g., methane, ethane, and propane according to the International Union of Pure and Applied Chemistry (IUPAC) and National Institute of Standards and Technology (NIST) database[35]) while many other binary hydrocarbon-water mixtures have questionable, inconsistent, and/or lacking data across this wide range of conditions. Despite the significant importance of these systems in many industries and the efforts to

measure the mutual solubilities accurately, significant disagreement exists in the experimental data. In fact, for many of the systems, the IUPAC-NIST solubility database[35] recommends limited to none of the available data when such data is available. Therefore, there is need for a predictive model to aid in differentiating the accuracy of experimental data sets and to predict water content for temperatures, pressures, and hydrocarbons that have not yet been measured.

Modeling these systems is difficult because they exhibit limited miscibility over a wide range of conditions (e.g., see Brunner[36]). The solubility of the hydrocarbon in water is several orders of magnitude lower than the corresponding solubility of water in the hydrocarbon. Additionally, the solubility of some hydrocarbons exhibits a minimum value at a low temperature; whereas, the water solubility is a monotonic function of the temperature.[37]

Cubic equations of state, for the most part, were originally developed for modeling hydrocarbon mixtures for the petroleum and refining industries. These models were applied with limited success to hydrocarbon-water systems using local composition[38,39] and density-dependent[40] mixing rules. Many other more involved approaches have been taken to further improve upon the basic cubic equations of state. One such approach is to use unconventional mixing rules (e.g., see Michel *et al.*[41] who took the hydrophobic effect into account through strong composition dependence of the water-water parameter). An alternative is to use a physically reasonable mixing rule for the hydrocarbon rich phase and a separate, accurate equation of state for the water rich phase. Such an approach was taken successfully by Yarrison *et al.*[33] for modeling water content in small,

light components (methane, ethane, propane, carbon dioxide, and hydrogen sulfide) using the Peng-Robinson equation of state[2] with a temperature-dependent binary interaction parameter. Another approach is to use other higher order semitheoretical equations of state that specifically account for molecular size and shape, hydrogen bonding and other anisotropic interactions. These models for associating fluids have been based on statistical mechanical contributions using chemical equilibrium, lattice theory, or perturbation theory to account for such interactions. In this work, we demonstrate advantages of combining the approach of Yarrison *et al.*[33] with a theoretical equation of state.

The statistical associating fluid theory (SAFT) equation of state (and its family of similarly based models)[19,42-55] is an example of a perturbation theory that has enjoyed remarkable success in predicting the effects of molecular size and shape, hydrogen bonding, polar interactions, composition, pressure, and temperature on the phase behavior of both associating and non-associating mixtures. In particular, the SAFT family has proven to be accurate in predicting the effect of molecular shape on phase behavior of alkanes to polymers. This molecular equation of state provides a framework for modeling the complex phenomena seen in many highly non-ideal systems such as hydrocarbon-water binary mixtures. Thus, the SAFT family of models is ideally suited to model water content from alkanes to polymers over a wide range of pressures and temperatures. However, there continues to be uncertainty in the best parameters for modeling water and mixtures of water and hydrocarbons with the SAFT family of equations of state.[56-59] The issue is to determine a unique set of SAFT

parameters for pure water. The parameters are not unique, since they are traditionally fit to pure fluid vapor pressure and saturated liquid density data, and at least 6 parameters are required if van der Waals interactions, association, and long range polar interactions are included. The nonlinearity of the SAFT model with respect to all these parameters will produce multiple equally good parameter sets using this fitting strategy.

There are two purposes of this chapter: (1) to determine the intrinsic van der Waals interaction parameters for water independent of hydrogen bonding or long range polar interactions and (2) to use a reliable theoretical equation of state to predict water solubility as a function of hydrocarbon size, temperature, and pressure to demonstrate the consistency (or lack thereof) of water content data. Finally, we discuss implications of the intrinsic water parameters on simulation models of water.

2.2 Theory and Model

Both objectives are accomplished through physically reasonable simplifying assumptions. Across a wide range of conditions, the solubility of alkanes in water and the solubility of water in alkanes are very small. We take advantage of this to estimate the fugacity of water in the water rich and hydrocarbon rich phases. The fugacity of water in the water rich phase can be estimated using an accurate equation of state for pure water. In the hydrocarbon rich phase, water is at sufficiently low solubility that a water molecule will rarely "see" any other water molecules. Thus, the water-hydrocarbon interaction will be the only important water interaction in determining the water fugacity in the

hydrocarbon rich phase. Since water only interacts with alkanes through short range repulsion and van der Waals attraction, other intermolecular forces associated with water such as hydrogen bonding and polar interactions can be neglected in the hydrocarbon rich phase. Assuming Lorentz-Berthelot mixing rules, this allows for the determination of the intrinsic van der Waals parameters for water independent of the hydrogen bonding or long range polar parameters. Such an approach can also be used for more complex molecules. Given the ability of SAFT to accurately predict the effect of molecular size and shape on phase behavior, it is believed that a purely predictive (no binary interaction parameter) model for the solubility of water in hydrocarbons from alkanes to polymers will be developed. Such a model can be used to check the level of consistency in experimental water content data.

In an attempt to make an accurate and predictive model from both an engineering and theoretical standpoint, several binary n-alkane-water systems were considered (carbon numbers (CN) 1, 2, 5-10, 14 and 16). The hydrocarbon rich phase is modeled using the perturbed-chain SAFT (PC-SAFT) equation of state,[42,43] and the aqueous phase is modeled using a NIST equation of state based on the work of Saul and Wagner.[60,61] This formulation for the aqueous phase provides quick and accurate calculations of the fugacity of pure water using minimal parameters.

2.2.1 Conditions for Equilibrium

For binary hydrocarbon-water systems in fluid-fluid equilibrium, the phase equilibrium relationship starts by equating the fugacity of each component in both

phases. As an example, consider a binary mixture of water (H_2O) and hydrocarbon (HC) in vapor-liquid equilibrium (VLE) where the hydrocarbon rich phase is a vapor. The phase equilibrium written in terms of water is

$$y_{H_2O}\hat{\phi}_{H_2O}\left(P,T,y_{H_2O}\right)P=(1-x_{HC})\gamma_{H_2O}\left(P,T,x_{HC}\right)\mathrm{f}_{H_2O}^{pure}\left(P,T\right), \qquad (2.1)$$

where y_{H_2O} is the mole fraction of water in the hydrocarbon rich phase, $\hat{\phi}_{H_2O}$ is the fugacity coefficient of water in the hydrocarbon rich phase evaluated using the PC-SAFT equation of state, P is the system pressure, T is the system temperature, x_{HC} is the mole fraction of hydrocarbon dissolved in the liquid water rich phase, γ_{H_2O} is the activity coefficient of water in this phase, and $\mathrm{f}_{H_2O}^{pure}$ is the fugacity of pure water evaluated using the NIST equation of state. While written for VLE, similar expressions can be written for liquid-liquid equilibrium (LLE) or vapor-liquid-liquid equilibrium (VLLE) by using the corresponding representations of the fugacity in the different phases. Based on the low solubility of the hydrocarbon in water, these equations are simplified by assuming that the aqueous phase is essentially pure. In terms of equation (2.1), this means $\gamma_{H_2O}\approx 1$ and $x_{HC}\approx 0$. This approximation can be relaxed by calculating the solubility of the hydrocarbon in water based on correlations for the Henry's law constant. However, the difference was found to be negligible in the cases studied here.

2.2.2 Calculating Aqueous Phase Fugacity

The fugacity of pure water was calculated using the NIST equation of state as presented by Saul and Wagner.[60,61] This formulation, which accurately

reproduces the fugacity of pure water with minimal parameters, is valid in the temperature range $274\ \text{K} < T < 647\ \text{K}$.

2.2.3 Calculating Hydrocarbon-Rich Phase Fugacity

The fugacity of water in the hydrocarbon rich phase is modeled with a version of the SAFT equation of state. The widely applied and highly successful SAFT equation of state was first derived by Chapman *et al.*[19,46-48,53] based on extensions and simplifications of Wertheim's first-order thermodynamic perturbation theory,[15-18] and there are several versions of SAFT in regular use today.[19,42-55] In this work, the PC-SAFT version, which uses a modified Barker-Henderson dispersion term developed by Gross and Sadowski,[42,43] was used to calculate the fugacity of water in the hydrocarbon-rich phase.

PC-SAFT applies the Barker-Henderson[62,63] second-order perturbation theory to a hard chain reference fluid. This results in a dispersion term dependent on the chain length of a molecule. Only the development relevant to this work is presented here. For greater detail, the reader is referred to the work of Gross and Sadowski.[42,43] For simplicity, the reduced Helmholtz free energy, $a = A/Nk_bT$, is used throughout this development where N is the number of molecules and k_b is the Boltzmann constant. For non-associating, non-polar systems, the dimensionless residual (res) Helmholtz free energy is

$$a^{res} = a^{hc} + a^{disp}, \tag{2.2}$$

where the superscripts hc and $disp$ denote the hard chain and dispersion contributions, respectively. This simple model accurately describes the

properties and phase behavior of hydrocarbons from alkanes up to polymers. Although the SAFT equation of state and its extensions can model anisotropic interactions such as hydrogen bonding and polar interactions,[54,55] the assumption is that water is dilute enough that two water molecules are never close enough to show substantial hydrogen bonding or polar interactions, which eliminates the need to fit these corresponding parameters.

The hard chain contribution to the free energy is written in terms of the hard sphere (hs) and chain connectivity $(chain)$ free energies as[46]

$$a^{hc} = a^{hs} + a^{chain}. \tag{2.3}$$

The hard sphere interaction originally developed by Carnahan and Starling[64] as extended to mixtures by Boublik and Mansoori *et al.*[65,66] is

$$a^{hs} = \frac{6}{\pi\rho}\left[\frac{\zeta_2^3 + 3\zeta_1\zeta_2\zeta_3(1-\zeta_3)}{\zeta_3(1-\zeta_3)^2}\left(\zeta_0 - \frac{\zeta_2^3}{\zeta_3^2}\right)\ln(1-\zeta_3)\right], \tag{2.4}$$

where $\zeta_{k=0,\ldots,3}$ are functions of the number density, ρ, and species mole fractions, x_i, according to

$$\zeta_k = \frac{\pi\rho}{6}\sum_{i=1}^{N_{cp}} x_i m_i d_i^3. \tag{2.5}$$

In this equation, N_{cp} is the number of components and m_i and d_i are the chain length and temperature dependent segment diameter of the i^{th} component. This temperature dependence is given by[49]

$$d_i = \sigma_i\left[1 - 0.12\exp\left(-\frac{3\varepsilon_i}{k_b T}\right)\right], \tag{2.6}$$

where σ_i is the hard sphere diameter and ε_i is the potential well depth of the i^{th} component (sometimes referred to as the segment dispersion energy).

The contribution to the Helmholtz free energy due to the chain length of molecules is given by Chapman *et al.*[19,46,53] as

$$a^{chain} = \sum_i x_i (1-m_i) \ln g_{ii}^{hs}(d_i), \tag{2.7}$$

where g_{ii}^{hs} is the pair correlation function of the hard sphere reference fluid for segment type i evaluated at contact as given by Boublik and Mansoori *et al.*[65,66]

The dispersion term developed by Gross and Sadowski is a sum of first-order and second-order terms given by[42,43]

$$a^{disp} = a_1^{disp} + a_2^{disp}, \tag{2.8}$$

where the two terms are

$$a_1^{disp} = -2\pi\rho I_1(\zeta_3, \bar{m}) \sum_{i=1}^{N_{cp}} \sum_{j=1}^{N_{cp}} x_i x_j m_i m_j \sigma_{ij}^3 \frac{\varepsilon_{ij}}{k_b T} \tag{2.9}$$

and

$$a_2^{disp} = -\pi\rho\bar{m} C_1 I_2(\zeta_3, \bar{m}) \sum_{i=1}^{N_{cp}} \sum_{j=1}^{N_{cp}} x_i x_j m_i m_j \sigma_{ij}^3 \left(\frac{\varepsilon_{ij}}{k_b T}\right)^2. \tag{2.10}$$

The undefined terms are the weighted average chain length, $\bar{m} = \sum_{i=1}^{N_{cp}} x_i$, the arithmetically averaged segment diameter, $\sigma_{ij} = (\sigma_i + \sigma_j)/2$, and the geometrically averaged dispersion energy, $\varepsilon_{ij} = (1-k_{ij})\sqrt{\varepsilon_{ii}\varepsilon_{jj}}$ with binary interaction parameter k_{ij} used to correct mixture property predictions. C_1 is from

the local compressibility approximation of Barker and Henderson[62,63] written in terms of the hard chain compressibility factor contribution as

$$C_1 = \left(1 + Z^{hc} + \rho \frac{\partial Z^{hc}}{\partial \rho}\right)^{-1} = 1 + \bar{m}\frac{8\zeta_3 - 2\zeta_3^2}{(1-\zeta_3)^4} + (1-\bar{m})\frac{20\zeta_3 - 27\zeta_3^2 + 12\zeta_3^3 - 2\zeta_3^4}{\left[(1-\zeta_3)(2-\zeta_3)\right]^2}. \quad (2.11)$$

The integral terms I_1 and I_2 in equations (2.9) and (2.10) are integrals over the pair correlation function of the reference fluid. These integrals have been fit to a power series in ζ_3 according to

$$I_1(\zeta_3, \bar{m}) = \sum_{i=0}^{6} a_i(\bar{m})\zeta_3^i \quad (2.12)$$

and

$$I_2(\zeta_3, \bar{m}) = \sum_{i=0}^{6} b_i(\bar{m})\zeta_3^i, \quad (2.13)$$

where the average chain length dependence of the coefficients is given by

$$a_i(\bar{m}) = a_{0i} + \frac{\bar{m}-1}{\bar{m}}a_{1i} + \frac{\bar{m}-1}{\bar{m}}\frac{\bar{m}-2}{\bar{m}}a_{2i} \quad (2.14)$$

and

$$b_i(\bar{m}) = b_{0i} + \frac{\bar{m}-1}{\bar{m}}b_{1i} + \frac{\bar{m}-1}{\bar{m}}\frac{\bar{m}-2}{\bar{m}}b_{2i}. \quad (2.15)$$

These coefficients, as reported by Gross and Sadowski,[43] were fit to a large set of pure component experimental data for the *n*-alkanes.

With this model, the fugacity coefficient can be determined from[48]

$$\ln\left(\hat{\phi}_{H_2O}\right) = \frac{\mu_{H_2O}^{res}}{k_bT} - \ln(Z) \quad (2.16)$$

where $\mu_{H_2O}^{res}$ is the residual chemical potential of water in the hydrocarbon rich phase and Z is the compressibility factor. Further details about the derivation of the contributing terms to the residual chemical potential and other undefined terms can be found in the original work by Chapman *et al.*[19,46-48,53] with specifics for the PC-SAFT dispersion term in the development by Gross and Sadowski.[42,43] This model requires only three undetermined parameters for each component — the chain length (m), the temperature-independent segment diameter (σ), and the segment-segment dispersion energy (ε). Pure component PC-SAFT parameters for the alkanes fit to saturated liquid density and vapor pressure experimental data have been tabulated by Gross and Sadowski.[43] The three parameters for water are determined and tested within this work.

2.3 Results and Discussion

The simplified thermodynamic model described above has the advantage that it requires the determination of only three intrinsic pure component water parameters $(m, \sigma$, and $\varepsilon/k_b)$. Since water is often modeled in molecular simulation as spherical, the choice was made to take $m = 1.00$. Any additional size effects will be absorbed by the other parameters. An attempt was made to determine the remaining two parameters by fitting to a variety of water content data using nonlinear least squares with the water parameters of Gross and Sadowski $(\sigma = 3.0007$ Å and $\varepsilon/k_b = 366.51$ K$)$[43] as an initial guess. Due to significant scatter in the available experimental data of water content in heavier alkanes (e.g., from the IUPAC-NIST database[35]) all of the data could not be fit

with physically realistic parameters. This led to exploring the solution space with a sensitivity analysis at several fixed values of the parameters. Figure 2.1 and Figure 2.2 are representative examples of the relative sensitivity of the model to independent changes in each parameter across a range of temperatures at a fixed pressure. It is clear that water content prediction is more sensitive to the well depth of the potential than to the segment diameter. Although not pictured here, similar conclusions were drawn when looking at a range of pressures at fixed temperature. With the relative insensitivity to the temperature-independent segment diameter in the hydrocarbon-water systems investigated, the segment diameter was set to $\sigma = 3.00$ Å based on some trial calculations, the value used in the SPC/E model,[67-69] and the value of Gross and Sadowski.[43]

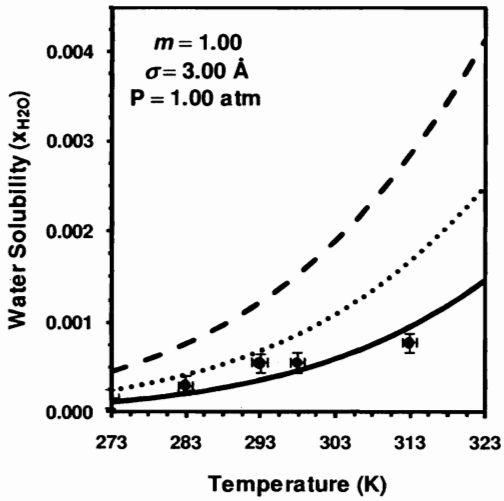

Figure 2.1 Heptane-water model sensitivity to the water segment-segment dispersion energy parameter. Points are from IUPAC-NIST experimental data collection[35] while lines are PC-SAFT predictions with $\varepsilon/k_b = 200$ K (solid), $\varepsilon/k_b = 250$ K (dotted), and $\varepsilon/k_b = 300$ K (dashed).

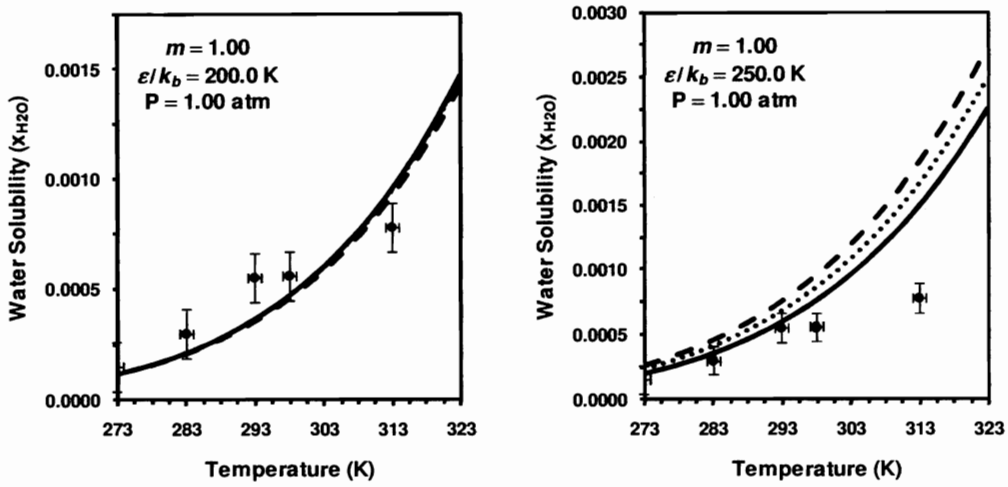

Figure 2.2 Heptane-water model sensitivity to the water temperature independent segment diameter. Points are from IUPAC-NIST experimental data collection[35] while lines are PC-SAFT predictions with $\sigma = 2.00$ Å (solid), $\sigma = 2.50$ Å (dotted), and $\sigma = 3.00$ Å (dashed).

With two of the three PC-SAFT water parameters set, returning to the nonlinear least squares fitting strategy yielded improved results for the potential well depth. Water content data for the linear alkanes with carbon numbers 5-13 and 16 from the IUPAC-NIST database[35] at 298 K and atmospheric pressure. It is considered as the expectation is water content data at ambient conditions is the most reliable since it is widely measured and reviewed. However, as seen in Figure 2.3, there is considerable uncertainty in the data. Table 2.1 shows the results of fitting the model to the data at ambient conditions. Although the overall average energy parameter suggested a logical choice, the potential bias due to an unnecessarily high value by the hexadecane result (which happens to have a 25% uncertainty) led to its omission in taking the average. This gives an average energy parameter of $\varepsilon/k_b = 207.30$ K. The performance of this parameter set in

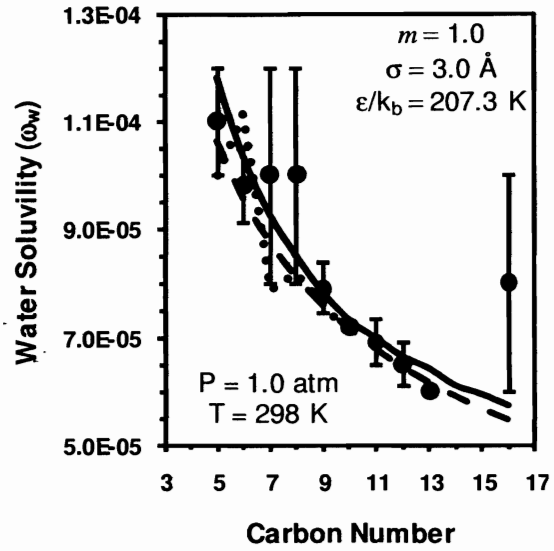

Figure 2.3 Comparison of current model predictions (solid) with IUPAC-NIST experimental data[35] (points) and correlation predictions from Tsonopoulos[70] (dashed) and Wagner[71] (dotted) for water solubility in hydrocarbon rich liquid phase at ambient conditions.

modeling the water solubility in liquid hydrocarbons at ambient conditions is shown in Figure 2.3. As expected, this model does a good job correlating all of the experimental data within the experimental uncertainty except for hexadecane. Based on the trend with increasing pair potential well depth observed in Figure 2.2, using the overall average of $\varepsilon/k_b = 209.84$ K given in Table 2.1 would shift the model curve up, decreasing its accuracy in all systems except that of hexadecane. This further substantiates the initial assumption that the large value for water content in hexadecane is probably in error and would unfavorably bias the performance of reported model parameters. The PC-SAFT model also gives the correct overall general trend of decreasing water content with increasing alkane carbon number. For comparison, two engineering correlations of water content are also presented. The correlation due to Wagner is based on fitting

Table 2.1 Optimized water segment-segment dispersion energy parameter for alkane hydrocarbon-water systems at 298 K and 1.0 atm using $m=1.0$ and $\sigma=3.00$ Å.

CN	ε/k_b (K)
5	201.24
6	202.96
7	213.45
8	220.19
9	207.93
10	206.01
11	206.30
12	205.51
13	202.11
16	232.69
Average	209.84
St. Dev.	9.85

water content in each alkane separately. For each carbon number, the author determined the best available data and determined separate parameters for each system. The scatter in available data accounts for the jagged curve connecting predictions for each carbon number. The model of Tsonopoulos is based on correlating reviewed data over a range of carbon numbers, giving a smooth curve similar to the model presented here.

With the single model parameter determined based on measurements of water content in the hydrocarbon rich phase at ambient conditions, validation of the model and its robustness is demonstrated through modeling systems at a myriad of extreme conditions. Figure 2.4 through Figure 2.7 show several examples of such conditions for methane, ethane, propane, hexane, octane, and decane. These results show excellent qualitative agreement with the experimental data and good quantitative agreement whether modeling the water

solubility in a vapor or liquid hydrocarbon. Figure 2.4 shows a comparison of the model with experimental data for the water solubility in liquid hydrocarbons hexane, octane, and decane at elevated temperature. Although PC-SAFT parameters were fit at ambient conditions, the model predicts water content in reasonable agreement with experimental data over a wide range of pressures and temperatures.

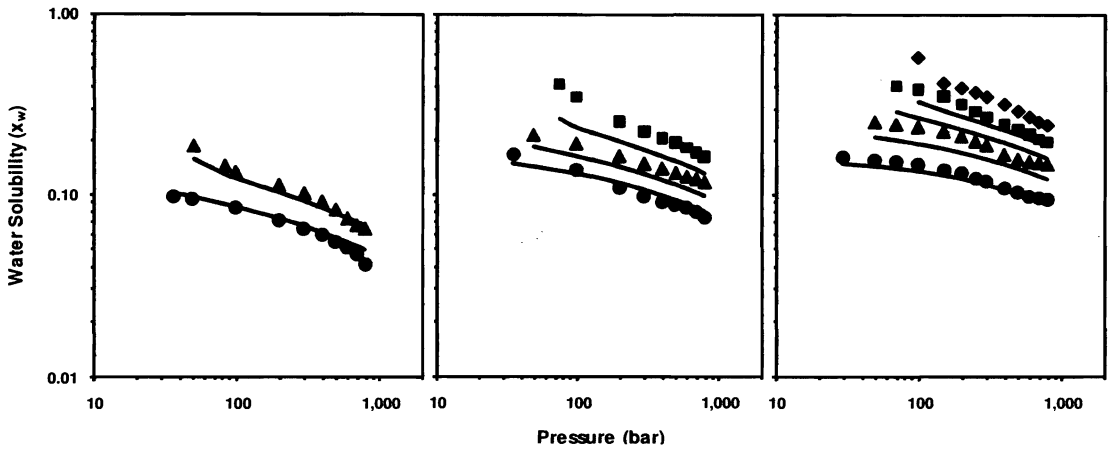

Figure 2.4 Comparison of current model predictions (curves) with experimental data (points) of the water solubility in the hydrocarbon rich phase for LLE systems. (Left) Hexane at 473.2 K (circles) and 493.2 K (triangles) from Skripka *et al.*[28,32] (center) Octane at 498.2 K (circles), 513.2 K (triangles), and 538.2 K (squares) from Gubkina *et al.*[27] (right) Decane at 498.2 K (circles), 523.2 K (triangles), 548.2 K (squares), and 563.2 K (diamonds) from Skripka *et al.*[28,32]

The single parameter for the water model was fit to liquid-liquid equilibria; however, it is expected the model will accurately predict water content in a gaseous hydrocarbon as well. In Figure 2.5 and Figure 2.6, comparisons of the model predictions with experimental data for water content in methane and ethane up to extreme temperature and pressure are made. Agreement is impressive considering that no binary interaction parameter has been set.

Agreement could be improved by fitting a temperature dependent binary interaction parameter. For the methane and ethane systems, Yarrison *et al.*,[33]

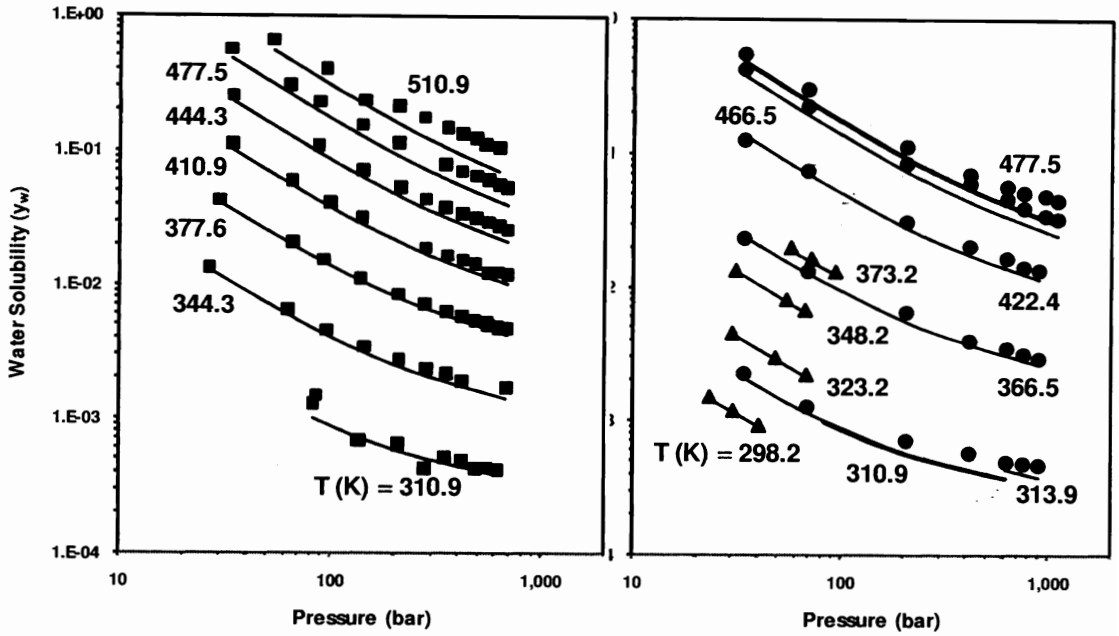

Figure 2.5 Comparison of current model predictions (curves) with experimental data from Olds *et al.*[29] (squares), Rigby and Prausnitz[31] (triangles), and Yarrison *et al.*[33] (circles) for the water solubility in the methane rich phase.

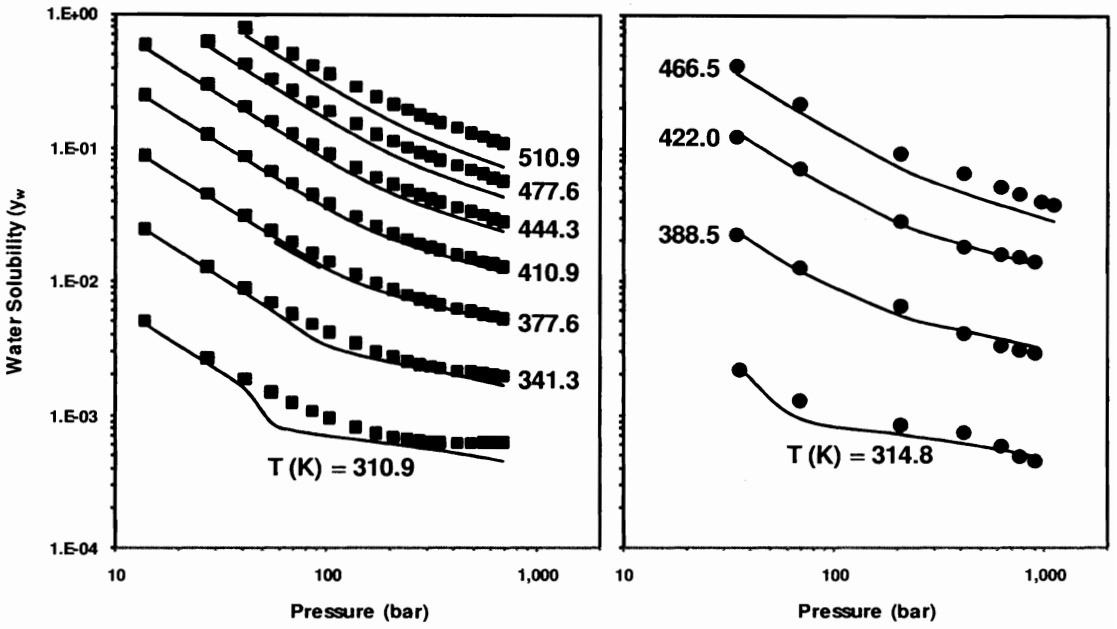

Figure 2.6 Comparison of current model predictions (curves) with experimental data from Reamer *et al.*[30] (squares) and Yarrison *et al.*[33] (circles) for the water solubility in the ethane rich phase.

using a cubic equation of state and a similar approach to that described here, found excellent agreement with data for water content in methane and ethane using such a parameter. Unlike the PC-SAFT equation of state, though, results using the cubic equation of state are expected to become worse for heavier hydrocarbons.

Except for the data reported by Yarrison *et al.*,[33] the model agreement for methane and ethane is within experimental error. A potential reason for less accurate quantitative performance at higher temperatures is the assumption of dilute solution. In the examples presented here, experimental water solubility has risen to over 2.0 wt%. It is not unreasonable to presume that this is sufficiently high that water-water interactions such as hydrogen bonding and polarity could no longer be negligible. To test the validity of this claim, hydrogen bonding and polarity parameters for water were fit to pure component vapor pressure and saturated liquid density data. The complete model was used to compare the accuracy of solubility predictions for the systems and conditions shown. Beyond concluding that these contributions are still largely insignificant with only slight improvements over the simple model, these parameters have yet to be sufficiently and rigorously studied enough to report.

The model accuracy was tested further by predicting the water content of the hydrocarbon rich phases of the propane-water system, which exhibits vapor-liquid-liquid equilibrium. Using the simplifying assumption proposed above that the solubility of the hydrocarbon is negligible in the water-rich phase, the phase partitioning of water between liquid and vapor propane phases is found by

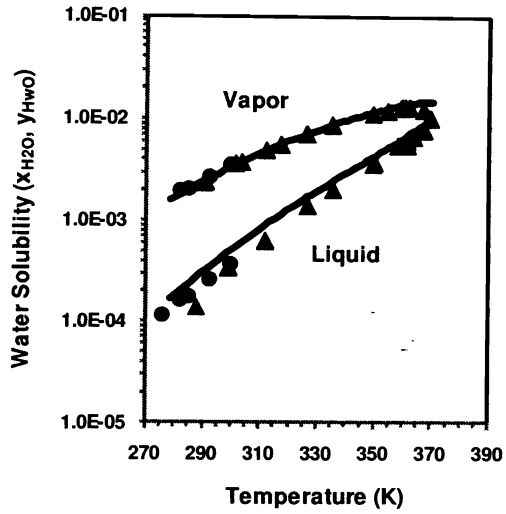

Figure 2.7 Comparison of current model predictions (curves) with experimental data from Song and Kobayashi[72] (circles) and Kobayashi and Katz[73] (triangles) for the water solubility and partitioning between propane rich phases.

equating the fugacity of water in all three phases. The fugacity of pure water was calculated using the previously mentioned Saul and Wagner correlation[60,61] while PC-SAFT with the intrinsic water parameters reported here was used for the hydrocarbon rich phases. This results in the phase envelope given in Figure 2.7 between the quadruple point and the critical point. Comparison with the experimental data of Song and Kobayashi[72] and Kobayashi and Katz[73] shows very good agreement outside the critical region. The model correctly predicts that the water mole fraction is higher in vapor propane than in liquid propane. The over-estimation of the critical point is expected and can be addressed for PC-SAFT using a renormalization group theory as shown by Bymaster *et al.*[4] The slight over-estimation of the liquid phase composition can be addressed by fitting a binary interaction parameter as mentioned above.

With a reasonably accurate set of parameters for water based on the fitting strategy of this work and correlations for PC-SAFT parameters for alkanes, the final objective was to extrapolate the predictive model $\left(k_{ij}=0\right)$ for engineering application. In Figure 2.8 and Figure 2.9, the limiting behavior of the water solubility is explored as a function of both temperature and pressure for several values of the alkane carbon number. These results indicate an essentially constant slope for log of water solubility versus the reciprocal of temperature across all carbon numbers for a fixed pressure and a small dependence on pressure for liquid alkanes. This linear dependence in the inverse temperature in Figure 2.8 and pressure independence for liquid alkanes in Figure 2.9 is consistent with experimental data. This is the basis of the correlation proposed by Wagner.[71] However, there is substantial pressure dependence for gaseous hydrocarbons where the 'kink' or discontinuity in the predictions for ethane indicates a phase change (vapor pressure). It is also suggested that the sensitivity of water content to carbon number decreases with increasing molecular weight, which provides the basis for a mechanism to extrapolate out to polymer-like molecules within this homologous series (i.e., polyethylene).

An advantage of the theoretical foundation of the SAFT family of equations of state is that the parameters for the potential model can be compared with potential parameters used in molecular simulation. For example, the potential parameters used in PC-SAFT for methane are similar to the Lennard-Jones parameters used for methane in molecular simulation. Therefore, it is interesting that the intrinsic energy parameter for water obtained here is more than twice the

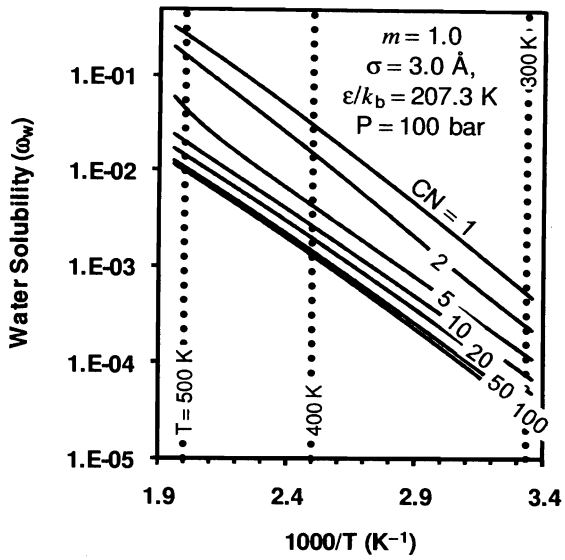

Figure 2.8 Effect of temperature and carbon number on the water solubility in the hydrocarbon rich phase at fixed pressure using the current predictive model.

Lennard-Jones energy values commonly used in simulation models of water. The simulation value can be justified based on the polarizability and ionization potential for water if one only considers the first term in the London dispersion energy. On the other hand, the value obtained here is based on reasonable physical arguments, an accurate correlation for water, and the Lorentz-Berthelot mixing rules. In both approaches, we are assuming the correctness of a repulsive contribution to the potential. It would be interesting to use our approach to fit an intrinsic water potential model from molecular simulation.

2.4 Conclusions

The purpose of this work was to develop a method for determining more robust PC-SAFT pure component parameters for complex molecules in the interest of modeling hydrocarbon-water systems. By making rather intuitive assumptions based on knowledge of the systems being studied to simplify the

model, it has been shown that it is possible to find the three intrinsic parameters using this approach. The accuracy of this simplified model and its set of parameters, specifically for binary hydrocarbon-water systems, have been demonstrated in both vapor-liquid and liquid-liquid phase equilibria over wide ranges of temperatures and pressures. In addition, the model was applied to the propane-rich vapor-liquid phase envelope assumed to be in equilibrium with pure water between the quadruple point and critical point. Excellent qualitative agreement in these studies was found along with relatively good quantitative agreement without having to introduce a binary interaction parameter. Employing this strategy helps separate the individual contributing effects and will subsequently reduce the complexity of the universally recognized approach of determining the pure component PC-SAFT parameters to a much simpler optimization problem. With the inherent nonlinearity of the PC-SAFT equation of state, this will reduce the parameter space and make the search for the optimal parameters that control anisotropic behavior less intensive. Additionally, such an accurate model can be useful in checking the consistency of subsequent experimental water content measurements in different alkanes. Further application of the approach would allow for predictions of water content in other alkanes (e.g., branched alkanes) and more complex hydrocarbon mixtures. Finally, a dispersion energy approximately twice the value being used in molecular simulation opens the question concerning the availability of an accurate potential model for water in simulation.

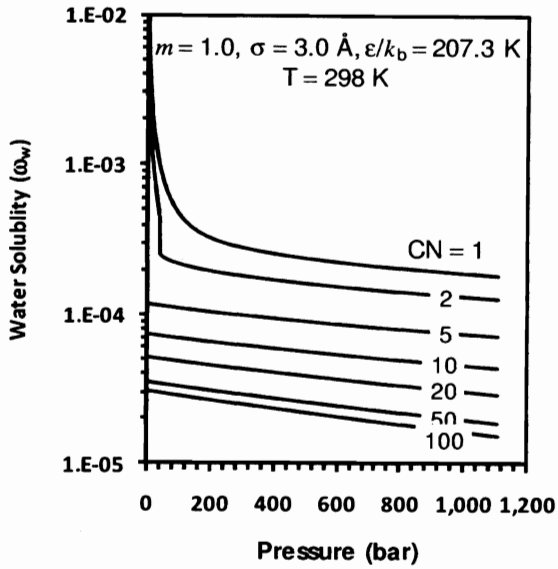

Figure 2.9 Effect of pressure and carbon number on the water solubility in the hydrocarbon rich phase at fixed temperature using the current predictive model.

2.5 Recommended Future Work

This study has demonstrated the capability of a proposed model reduction (simplification) with the purpose of separating some of the multiple model complex fluid parameters in sophisticated equations of state. This has been demonstrated specifically for water and the PC-SAFT equation of state. The first logical extension of this work is fitting the anisotropic parameters to give a complete parameter set for water. This would require greater testing of the resulting parameters to demonstrate their performance in comparison with currently available published parameter sets. Due to the anomalous behavior of pure water specifically, this could involve extensions to the currently available models as they have been unable to reproduce properties such as the density maximum. One such idea is cooperative hydrogen bonding which was initially suggested by Frank and Wen.[74] Their idea, which was confirmed with infrared

spectroscopy by Luck,[75] is that hydrogen bonds are not formed and broken one at a time, but they form in clusters due to electron rearrangement. Work by Truskett and coworkers,[76-79] has demonstrated some success with applying a variable hydrogen bonding energy, and this idea was further developed within a perturbation theory construct by Sear and Jackson.[80] Another potential approach to accounting for this behavior is through an additional density and/or temperature dependence of the hydrogen bonding orientation parameter. Coupling these different approaches with the modified fitting strategy could provide a more accurate picture of complex fluid behavior.

Extending the application of the approach suggested here to more species and models could provide greater insight into the sensitivity of such models. Through the aid of multiple degrees of freedom and correction factors such as the binary interaction parameter, the simplest techniques are often employed for determining model parameters and accurately reproducing observed experimental data for the specific systems of interest. This can often lead to overestimating or underestimating the importance of different contributions to the governing physics. For example, a smaller segment-segment dispersion energy can give the same physical behavior, but it would require an increase of anisotropic characteristics such as hydrogen bonding or polarity. This change in the parameters can lead to difficulties in extending their application to systems and conditions for which they were not fit. Thus, two studies are proposed to gauge the performance of current fitting strategies. First, the technique suggested here could be extended further by incorporating multiple mixture

environments. This could provide greater stability and less influence by a few outliers, as was the case with the water solubility measurement in hexadecane here. Another possibility would be creating a large interconnected network of pure component and mixture data used to simultaneously fit the parameters of many compounds at once. This could be aided by implementation on a parallel cluster which could quickly perform multiple calculations on several processors. This second approach could also be greatly assisted through the implementation of a global optimization strategy. Many current minimization routines used to do parameter fitting are only capable of finding the closest minimum in the deviation measurement which is highly depended on the initial guess. This is how multiple equally effective parameter sets are found, but a search algorithm specifically designed for global optimization of nonlinear multivariate functions, such as Tabu search,[81,82] could produce the overall best parameter set much more efficiently.

CHAPTER 3 RECENT ADVANCES IN CLASSICAL DENSITY FUNCTIONAL THEORY FOR ASSOCIATING AND POLYATOMIC MOLECULES[14]

3.1 Introduction

Over the past forty years, molecular modeling has largely been focused on understanding and explaining bulk homogeneous fluid behavior. For this reason, a significant increase in the number of approaches and accuracy of such approaches has been seen. The increase in both understanding and approaches came as the model complexity progressed from understanding simple hard spheres to associating hard spheres to non-spherical and polyatomic molecules. Provided these advances, there has been steady progress to further the understanding of inhomogeneous fluids, but this progress understandably lags behind bulk phase modeling as inhomogeneous theories are commonly perturbations to the homogeneous model. However, it is believed that this approach is the reason difficulties in modeling bulk fluid behavior still exist. That is, a complete and accurate picture of complex bulk fluid behavior (e.g., in the critical region or hydrogen bonding networks) is unattainable without a better understanding of the inhomogeneous fluid. In response to these sentiments, a shift in research and development emphasis toward molecular modeling of such inhomogeneous fluids has occurred. Accompanying the beliefs of many in this field is a wide-ranging scientific and industrial interest from technological processes involving interfaces, confined fluids, and self assembly. Thus, it is necessary to develop a theoretical tool capable of handling mixtures (potentially

with trace components) where characteristics such as the size, shape, and hydrogen bonding of species are important.

Density functional (DF) methods serve as a valuable theoretical tool in the study of inhomogeneous fluids. Many of the interesting phenomena observed in biological and soft material systems involve time and length scales that are inaccessible by the more traditional methods such as experimentation and molecular simulation. DF methods have proven to be advantageous in providing information unavailable from these other methods. Experimental methods can often be difficult to apply and interpret on microscopic (or smaller) scales. This, in turn, makes it difficult to separate the effects of individual molecular forces on the system behavior meaning the relevance of competing effects is indiscernible. Molecular simulations are applicable on such scales; however, computational cost limits these approaches to systems of small to medium size molecules without significant coarse-graining for short time periods, while many times neglecting the solvent. Similar to experimental methods, results from molecular simulations typically require additional analytical methods to explain the underlying physics of the problem through indirect calculation from mechanical variables. On the other hand, density functional methods can take advantage of system symmetries to offer a less computationally demanding approach applicable to a wide range of problems where molecular level physics are included explicitly and thermodynamic properties are calculated directly from the free energy functional. Such systems include copolymers of varying lengths with nanoparticles or surfaces subject to a myriad of conditions and easily accounting

for solvents explicitly. This advantage comes about because molecular simulations require detailed information about all of the constituent particles in a system, while density functional methods focus on the direct connection between free energy and the density distributions of components. The theory incorporates enough molecular level detail to quickly and accurately provide physical insight to the system, even in complex situations, by calculating average properties directly without considering the detailed motions of individual particles.

The last two decades have seen the increased usage of density functional methods to predict the microstructure and thermodynamics of both simple atomic and complex polyatomic bulk and inhomogeneous fluids. The phrase density functional theory (DFT) refers to both the quantum approach developed by Hohenberg and Kohn[83] and Kohn and Sham[84] and the classical approach first applied by Ebner, Saam, and Stroud.[85] The work of Kohn and co-workers is based in quantum chemistry, and their DFT was originally developed to explain the electronic structure of an inhomogeneous ground state electronic liquid. The evolution of DFT eventually led to its application to a classical system by Ebner *et al.* to model the interfacial properties of a Lennard-Jones (LJ) fluid. The classical approach forms the basis of the work presented here, as it was a specific theoretical development to model inhomogeneous fluids. For this reason, any further mention of density functional theory refers to the classical version where the functionals apply to spatial distribution of molecules rather than electrons. For a detailed background and complete mathematical development, the reader is referred to the work by Evans.[5]

Density functional theory has a statistical mechanics foundation with a motivation to express the free energy of an inhomogeneous system as a unique functional of the density of its constituent molecules $\rho(\mathbf{r})$ independent of any external potential. With this functional, DFT can be used to calculate the equilibrium structure and thermodynamic functions such as phase behavior, interfacial properties, surface forces, and molecular structure.[86] Developments have also been made to allow for dynamic and non-equilibrium problems to be solved by DFT.[87] Because density functional theory can be used to model a wide variety of physical systems, DFT is more of a framework to work within rather than simply a theory as its name implies. The remainder of this review outlines the basic structure of the theory, addresses approximations for the free energy functional, and discusses relevant recent developments within the theory. In addition, several applications to complex fluid systems are presented and the future direction of the field is discussed.

3.2 General Formalism

The formalism presented here simply demonstrates the structural basics of a density functional theory. For this reason, it is presented for a simple, pure component monatomic fluid. In more complex cases, it is possible to generalize the DFT to accommodate polyatomic chains of like or unlike species; however, the general framework presented here is the same. One must simply make appropriate approximations of all the underlying physics of the problem and validate such approximations with experimental or molecular simulation data.

This development presumes an adequate understanding of basic statistical mechanics (see standard texts by McQuarie[86] and/or Huang[87]).

Consider a monotonic fluid of n molecules, each of mass m at temperature T and volume V. The Hamiltonian of such a system has contributions due to kinetic energy (K), potential energy (U), and the external potential (E). The n molecule Hamiltonian is then defined as

$$\begin{aligned} H_n &= \sum_{\alpha=1}^{n} \frac{|\mathbf{p}_\alpha|^2}{2m} + \sum_{\alpha=1}^{n}\sum_{\beta=1}^{n} u_{\alpha\beta}\left(|\mathbf{r}_\alpha - \mathbf{r}_\beta|\right) + \sum_{\alpha=1}^{n} v_\alpha(\mathbf{r}_\alpha) \\ &= K + U + E \end{aligned} \tag{3.1}$$

where $\mathbf{p}_\alpha$ is the momentum of molecule α, $\mathbf{r}_\alpha$ is the coordinate vector of that molecule, $u_{\alpha\beta}$ is the intermolecular potential between molecules α and β at separation $|\mathbf{r}_\alpha - \mathbf{r}_\beta|$, and v_α is the external potential acting on molecule α. Given the definition of the system, the grand canonical ensemble proves to be the most appropriate, as it has fixed V, T, and chemical potential (μ). The partition function in this ensemble is written in terms of the Hamiltonian as[88]

$$\Xi = \sum_{n=0}^{\infty} \frac{\exp(\beta\mu n)}{n! h^{3n}} \int\!\!\prod_{\alpha=1}^{n} d\mathbf{p}_\alpha d\mathbf{r}_\alpha \exp(-\beta H_n). \tag{3.2}$$

In this definition, $\beta = 1/k_b T$ is known as the Boltzmann factor, while k_b and h are the Boltzmann and Planck constants, respectively. The definition of the grand potential, Ω, then follows as the logarithm of the partition function according to

$$\beta\Omega = -\ln \Xi. \tag{3.3}$$

The necessary conditions for phase coexistence in any ensemble are equivalent pressures (mechanical stability), temperatures (thermal stability), and chemical

potentials (chemical stability) in all phases. Two of these conditions (equal temperature and chemical potential) are implicit by working in the grand canonical ensemble. The equal pressure condition is implied by further requiring a fixed grand potential.

In this development, the Hamiltonian and consequently the grand potential are a functional of $\nu_\alpha(\mathbf{r}_\alpha)$, making them a functional of the combined term

$$\phi(\mathbf{r}) = \beta\left[\mu - \nu(\mathbf{r})\right]. \tag{3.4}$$

Using equation (3.4) in conjunction with the definition of the thermal de Broglie wavelength $\left(\Lambda = \sqrt{h^2/2\pi m k_b T}\right)$, the integration over the momentum coordinates in equation (3.2) can be carried out and simplified to give

$$\Xi = \sum_{n=0}^{\infty} \frac{1}{n!\Lambda^{3n}} \int \exp(-\beta U_n) \prod_{\alpha=1}^{n} d\mathbf{r}_\alpha \exp\left(\beta \sum_{\alpha=1}^{n} \phi(\mathbf{r}_\alpha)\right). \tag{3.5}$$

It is now necessary to define the microscopic density operator

$$\hat{\rho}(\mathbf{r}) = \sum_{\alpha=1}^{n} \delta(\mathbf{r} - \mathbf{r}_\alpha) \tag{3.6}$$

where δ is the multidimensional Dirac delta function. The equilibrium density is then defined by the ensemble average according to

$$\rho(\mathbf{r}) = \left\langle \hat{\rho}(\mathbf{r}) \right\rangle. \tag{3.7}$$

Combining these definitions allows one to redefine the potentials in terms of the density profile $\rho(\mathbf{r})$. Application to equation (3.5) reduces the expression to

$$\Xi = \sum_{n=0}^{\infty} \frac{1}{n!\Lambda^{3n}} \int \exp(-\beta U_n) \prod_{\alpha=1}^{n} \exp\left(\beta \int \phi(\mathbf{r}) \rho(\mathbf{r}) d\mathbf{r}\right) d\mathbf{r}_\alpha. \tag{3.8}$$

Functional differentiation of this expression and application of the definition of the ensemble average leads to the conclusion

$$\rho(\mathbf{r}) = \langle \hat{\rho}(\mathbf{r}) \rangle = \frac{1}{\Xi} \frac{\delta \ln \Xi}{\delta \phi(\mathbf{r})} = -\frac{\delta \ln \Omega}{\delta \phi(\mathbf{r})}. \tag{3.9}$$

Thus, to determine the fluid structure and thermodynamic properties, a functional for the grand potential must be written in terms of the density profile $\rho(\mathbf{r})$. This is done with a Legendre transform of Ω to give[89]

$$A[\rho(\mathbf{r})] = -\ln \Xi + \int d\mathbf{r} \frac{\delta \ln \Xi}{\delta \phi(\mathbf{r})} \phi(\mathbf{r}) = \Omega + \int d\mathbf{r} \rho(\mathbf{r}) \phi(\mathbf{r}) \tag{3.10}$$

where $A[\rho(\mathbf{r})]$ is the intrinsic Helmholtz free energy functional.

In the context of this derivation, this Helmholtz free energy functional is the equilibrium free energy of a system with equilibrium density profile $\rho(\mathbf{r})$ subject to external field $v(\mathbf{r})$. Writing the equivalent expression for an arbitrary non-equilibrium density $\tilde{\rho}(\mathbf{r})$ gives

$$\tilde{\Omega} = A[\tilde{\rho}(\mathbf{r})] - \int d\mathbf{r} \tilde{\rho}(\mathbf{r}) \phi(\mathbf{r}). \tag{3.11}$$

It has been shown that Ω is the minimum value of $\tilde{\Omega}$ for some fixed $\phi(\mathbf{r})$ when $\tilde{\rho}(\mathbf{r})$ is the equilibrium density profile.[5] This produces the mathematical relations

$$\left.\begin{array}{l} \left.\dfrac{\delta \tilde{\Omega}[\tilde{\rho}(\mathbf{r})]}{\delta \tilde{\rho}(\mathbf{r})}\right|_{\tilde{\rho}=\rho} = 0 \\ \tilde{\Omega}[\rho(\mathbf{r})] = \Omega \end{array}\right\}. \tag{3.12}$$

This gives rise to a procedure for approximating the equilibrium density and grand potential by first approximating the intrinsic Helmholtz free energy functional $A[\rho(\mathbf{r})]$ (and implicitly $\tilde{\Omega}$) and then satisfying the relationships in equation (3.12).

The exact functional form of $A[\rho(\mathbf{r})]$ is only known for an ideal fluid in two or three dimensions. Thus, different methods for approximating this free energy functional for more complex systems have been devised out of molecular simulations and/or theoretical developments. These are the basis of different DFTs and some of the more prominent and influential approaches are detailed in the following section.

3.3 Helmholtz Free Energy Functional Approximations

In order to determine the structure and thermodynamic properties of a more realistic physical system, it is necessary to approximate the Helmholtz free energy functional. The methods for making such an approximation can be generally classified into one of three categories – density expansion, integral equation theory, or thermodynamic perturbation. The density expansion method originated with van der Waals theory for capillarity, and its simplicity has continued to make it attractive for many realistic applications. Several theories for interfacial phenomena and phase transitions that are closely related include those of Cahn-Hilliard, Ginzburg-Landau, and Flory-Huggins-de Gennes-Lifshitz.[13] Despite their popularity, the density expansion methods are only accurate for systems with weak inhomogeneity or slowly varying density profiles. Integral equation theories are often considered to be a subclass of the density

expansion methods, as they also involve a truncation of the free energy at the quadratic term. These approaches gained support with the publication of the reference interaction site model (RISM) by Chandler and Andersen[90] and its extension to polyatomic molecules (PRISM) by Schweizer and Curro.[91] A similar approach was introduced by Cummings and Stell[92] in the context of a site-site Ornstein-Zernike equation. Although integral equation theory predictions have also shown good agreement with simulation and generally better performance than the density expansion theories, truncation of the Helmholtz free energy term limits their application to slowly varying density profiles and systems that do not exhibit phase transitions consistent with multiple minima in the free energy such as wetting.[13] The purpose of the remainder of this section is to highlight some of the more important atomic and polyatomic methods that have been employed with special focus on the use of thermodynamic perturbation theory. Thus, the reader is directed to several review papers that discuss the density expansion and integral equation theory methods more extensively.[13,93]

3.3.1 Atomic Fluids

The primary concern of approximating the free energy functional for monatomic fluids comes from the excluded volume effects (excess free energy contribution). This follows logically from the availability of an explicit expression for the ideal free energy functional of monatomic fluids.[93] For this reason, it is common to write $A\left[\rho(\mathbf{r})\right]$ as the sum of ideal and excess contributions according to

$$A\left[\rho(\mathbf{r})\right] = A^{id}\left[\rho(\mathbf{r})\right] + A^{ex}\left[\rho(\mathbf{r})\right]. \tag{3.13}$$

These excess contributions result from intermolecular interactions. The exact form of the ideal functional for a monatomic fluid is given by[93]

$$\beta A^{ideal}\left[\rho(\mathbf{r})\right] = \int d\mathbf{r}\rho(\mathbf{r})\left[\ln\rho(\mathbf{r})-1\right]. \tag{3.14}$$

While it can be common to include the de Broglie wavelength in this equation, it has been omitted here due to its lack of influence on fluid structure and residual thermodynamic properties (i.e., it does not change equilibrium density profiles or phase behavior).

Evans[5] discusses many of the approaches for approximating the excess contribution to the free energy functional. One of the more popular techniques is the weighted density approximation (WDA). Its popularity stems from both its high accuracy and adaptability to most systems.[5] WDA is capable of handling systems with highly oscillatory density profiles much better than other techniques based on Taylor series expansions because it does not correspond to any finite order expansion in density of the excess free energy functional.

The weighted density approximation is actually a modification of the local density approximation (LDA) approach. In LDA, one approximates the free energy functional per molecule in the inhomogeneous system, $a^{inhom}\left[\rho(\mathbf{r})\right]$, at position $\mathbf{r}$ with density $\rho(\mathbf{r})$ by the free energy per molecule in the homogeneous bulk system, $a^{bulk}\left[\rho(\mathbf{r})\right]$, with the same density $\rho(\mathbf{r})$. Thus, the excess free energy functional is written as

$$\begin{aligned} A^{excess}\left[\rho(\mathbf{r})\right] &= \int d\mathbf{r}\rho(\mathbf{r})a^{inhom}\left[\rho(\mathbf{r})\right] \\ &= \int d\mathbf{r}\rho(\mathbf{r})a^{bulk}\left(\rho(\mathbf{r})\right) \end{aligned}. \tag{3.15}$$

The disadvantage to this approximation comes with largely oscillating density profiles in the inhomogeneous system. Realistic cases exist where the peaks in the density profile exceed the close-packed limits of the bulk fluid causing the bulk free energy functional to yield unphysical results since the direct correlation function is a delta function applicable only to a weak inhomogeneity.

WDA constructs a weighted (also known as smooth or coarse-grained) density $\bar{\rho}(\mathbf{r})$ that prevents such unphysical values for the free energy. The smooth density is a weighted average of the density $\rho(\mathbf{r})$ over a local volume. The size of this local volume is governed by the range of intermolecular forces. This produces the same form for the excess free energy functional given in equation (3.15) for the LDA, except now the bulk free energy per molecule is evaluated at the weighted density according to

$$A^{excess}\left[\rho(\mathbf{r})\right] = \int d\mathbf{r}\rho(\mathbf{r})a^{bulk}\left[\bar{\rho}(\mathbf{r})\right], \tag{3.16}$$

where the weighted density is given by

$$\bar{\rho}(\mathbf{r}) = \int d\mathbf{r}'\rho(\mathbf{r}')\omega\left(|\mathbf{r}-\mathbf{r}'|;\bar{\rho}(\mathbf{r})\right). \tag{3.17}$$

Different WDA versions come from different choices for the weighting function ω. The majority of forms for the weighting function are chosen to obtain correct fluid structure in the bulk limit. Evans[5] gives further details on several specific approximations for hard sphere systems including work by Tarazona,[94,95] Curtin-Ashcroft,[96] Rosenfeld,[97] and Meister-Kroll.[98]

3.3.2 Polyatomic Fluids

In polyatomic fluids, the system behavior is governed by intermolecular interactions even in the ideal chain. Therefore, making the appropriate choice of the ideal system that includes and/or excludes these interactions must be made. Differences in modern DFTs for polyatomic fluids arise in whether these intermolecular interactions are dealt with in the ideal functional, excess functional, or a combination of both. This differs from the atomic fluid where all the intermolecular interactions are dealt with in the excess contribution since the ideal contribution is known exactly. With these differences in dealing with intermolecular interactions come differences in modeling accuracy and computational difficulty.

Application of DFT to a polyatomic system was introduced in 1986 by Chandler, McCoy, and Singer (CMS-DFT)[99-101] and later by McMullen and Freed[89] in 1990. Both of these approaches use a segment density basis, but they differ in how they deal with intramolecular interactions. The CMS-DFT separates all of the intramolecular interactions into the ideal functional and the intermolecular interactions into the excess functional. This produces accurate results for an ideal system. In fact, it reproduces the exact ideal chain free energy contribution. With accuracy comes the drawback of computational cost, as the intramolecular correlation functions are obtained from a single chain Monte Carlo simulation. There are also inconsistencies between the interface and the bulk due to approximations introduced by PRISM[91] used to describe the bulk fluid structure, which is needed in computing the excess free energy

functional. The McMullen and Freed approach is to deal with the intramolecular interactions in the excess free energy functional. This produces erroneous results when modeling strongly inhomogeneous systems with a rapidly varying external field.[102]

Another common approach is to write the free energy functionals in terms of a molecular density, $\rho(\mathbf{R})$, rather than individual segment densities. In this case, $\mathbf{R}=\{\mathbf{r}_1,\mathbf{r}_2,\ldots,\mathbf{r}_N\}$ is a multidimensional vector containing the positions of all N monomers of a polyatomic molecule. In such approaches, it is only the ideal functional that is written in terms of this molecular density. The excess functional is still approximated in several different ways in terms of segment densities, as it is unknown in terms of molecular density. Thus, the intrachain correlations introduced in the ideal functional are not maintained in the overall functional. The appeal of such an approach is the ability to write the exact ideal contribution from statistical mechanics. As with the CMS-DFT, exactness comes with increased computational cost, as the many-bodied nature and bonding constraints of a polyatomic molecule produces N^{th} order implicit equations for the density profile. Yethiraj and Woodward[103] used such a technique by combining DFT with Monte Carlo molecular simulations. Again, similar to the CMS-DFT, they solve for the exact ideal chain functional using a single-chain simulation. Rather than performing expensive simulations, others, such as Kierlik and Rosinberg,[104-106] implemented numerical techniques to solve the implicit integral equations. However, such an approach has proven to be even more expensive than the simulations.[103]

Weighted density approximations are also quite common for estimating free energy functionals in polyatomic DFT approaches as presented in the previous section for atomic fluids. The procedure for implementation is much the same as described for atomic fluids.

3.3.3 Developments Using Wertheim's TPT1

Most DFTs employ a segment based density for the overall functionals. In recent years, there are two prominent frameworks for such a DFT. The first is that of Chandler, McCoy, and Singer[99-101] as described briefly in the previous section. The other approach is based on Wertheim's first-order thermodynamic perturbation theory (TPT1).[15-18] Wertheim's TPT1 has been implemented in modeling a wide range of systems with many specific and general applications. Most prominent of these is the development of the statistical associating fluid theory (SAFT) equation of state by Chapman *et al.*[19,46,53] in 1988. The SAFT model has seen popular application in research and industry for modeling bulk complex fluid properties. Chapman[46] also outlined how Wertheim's theory, in the form of a free energy functional, could be applied to inhomogeneous fluids. While Chapman's group developed a density functional theory for associating atomic molecules and later polymers,[20,21,24-26] Kierlik and Rosinberg[104-106] were the first to apply Wertheim's theory to produce a DFT for polyatomic molecules. Some of the many groups that have used Wertheim's TPT1 for association in a DFT formalism include Kierlik and Rosinberg,[104-106] Chapman *et al.*,[20-26,102,107-117] Wu *et al.*,[118-123] Sokolowski *et al.*,[124-134] Jackson *et al.*,[135-139] Telo da Gama *et al.*,[140-143] and Vega *et al.*[144,145]

3.3.3.1 Atomic Associating Fluids

Segura, Chapman, and Shukla[20,21] introduced a DFT for atomic associating fluids based on Wertheim's thermodynamic perturbation theory in a series of papers. These early developments have served as the basis of later approaches to polyatomic DFTs by Wu *et al.*,[118-123] and Tripathi and Chapman.[25,26]

Segura *et al.* successfully used the Tarazona[94,95] method for hard spheres and two different perturbative approaches to account for association. Due to their relevance in later theoretical developments, these approaches are detailed here. The two approaches are: (1) application of Wertheim's associating fluid functional as a perturbation to a reference fluid functional (the Tarazona hard sphere fluid in Segura's case) and (2) application of a weighted density functional theory to the bulk equation of state for associating fluids.

In the first technique, the excess free energy functional is written as[46]

$$A^{ex}\left[\rho(\mathbf{r})\right] = A^{ex,hs}\left[\rho(\mathbf{r})\right] + A^{ex,assoc}\left[\rho(\mathbf{r})\right], \tag{3.18}$$

where the superscripts hs and $assoc$ denote the hard sphere and association contributions to the excess free energy functional, respectively. The hard sphere contribution is similar to equations (3.16) and (3.17) with

$$A^{ex,hs}\left[\rho(\mathbf{r})\right] = \int d\mathbf{r}\rho(\mathbf{r})\, a^{hs}\left[\bar{\rho}(\mathbf{r})\right] \tag{3.19}$$

and the ω that were used were the Tarazona weighting functions.[94,95] Then, the association term for simple spherical molecules with M association sites is given by[19-21]

$$A^{ex,assoc}\left[\rho(\mathbf{r})\right] = Mk_bT\int d\mathbf{r}\rho(\mathbf{r})\left(\ln\chi_A(\mathbf{r}) - \frac{\chi_A(\mathbf{r})}{2} + \frac{1}{2}\right), \tag{3.20}$$

where $\chi_A(\mathbf{r})$ is the fraction of molecules at $\mathbf{r}$ not bonded at site A defined as

$$\chi_A(\mathbf{r}) = \frac{1}{1+\int d\mathbf{r}'\Delta\chi_A(\mathbf{r}')\rho(\mathbf{r}')}, \tag{3.21}$$

where the spatial dependence of Δ is given by

$$\Delta = 4\pi\kappa g\left(\mathbf{r},\mathbf{r}',\rho(\mathbf{r}')\right)f \tag{3.22}$$

and whose derivation from Wertheim's theory[15-18] can be found in the original work by Segura *et al.*[20,21] They assumed further that the pair correlation function for the inhomogeneous fluid could be approximated by the hard sphere pair correlation function at contact in the bulk, such that

$$\Delta \approx 4\pi\kappa g_{hs}\left(\sigma,\rho_{bulk}\right)f \tag{3.23}$$

where f is the Mayer-f function defined in terms of the association bonding energy $\left(\varepsilon^{assoc}\right)$ by

$$f = \exp\left(\beta\varepsilon^{assoc}\right) - 1 \tag{3.24}$$

and κ is a constant geometric factor[21] that accounts for the available bonding volume between two molecules. Alternatively, the hard sphere pair correlation function can be estimated using a weighted density approach where the weights are chosen such that they reduce to the bulk value in the homogeneous limit.

By minimizing the grand potential function given in equation (3.11) the following set of equations[21] analogous to the Tarazona Mark II DFT for hard spheres[5] were obtained:

$$\ln \rho(\mathbf{r}) = \beta\left(\mu - v(\mathbf{r}) - \lambda(\mathbf{r})\right) \tag{3.25}$$

where the chemical potential of the bulk fluid is given by

$$\beta\mu = \ln \rho_{bulk} + \beta\mu^{ex,hs} + \beta\mu^{ex,assoc} \tag{3.26}$$

and

$$\lambda(\mathbf{r}) = a^{hs}\left[\rho(\mathbf{r})\right] + \frac{\delta A^{ex,assoc}\left[\rho(\mathbf{r}')\right]}{\delta\rho(\mathbf{r})} + \int d\mathbf{r}' \frac{\partial\bar{\rho}(\mathbf{r}')}{\partial\rho(\mathbf{r})}\bar{\rho}(\mathbf{r}')a^{hs}\left[\bar{\rho}(\mathbf{r}')\right]. \tag{3.27}$$

The well-recognized Carnahan and Starling equation of state[64] is used for the hard sphere contribution, and the bulk fluid excess chemical potential due to association is fixed by the bulk density and the association bonding site energy.

The second method by Segura *et al.* assumes that the hard sphere and association interactions are of similar range, giving credence to the application of a weighted DFT to the bulk equation of state. Thus, a weighted density can be applied to both excess free energy functionals. The Carnahan and Starling equation of state[64] is still used for the hard sphere term, but the bulk relations are used for the association free energy functional according to[21]

$$a^{ex,assoc}\left[\bar{\rho}(\mathbf{r})\right] = Mk_bT\left(\ln \bar{\chi}_A(\mathbf{r}) - \frac{\bar{\chi}_A(\mathbf{r})}{2} + \frac{1}{2}\right). \tag{3.28}$$

The weighted density and weighted fraction of molecules not bonded at site *A* are then replaced by the homogeneous terms from Wertheim's theory.[15-18,46] Using these approximations with the bulk fluid values, as opposed to the full inhomogeneous form of Wertheim's theory, can greatly reduce the computation time.

Both of these approaches have proven to be successful DFT applications for atomic associating fluids. Although the second method is much simpler, the first method shows how Wertheim's association functional can be used as a perturbation to a reference fluid functional which forms the basis of a polyatomic DFT introduced by Tripathi and Chapman.[25,26,102] The second method has been applied with many different types of weighting functions, but the concept of applying a weighting function to a bulk equation of state is the same in all these approaches. This includes investigating the effects of confinement on the interfacial and phase behavior of associating fluids by Segura and Chapman,[20-23] Sokolowski *et al.*[130,132] who used modified Meister-Kroll[98] weighting, Wu *et al.*[121,123] who used Rosenfeld[97,146] weighting, and Tripathi and Chapman[115,116] who also used Tarazona[94,95] weighting. This second approach is also used as the basis of a polyatomic DFT introduced by Yu and Wu.[122,123] Comparisons of both techniques against Monte Carlo molecular simulations have shown good agreement.

In addition to the two approaches presented by Segura and Chapman, there have also been atomic DFT schemes based on Wertheim's theory using the local density approximation discussed previously (instead of the weighted density approximation) or using a density gradient approach. As mentioned above, the LDA approach approximates the free energy functional at the local density. The LDA suppresses large oscillations in the density profile that should be present in cases of strong inhomogeneity. This fundamental issue with the LDA approach is explained by the neglecting of short-range correlations in the

fluid[135] which reduces the LDA to a van der Waals treatment for non-uniform fluids.[147] Despite this problem, an LDA approach can be used successfully in determining the interfacial properties of a smoothly varying system such as a vapor-liquid interface, where the van der Waals treatment is sufficient. Jackson *et al.*[45,136-139] have shown the successful application of the LDA approach in the context of a DFT based on Wertheim's theory to describe the vapor-liquid interfacial properties of inhomogeneous associating fluids.

3.3.3.2 Polyatomic Fluids

As mentioned above, Kierlik and Rosinberg[104-106] were the first to introduce a polyatomic DFT based on Wertheim's TPT1. Their approach was developed on the basis of a molecular density distribution. Since this approach retains information about segment connectivity when taken in the limit of complete association, it is exact for ideal chains. Using this exact expression for the ideal free energy functional, the excess free energy functional contains all non-bonding intramolecular and intermolecular interactions. In doing so, they express chain connectivity in terms of a first-order perturbation theory and short-ranged correlations in terms of density-independent weighted functions of their own.[101,148] A positive feature of their theory is the consistency of intramolecular correlations between the inhomogeneous and bulk fluid regions leading to consistency in the density profiles across this transition. While naturally desired, this is not the case with all approaches, as was indicated with the CMS-DFT where approximations from PRISM produced inconsistencies.

This DFT has been applied to rigid molecules,[104] flexible molecules,[105] and freely-jointed chains in slit-like pores.[106] Their DFT is relatively accurate when compared with molecular simulation;[149] however, it overestimates chain enhancement near a wall at high density and underestimates chain depletion near a wall at low density. The theory shows greater accuracy at describing terminal segment density distributions than those of middle segments.[106] Kierlik and Rosinberg explain this by the relative hard-sphere-like structure of the end segments (compared to the middle segments) induced by forced chain connectivity. Thus, the wall preferentially attracts terminal segments to reduce the energetic penalties of configurational changes in the chain by adsorbing middle segments. Another advantage of the Kierlik and Rosinberg approach is it required no additional parameters for implementation.

Despite the improved modeling capabilities (density profiles and thermodynamics) of this approach over others, such as integral equation theory and polymer self-consistent field theory (SCFT), there are significant drawbacks. As mentioned, there are significant increases in computational costs associated with the numerical methods required in the application of the theory. Additionally, Kierlik and Rosinberg are unable to introduce more realistic intermolecular interactions such as hydrogen bonding.

Yu and Wu[122,123] have also developed a polyatomic DFT using a molecular density basis. As mentioned in section 3.3.3.1, the second approach for atomic associating fluids introduced by Segura *et al.*[21] and modified by Yu and Wu[122,123] serves as the theoretical basis for this polyatomic DFT. Their approach uses a

combination of Wertheim's perturbation theory with the weighted densities of the fundamental measure theory (FMT) from Rosenfeld.[97,146,150] Similar to the DFT of Kierlik and Rosinberg, the molecular density basis for the ideal chain free energy functional requires the implementation of expensive numerical techniques to solve for the structural and thermodynamic properties.

The DFT of Yu and Wu has also been compared with the same molecular simulation data[149] as the Kierlik and Rosinberg DFT was. Yu and Wu still showed underestimation of chain depletion near a wall at low density, but their approach improves the predictions. This improvement comes at a cost of reduced accuracy in the end and middle segment densities of the longer chain. They assert that this apparent deficiency is a byproduct of the respective cavity correlation functions being used for chain connectivity. The Kierlik and Rosinberg approach uses the inhomogeneous cavity correlation function, while Yu and Wu use Wertheim's TPT1 for a bulk fluid.

In addition to these initial validating results for the Yu and Wu DFT, their theory has seen application in many other complex systems. Within their own research group, Wu *et al.* have published applications to polymer mixtures,[123] block copolymers near selective surfaces,[119] and semiflexible polymers.[118] Others have shown the versatility of this approach such as Bryk, Sokolowski, and coworkers who have studied polymer adsorption,[124] polymer surface induced phase transitions,[125] capillary condensation of polymers,[126] and star polymer fluids.[129] Despite this diverse set of applications, it proves difficult to continue to extend this approach to more complex systems such as branched polymers,

since the theory does not allow for assigning functionality to specific segments along a chain backbone. Additionally, an inherent assumption in their theory is a homonuclear chain. Again, this restricts their ability to handle more complex fluids such as block copolymers or surfactants with significantly different sized segments or locating association sites on specific segments.

In 2005, Tripathi and Chapman[25,26] developed a DFT for inhomogeneous polyatomic fluids using the first approach of Segura *et al.*[21] discussed in the previous section with free energy functionals derived from TPT1. Their theory, called interfacial statistical associating fluid theory (*i*SAFT) , is also self-consistent in its transition from homogeneous to inhomogeneous regions with the attractive characteristic that the bulk limit is the SAFT equation of state.[19,46,53] Thus, this approach provides a single framework for taking advantage of the bulk modeling characteristics of SAFT while also predicting the inhomogeneous fluid microstructure. Their conceptual mechanism is to model a polyatomic fluid as a mixture of associating atomic spheres in the limit of complete association. Through this assumption, Tripathi and Chapman achieve a much more tractable (computationally simpler) polyatomic DFT, as it retains the form of the atomic DFT. Along with the improved computational efficiency of the theory, they also produce comparable, if not improved, accuracy over the molecular density and simulation based approaches detailed above. The basics of this segment density based approach start with an expression for the total Helmholtz free energy functional given by

$$A^{total}\left[\rho_\alpha(\mathbf{r})\right] = A^{id}\left[\rho_\alpha(\mathbf{r})\right] + \Delta A^{ex,hs}\left[\rho_\alpha(\mathbf{r})\right] + \Delta A^{ex,assoc}\left[\rho_\alpha(\mathbf{r})\right] + \Delta A^{att}\left[\rho_\alpha(\mathbf{r})\right] \quad (3.29)$$

where the subscripts indicate the α^{th} segment on the chain and the superscripts, from left to right, denote the contributions due to an ideal gas atomic mixture, excluded volume of the monomer segments, association between segments for chain formation, and other long-range attractions. The ideal contribution is similar to that of equation (3.14) while the excess free energy due to segment association can be dealt with using any of the previously mentioned weighted density approximations. Tripathi and Chapman utilized the Rosenfeld formalism,[97,146] which has already been derived for asymmetric mixtures. This term, as derived from Wertheim's theory, is given by Segura *et al.* as[19,21,47]

$$\beta\Delta A^{ex,assoc} = \int d\mathbf{r} \sum_{\alpha=1}^{m} \rho_{\alpha}^{seg}(\mathbf{r}) \sum_{A\in\Gamma^{\alpha}} \left(\ln \chi_A^{\alpha}(\mathbf{r}) + \frac{\chi_A^{\alpha}(\mathbf{r})}{2} - \frac{1}{2} \right), \tag{3.30}$$

where the summations are over all m segments in the chain and the set of all association sites on the current segment, Γ^{α}. The fraction of α segments not bonded at site A, $\chi_A^{\alpha}(\mathbf{r})$, is defined as

$$\chi_A^{\alpha}(\mathbf{r}) = \frac{1}{1 + \int d\mathbf{r}' \chi_B^{\alpha'}(\mathbf{r}') \Delta^{\alpha\alpha'}(\mathbf{r},\mathbf{r}') \rho_{seg}^{\alpha}(\mathbf{r}')}. \tag{3.31}$$

In the limit of complete association, all the segments form chains such that $\chi_A^{\alpha}(\mathbf{r}) \to 0$. Tripathi and Chapman assumed that all association sites on a given chain approach this complete bonding limit at the same rate (i.e., $\chi_A^{\alpha}(\mathbf{r}) \approx \chi_B^{\alpha'}(\mathbf{r}')$) which simplifies equation (3.31) to

$$\chi_A^{\alpha}(\mathbf{r})^2 = \frac{1 - \chi_A^{\alpha}(\mathbf{r})}{\int d\mathbf{r}' \Delta^{\alpha\alpha'}(\mathbf{r},\mathbf{r}') \rho_{seg}^{\alpha}(\mathbf{r}')}. \tag{3.32}$$

In these expressions,

$$\Delta^{\alpha\alpha'}(\mathbf{r},\mathbf{r}') = y^{\alpha\alpha'}(\mathbf{r},\mathbf{r}')F^{\alpha\alpha'}(\mathbf{r},\mathbf{r}')\mathrm{K} \tag{3.33}$$

where $y^{\alpha\alpha'}(\mathbf{r},\mathbf{r}')$ is the cavity correlation function between segment α and its neighbor α', and K is a constant geometric factor[21] that accounts for the volume available for bonding between two segments. The Mayer-F function is

$$F^{\alpha\alpha'}(\mathbf{r},\mathbf{r}') = \exp\left[\beta\left(\varepsilon_0 - v^{\alpha\alpha'}(\mathbf{r},\mathbf{r}')\right)\right] - 1, \tag{3.34}$$

where ε_0 represents the association energy of interaction between segments and $v^{\alpha\alpha'}(\mathbf{r},\mathbf{r}')$ is the energy of the bond (e.g., harmonic bonding potential for bond vibration). By taking the limit of complete association ($\chi_A^{\alpha}(\mathbf{r}) \to 0$ as $\varepsilon_0 \to \infty$) the chain functional is obtained. For the same reason the thermal de Broglie wavelength was dropped from the ideal free energy functional in section 3.3.1, the density-independent constants $\beta\varepsilon_0$ and $\ln \mathrm{K}$ can be eliminated here, leaving

$$\beta\Delta A^{chain} = \int d\mathbf{r} \sum_{\alpha=1}^{m} \rho_{\alpha}^{seg}(\mathbf{r}) \sum_{\alpha}^{\{\alpha'\}} \left[-\frac{1}{2} \ln \int d\mathbf{r}' y^{\alpha\alpha'}(\mathbf{r},\mathbf{r}') \rho_{\alpha'}^{seg}(\mathbf{r}') \exp\left(-\beta v^{\alpha\alpha'}(\mathbf{r},\mathbf{r}')\right) + \frac{1}{2} \right]. \tag{3.35}$$

Since the cavity correlation function of an inhomogeneous fluid is unknown, the assumption is made that it can be approximated using the bulk hard sphere pair correlation function evaluated at contact using a weighted density.

Tripathi and Chapman[25,26] were able to show the *i*SAFT DFT performs very well in comparison with those of Kierlik and Rosinberg[106] and Yu and Wu[123] for the same systems. They were able to show accurate density profile predictions for entire chains as well as end and middle segments despite the other theories having exact expressions for the ideal free energy functional. They determined this was because *i*SAFT has better approximations for the

excluded volume effects. It is also worth noting that *i*SAFT only requires solving a set of first-order integral equations that are independent of chain length. With that, it is possible to perform these calculations using simpler numerical methods similar to those used in atomic DFTs,[21,23,25,26,115-117] which gives it another distinct advantage over other polyatomic DFTs.

The *i*SAFT DFT has also been applied in several different complex polyatomic systems. Tripathi and Chapman[26] applied it to inhomogeneous solutions and blends of linear and branched chains. Application to branched chains is another advantage for this approach, as they are implemented by simply designating additional bonding sites on desired branching segments in the chain backbone. The theory has also been applied to lipids in solution, lipid bilayers, surface tension of polymer melts,[151] and surfactant adsorption in copolymer thin films. Dominik *et al.*[151] also demonstrated the capability of modeling both the bulk phase and interfacial properties using the same set of parameters. This makes *i*SAFT a fully functional single framework for computing both bulk and interfacial properties with the single set of already well documented SAFT parameters.

Despite these successes, instances of inaccuracy led to a modification of the theory by Jain *et al.* in 2007.[24] They discovered that the approximations in *i*SAFT make it most accurate for the average segment density of homonuclear chains. The theory becomes less accurate when the segments of the chain become too dissimilar. In addition, even in the case of homonuclear chains, the theory does not constrain the segments to satisfy stoichiometry. This arises from

the assumption that the rate of complete association is the same for all sites on all segments, so each segment only has information about its immediate neighbors. Thus, Jain *et al.*[24] proposed modified *i*SAFT, which altered the approach to calculating the association term. This contribution to the excess free energy functional was improved by systematically calculating the fraction of segments not bonded at a particular site. This effectively allows for information to be transferred from one segment to the next along the entire length of the chain. With each segment in the chain now having information about all the other segments in the chain, this results in a self-consistent DFT that now constrains the segments for stoichiometry.

This modified *i*SAFT DFT (hereafter referred to simply as *i*SAFT) has produced excellent results in its comparison with both simulation and the other polyatomic DFTs discussed in this section. Jain *et al.*[24] showed excellent agreement with simulation for end, middle, and average segment density profiles of ideal chains. In fact, the minor deviations were attributed to numerical truncation errors and it was concluded that *i*SAFT gives the exact ideal chain functional. They also showed excellent agreement with molecular simulation of an equimolar mixture of a hard chain and solvent confined in a pore. Further work has led to applications in more complex systems such as lamellar structures of confined diblock copolymers,[113] tethered polymers,[112,114] the effect of solute and temperature on structural and interfacial properties of water,[107] polymer depletion/colloid aggregation forces in a polymer-colloid system,[108] temperature induced phase transitions in associating polyatomic fluids,[109,110] and

effects of surfactant structure and concentration on a planar oil-water-surfactant interface.[111]

3.3.4 Extensions of the Theory

The outline and review of classical DFT approaches discussed above for both atomic and polyatomic molecules handles many of the molecular level physics required in predicting the equilibrium microstructure and thermodynamic properties of relatively simple substances. However, given the validation of both the methodology and the accuracy of the basic perturbation terms, the range of applicability is only limited by further development of additional approximations to the increasingly complex physics. This has led to implementing different strategies for handling hydrogen bonding, chain stiffness, polyelectrolytes, critical scaling, non-mean-field long-range attraction models, and off-equilibrium or dynamic systems.

As mentioned in section 3.3.3.2, an attractive characteristic of polyatomic DFTs based on Wertheim's TPT1 is that they reduce to the popular SAFT equation of state in the homogeneous limit. The formulation of the theory presented here does not address the additional perturbation term used for long-range segment-segment attraction. However, this bulk SAFT limit is only reached when the approximation is made that any correlations are negligible leading to a mean-field Van der Waals type fluid. While this is capable of producing accurate qualitative results, an adequate treatment of correlations in the attractive term is crucial for a quantitatively accurate description of both the fluid phase equilibria and interfacial properties of real systems. There have been

several subsequent versions of the bulk SAFT equation of state that have improved the accuracy by implementing different methods for handling these correlations. Some of these include CK-SAFT,[152,153] LJ-SAFT,[47,154] SAFT-VR,[155,156] and PC-SAFT.[42,43] On the other hand, there has been little emphasis put on adapting polyatomic DFTs to incorporate these correlations since the early work of Toxvaerd.[157-159] Several other averaging approaches have been used to approximate the inhomogeneous pair correlation function, but it is not always clear how to approximate this function such that it reduces to the bulk equivalent in the homogeneous limit for these SAFT-based schemes within a polyatomic DFT. Gloor and Jackson[137,138] have implemented the SAFT-VR approach to model a vapor-liquid interface. Given the fairly smooth density profiles in such a system, they were able to apply the LDA to give very good quantitative agreement with the experimental interfacial tension. Similar studies of the structure and properties of liquid-vapor interfaces using the LDA have been done by Winkelmann and coworkers[160-162] for LJ-SAFT and Tang and Gross[163,164] for PC-SAFT. In fact, Gross further extended the theory to include a model for the capillary wave number contribution to the surface tension based on a first-order extension of universal critical scaling, a WDA approach to a second-order thermodynamic perturbation term, and an LDA approach to polar interactions. These developments were introduced assuming a pure component heteronuclear chain. Implementing more accurate approximations for the pair correlation function than the simple mean-field approximation, whether in the spirit of SAFT-VR, LJ-SAFT, or PC-SAFT, show similar significant improvement to the property

predictions, but the use of the second-order perturbation term had negligible effect. The critical scaling/renormalization group theory resulted in excellent results for non-polar to moderately polar substances, and polar PC-SAFT showed consistent improvement over using just PC-SAFT when considering prototypically strongly polar substances. However, while the results are excellent for the quadrupolar fluid carbon dioxide, there is a molecular orientation for strongly dipolar fluids such as acetone that has yet to be taken into account, which limits the improvement in the model.

The developments in polyatomic DFTs discussed in sections 3.3.2 and 3.3.3.2 were largely simplified by neglecting the angular dependence of chain-forming covalent bonds. This produces the fully-flexible chain or pearl necklace model. In nature, though, more interesting phases and system behavior result from chain stiffness and bond flexibility such as in liquid crystals. The general approach to account for semiflexible and stiff chains is to introduce an additional pseudo-bond between the terminal segments of the chain where the strength and/or distance of this additional bond determines the bond angle. This was originally suggested by Kierlik and Rosinberg[104,105] and later adapted by groups such as Woodward, Forsman, and Yethiraj[165-167] and Cao and Wu.[118,120] While these groups are able to show excellent agreement with molecular simulation data, the pressure in the homogeneous limit does not retain the orientation dependence introduced in the density functional theory as the conformation is that of an isolated molecule. This means the framework is no longer self-consistent across the transition from the interface to the bulk. Suggestions of

ways to correct these deficiencies are to go to higher order in perturbation theory, introducing the need for the appropriate triplet correlation functions or implementing a mechanism for adjusting the chain stiffness to fit some known bulk property like the end-to-end distance.

Another interesting common physical attribute that has recently been introduced into the theory is adding functionalized associating (hydrogen bonding) segments in specific locations on the molecule. The addition of these temperature dependent sites can allow for reversible non-covalent bonds which may affect self-assembly, phase behavior, physical properties, etc. The ability to control the functionality and behavior of a system from the molecular level has many potential applications such as biosensors, separation devices, drug delivery, and novel "smart materials", where chemical, electrical, mechanical, or optical properties can all be controlled. The ability to study these features of an atomic molecule within a TPT1 DFT have already been outlined in section 3.3.3.1, where the association free energy functional is either used directly as a perturbation functional to a reference fluid functional or it is approximated by evaluating the bulk association free energy at an effective density. These two strategies were also used in the limit of complete association as a basis for the polyatomic DFTs, and they can be reapplied with finite association energy to give approaches for studying inhomogeneous polyatomic associating fluids. Using the bulk association free energy evaluated at an effective density has recently been applied to study the structure of associating molecules at vapor-liquid interfaces,[121,128,137,138] in slit-like pores,[128] and at solid surfaces.[168] These studies

used simple association schemes with a single association site on each polymer segment. Such approaches are dependent on the accuracy of the weighting functions and can give the wrong free energy in the limit of strong association under certain conditions. Even more recently, the association free energy functional was applied to the *i*SAFT DFT, where its versatile application to any association scheme was demonstrated through observations of how reversible bonding can affect the microstructure of an associating chain near a surface, the formation of supramolecules and complex architectures, and the phase behavior of the system, which included reentrant order-disorder phase transitions.[109,110]

In perturbation DFTs, free energy changes due to electrostatic interactions are written down as an independent contribution to the intrinsic free energy functional. There are two major approaches to describe the electrostatic interactions. The most popular is a second-order Taylor expansion of the electrostatic functional about its bulk limit.[150,169,170] This method requires the pair direct correlation functions (DCFs) for charged hard spheres as input. These DCFs are typically derived from exact solutions[171-175] of the mean spherical approximation (MSA) within the integral equation theory framework for charged hard sphere systems. Depending on the assumptions made in the derivations, the resulting DFT[150,169,170,176-178] represents the restricted primitive model (all solutes are the same size with a continuum solvent), primitive model (continuum solvent), or civilized model (molecular solvent). The second approach for the electrostatic functional follows the idea of Segura and Chapman[21] by applying a bulk charged fluid free energy term evaluated at a local weighted density.

Example DFTs using this approach include the works of Bryk,[127] Pizio,[133,134] and Smagala.[179]

Thus far, the discussion and developments have been under the guise of determining the equilibrium microstructure and thermodynamic properties. There are also invertible mappings among the time-dependent density profiles, momentum distributions, and external field for use in calculating dynamic properties.[180,181] Even so, a microscopically based dynamic theory has yet to be developed for general practical application. The current state-of-the-art for dynamic properties of complex fluids is to acquire the Helmholtz free energy from an equilibrium DFT calculation and use it in a pseudo-equilibrium approximation of a phenomenological equation. A detailed review of these types of approaches were presented by Wu and Li. [13]

3.4 Examples of Applications

Previous reviews of DFT by Wu[12] and Wu and Li[13] detail applications to a wide variety of inhomogeneous systems. This section aims to expand this diverse list by focusing on emerging novel applications from more recent work using polyatomic DFTs derived from Wertheim's TPT1. The applications presented here can be separated into 4 general categories — polymer nanocomposites, associating polymers, self-assembly of heteronuclear molecules, and tethered polymers.

3.4.1 Polymer Nanocomposites

Mixtures of polymers and nanoparticles are important in both theoretical studies of self assemblies and practical applications. On one hand, nanoparticle

(colloid) additives in a polymer matrix could efficiently enhance the mechanical, chemical, electrical, magnetic, or optical properties of already broadly applied polymeric materials. Such composite materials have a promising future to be the next generation of catalysts, semiconductors, batteries, microelectronics, and self-healing materials.[182-184] On the other hand, the mixture of non-adsorbing polymers with sterically stabilized colloidal suspensions has been an important field in fundamental physics study for several decades. Pusey and coworkers[185] have shown that certain colloidal suspensions behave almost perfectly as hard spheres. The addition of non-adsorbing polymers could establish an athermal system and induce an entropic depletion, which leads to tunable physical and thermodynamic behavior in both homogeneous and confined environments. These systems provide an excellent tool to study equilibrium phase behavior, phase transition kinetics, interfacial fluctuations, and wetting and layering transitions. [186-189]

The challenges of theoretically describing these mixtures originate from the distinctive nature of the two components and their multiple interacting length scales. With addition of particle-polymer and polymer-polymer interactions, the properties of these mixtures are affected by even more complex parameters. Early theories such as the Asakura-Oosawa (AO) theory[7] and its derivatives (see review of Poon[190]) treat the nanoparticles as hard spheres and polymers as non-interacting points that are restricted from coming within a certain distance of the hard spheres. These theories could reasonably predict the bimodal of the (polymer rich) gas–(nanoparticle rich) liquid separation and the depletion force

when compared to simulation, but they clearly neglect the internal structure of the polymers, polymer-polymer interactions and correlations. More sophisticated theories, such as SCFT[9] and IET[91,191,192] also suffer from limitations. SCFT is known to be capable of capturing the physics of polymers, but it does not retain segmental information and local density fluctuations. Thus, it is not suitable to describe the free energies of individual spheres. To remedy this disadvantage, combinations of polymer free energy description by SCFT and particle description by DFT[193,194] or simulation[195] have been proposed. They have found successful applications in modeling block copolymer-nanoparticle composites. PRISM[196,197] can provide accurate descriptions of polymeric fluids at the microscopic level; however, it is considered to be sensitive to the particular closure employed and unreliable at high polymer densities.[198-200]

Classical DFTs derived from Wertheim's TPT1 have demonstrated the ability to accurately handle both the nanoparticle and polymer species more efficiently than molecular simulations. DFTs have the advantage of accounting for multiple length scales and competitive interactions within a consistent framework as well as the applicability to various concentration regions. Depletion force calculations have been discussed in the review of Wu,[12] while the focus here is on several new applications displaying interesting physical behavior.

3.4.1.1 Polymer Nanocomposite Film on a Hard Substrate

Multilayered polymer films on a substrate represent an important class of technological applications including insulation layers, paints, adhesives, and communication devices. Most of these applications require a uniform and

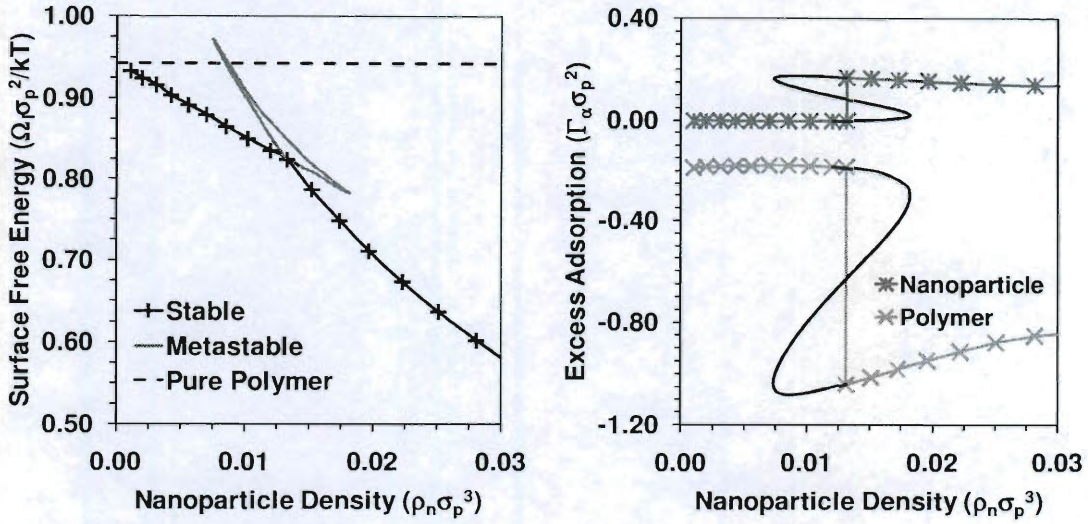

Figure 3.1 (Left) Surface free energy for a mixture of a 40-mer at a fixed overall packing fraction, $\eta = 0.3665$. The abrupt change in slope of the curve of stable configurations at $\rho_n^* = 0.01317$ indicates a first-order phase transition. The dashed curve is the free energy of a neat 40-mer with $\eta = 0.3665$. (Right) Excess adsorption of blend components as a function of nanoparticle density.

homogeneous medium. However, either due to nanoscale manufacturing defects, which are hard to resolve, or the dewetting behavior of the polymers on the substrates, cracks or ruptures could form and propagate leading to failures of these materials. Recent experiments[201,202] and simulations[182,203] found that nanoparticle fillers in these materials could migrate to interfaces such as cracks, substrates, and those between block copolymers. To fully utilize this behavior to design so-called self-healing materials, the underlying physics at the microscopic scale needs to be better understood.

McGarrity and coworkers[204,205] applied the original *i*SAFT DFT[25,26] to an athermal blend of nanoparticles (hard spheres) and polymers (hard chains) at a hard substrate. The system was set to be purely entropic to mimic a system

where the polymers are chemically identical to the nanoparticles. They tracked the surface free energy of the system with increasing nanoparticle concentration at fixed total packing fraction and found the addition of nanoparticles decreased the surface free energy. They also observed a discontinuity in the slope of the free energy curve when plotted as a function of particle density, which indicates a first-order phase transition. Figure 3.1 shows the free energy profile (left) and excess adsorption on the surface (right) calculated from *i*SAFT. The system demonstrates a sudden increase in the surface adsorption of nanoparticles at the corresponding phase transition. This implies the migration of nanoparticles to the surface, which is confirmed by the density profiles before and after the phase transition shown in Figure 3.2. The comparison between the profiles before the transition (left) and after the transition (right) clearly shows the formation of a monolayer of nanoparticles on the surface, exclusion of the polymer from the surface, and a decrease in the nanoparticle bulk density. Predictions of polymer and nanoparticle structure are in good agreement with molecular dynamics simulations as demonstrated by McGarrity *et al.*[204,205] The theory also predicts the relationship between nanoparticle size and concentration at which the phase transition occurs. Predictions of the nanoparticle concentration and surface free energy at the phase transition are slightly different with *i*SAFT as compared to the original *i*SAFT calculations of McGarrity *et al.* Further investigations showed that formation of subsequent layers of nanoparticles are also possible.

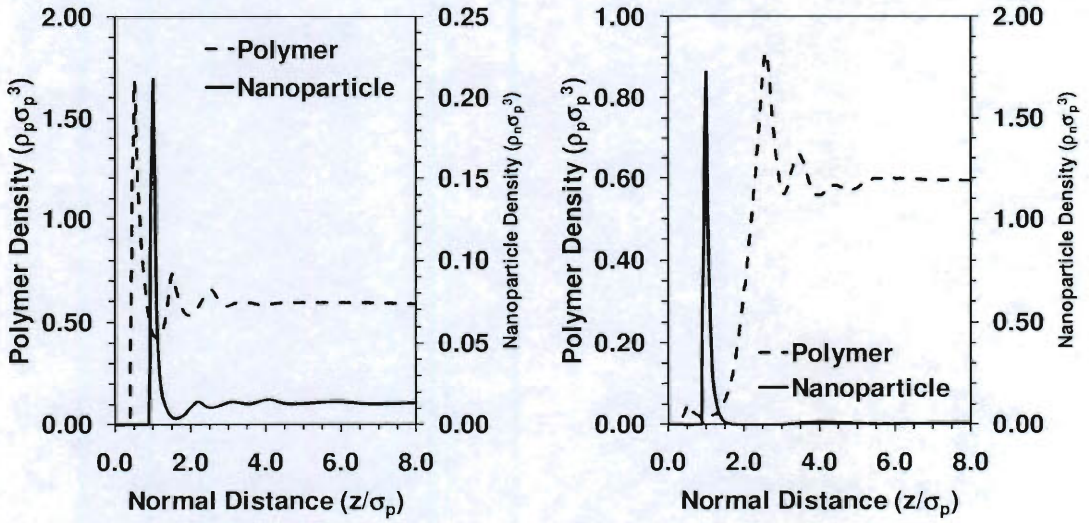

Figure 3.2 Polymer and nanoparticle density profiles calculated by *i*SAFT at the phase transition point. Profiles computed by setting density to the transition point and using a converged profile from a lower (left) and higher (right) density as the initial guess.

3.4.1.2 Block Copolymer Nanocomposites

Block copolymers are essential tools in synthesizing precisely controlled microstructures in modern materials engineering. The combination of block copolymers with nanoparticles enables even broader applications. Selective nanoparticles can be localized either at the center of a certain block domain or at the interface of blocks with nanoscale precision. Such potential applications could be in high efficiency storage media, nanolithography,[206] solar cells and photonic crystals. The realization of these applications would require understanding the effects of copolymer structure, copolymer size (molecular weight), nanoparticle concentration, and particle surface energies on the distribution of nanoparticles and phase behavior.

Molecular simulations[207-210] have shown qualitative agreement with experimental results for the distribution of nanoparticles. Investigations of the phase diagrams have also been done,[211] revealing multiple structures such as lamellae, perforated lamellae, hexagonally packed cylinders, and bicontinuous phases depending on the concentration of nanoparticles and their interaction energy with the different blocks. These simulations are limited to short copolymers because of the computational expense. As mentioned above, SCFT combined with the hard sphere free energies from DFT has also been applied and complex morphologies, especially cylindrical phases, have been observed.[193,194,212,213] Although it is unclear whether the typical local incompressibility condition of SCFT is valid within a continuous DFT framework, the SCFT-DFT hybrid method is computationally more efficient than classical DFTs. Most of the aforementioned complex phases would require 2 or 3 dimensional calculations to identify, thus DFT on its own may not be efficient for exploring these phase boundaries. This is the reason applications of classical DFTs[214,215] are currently limited to studying density distributions of components. Figure 3.3 shows a quantitative comparison between *i*SAFT predictions and simulation results[210] for an AB diblock copolymer blend with nanoparticles. The theory shows excellent agreement with these simulation results for various nanoparticle sizes and surface energies.

3.4.2 Associating Polymers

Associating macromolecules containing functional groups capable of forming reversible non-covalent (hydrogen or ionic) bonds can display complex

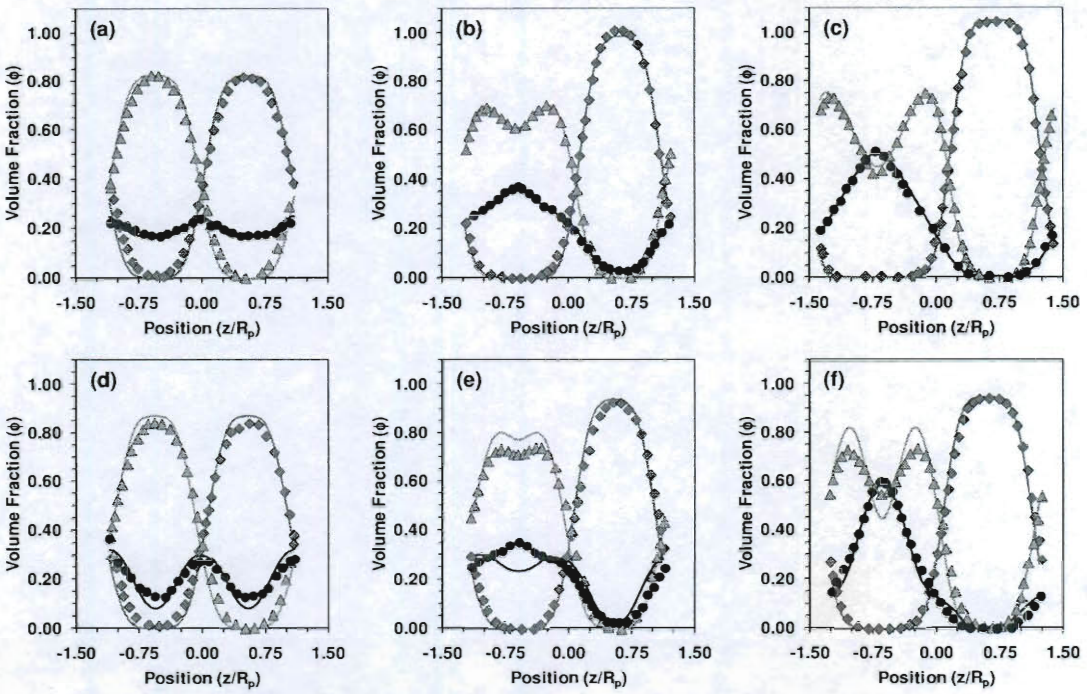

Figure 3.3 Concentration profiles of AB block copolymer nanocomposites for size ratios $\sigma_p^* = \sigma_{np}/\sigma_p = 1$ (top row) and $\sigma_p^* = 2$ (bottom row) with square shoulder interaction energy ratios $\varepsilon_p^* = \varepsilon_{np,A}/\varepsilon_{A,B} = 0$ (left), $\varepsilon_p^* = 1$ (center), and $\varepsilon_p^* = 2$ (right). Average packing fractions are $\eta_p = 0.28$ and $\eta_{np} = 0.07$. R_p is the athermal copolymer end-to-end distance implied by the theory. Lines are *i*SAFT predictions and symbols are molecular simulations of Schultz *et al.*[210] for the A block (dark grey), B block (light grey), and nanoparticle (black).

molecular architectures, interesting phase transitions, and unique self-assembled patterns or microstructures. The reversible nature of the associating components allows the control of molecular connectivity via temperature. Hence the phase behavior (macrophase separation, polymer-polymer miscibility, and self-assembly into mesostructures) and the unique material properties (physical properties and processability) of the system can all be tuned with temperature. Current and potential applications where such technology can be utilized include biosensors, separation devices, controlled drug delivery,[216] thermal manipulation

of the viscosity,[217] and the development of temperature controlled "smart materials".[218,219] SCFT and mean-field theories have been applied to study the self-assembly of associating supramolecular polymers. However, they are deficient in describing cases of macromolecules near solid surfaces or in confined nanoslits,[10,11] where local density fluctuations and liquid-like ordering play a significant role. On the contrary, a segment based DFT retains statistical segmental information rather than a field description of polymers at an expense significantly lower than molecular simulation methods. As mentioned previously, Segura *et al.*[21] introduced and successfully demonstrated two approaches to include association between atomic species. Yu and Wu[122,123] implemented an effective weighted density in the bulk theory for finite association in their polyatomic DFT to study some of these phenomena. Bymaster and Chapman[109,110] compared both approaches for a dimerizing hard sphere fluid within *i*SAFT and the more rigorous approach of using the association functional as a perturbation to a reference fluid functional showed superior performance in comparison with simulations. This was especially significant at low densities and high association strength.

Bymaster and Chapman[109,110] also demonstrated how versatile the implementation of the association free energy functional is through examples to several different association schemes. The more rigorous approach is shown to be capable of self-consistently mimicking the natural formation of complex supramolecules from simple associating species. In Figure 3.4, *i*SAFT predicts the same density distribution for 3 different schemes of forming the same star

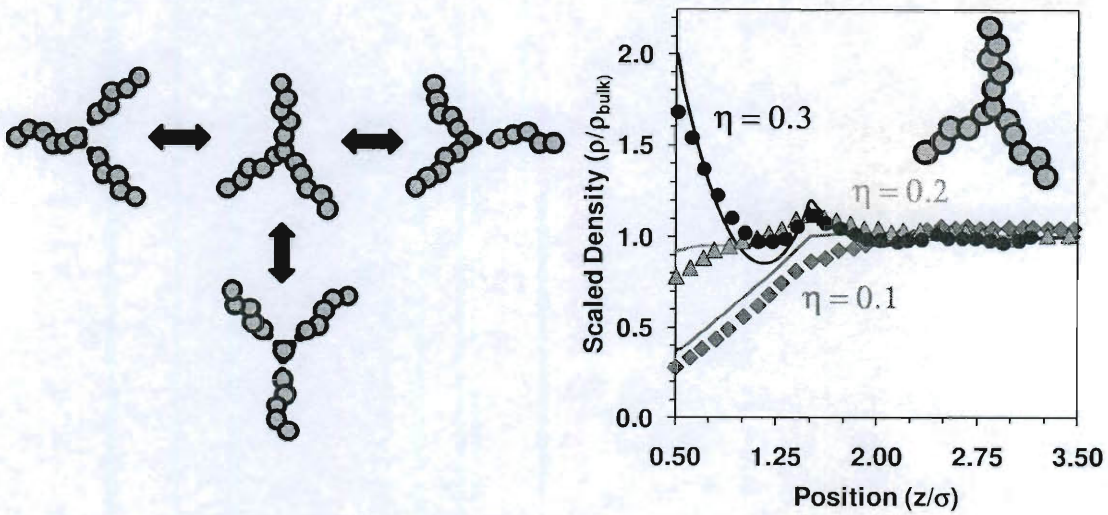

Figure 3.4 (Left) Association schemes for forming a star polymer with 3 arms and $N = 16$ segments at high association strengths. (Right) Density profiles of the star polymer between two hard walls at separation distance $H = 16\sigma$ and $\eta_{avg} = 0.1$ (dark grey), $\eta_{avg} = 0.2$ (light grey), and $\eta_{avg} = 0.3$ (black) normalized by the bulk density. A high population of star polymers is formed in the melt at high bonding strengths (e.g., $\beta\varepsilon_{assoc} = 30$) using any of the association schemes. Symbols are molecular simulation data from Yethiraj and Hall[167] and lines are *i*SAFT predictions. Figure taken from Bymaster and Chapman.[110]

polymer from smaller associating polymers and the density distribution agrees well with simulation at various densities. This application demonstrates the opportunity of applying such a technique to study the structure of even more complex supramolecules such as dendrimers. The phase behavior of chemically incompatible but symmetric polymers with associating end functional groups is also studied at typical polymer melt densities. Figure 3.5 gives the phase boundaries for systems with different polymer sizes. Aside from a homogeneous disordered phase and a lamellar phase, which are also identified in block copolymer melts, macrophase separations into 2 phases of individual polymers are also possible. The phase diagram shows theoretical predictions of phase

transitions from a lamellar microphase to a disordered phase to a macrophase 2 phase split back to a reentrant disordered phase as temperature is increased at high association strength. This same series of transitions has been observed experimentally.[220]

3.4.3 Self-assembly of Heteronuclear (Amphiphilic) Molecules

Chemically dissimilar species constrained by connectivity tend to self-assemble into distinct molecular level subdomains to help reduce the surface area of unfavorable interfaces. The morphology of these domains depends on the interaction between like and unlike species and the partitioning of the individual molecules. A theoretical model that is both qualitatively and quantitatively accurate in describing self-assemblies could provide vital guidance

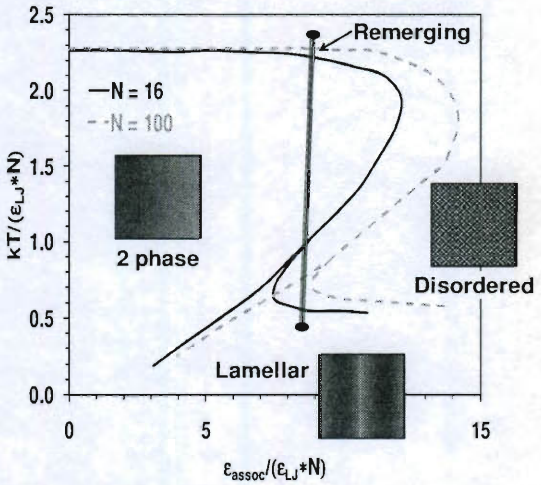

Figure 3.5 Phase diagram for associating polymer mixtures highlighting the effect of chain length and temperature on the phase behavior. The distinct observed phases are: (1) a disordered phase, (2) a macrophase split, and (3) a lamellar microphase. Remerging phase behavior is observed (disordered-macrophase split-disordered and lamellar-disordered-lamellar) upon changing the temperature. Figure taken from Bymaster and Chapman.[110]

to material design and the understanding of biological processes. Wu's review[12] briefly discusses earlier efforts to study self-assembling systems. In this section, the emphasis is on the excellent quantitative accuracy of current DFTs in comparison to molecular simulation and the promise for future application.

3.4.3.1 Surfactants at a Liquid-Liquid Interface

When introduced into a mixture of two substances with low affinities for one another (e.g., water-like and oil-like solvents), amphiphilic molecules like surfactants tend to partition or self-assemble themselves at the interface. This is due to multiple competing attractive and/or repulsive energies for the different solvents for different regions of the same molecule. Aggregation of these molecules on the surface effectively screens unfavorable interactions between the solvents, which in turn reduces the interfacial tension. The correlation between surface tension with bulk surfactant concentration is well studied for many practical systems;[121,151] however, the structuring of the surfactant at the interface is rarely addressed. Molecular simulations are inherently inefficient in studying this system. First, to maintain acceptable statistics, the very low bulk surfactant concentration would require a large number of solvent molecules for the two macrophases resulting in a computationally expensive simulation. Second, the bulk phase densities, directly measurable in experiments, are difficult to control in a common canonical ensemble molecular simulation in which the total number of molecules or the average density is fixed. On the contrary, DFTs are very suitable for these phase coexistence calculations, where bulk chemical potentials and bulk densities are easily monitored since they are

derived in the grand canonical ensemble and computation is not affected by the low concentration of surfactants.

Very recently, Emborsky and coworkers[111] applied *i*SAFT to the Telo da Gama and Gubbins model[222] for surfactants to study the interfacial tension and microstructure of an oil-water-surfactant system. In this model, oil and water molecules are hard spheres with a Weeks-Chandler-Andersen[223,224] attraction between like species at a dimensionless temperature of $T^* = k_b T/\varepsilon = 1$. Surfactant molecules are constructed by bonding m water-like head segments (H) to n oil-like tail segments (T) to form an $H_m T_n$ structure. Figure 3.6 shows the comparison between the theoretical predictions and the molecular

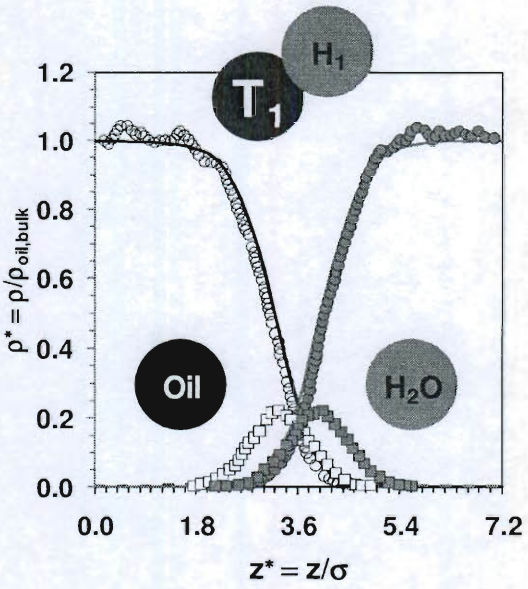

Figure 3.6 Comparison of *i*SAFT predictions (curves) with the simulation data of Smit[221] for the microstructure of 24 H1T1 surfactant molecules at an oil-water interface. Symbols are segment densities of oil (white circles), water (grey circles), tails (white squares), and heads (grey squares). Figure taken from Emborsky *et al.*[111]

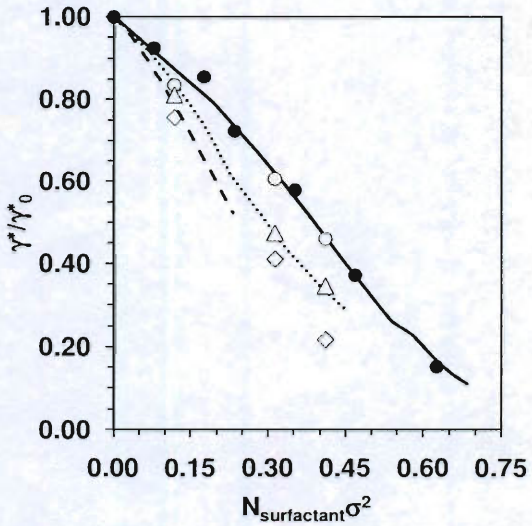

Figure 3.7 Comparison of the scaled interfacial tension *i*SAFT predictions with the molecular simulations of Smit[221] (solid symbols) and Smit *et al.*[225] (open symbols) as a function of surfactant loading. Different curves are for H1T1 (circles and solid line), H1T3 (triangles and dotted line), and H1T5 (diamonds and dashed line) surfactant structures. Figure taken from Emborsky *et al.*[111]

simulations of Smit *et al.*[221,225] of the microstructure of the interface for an H_1T_1 surfactant system. Figure 3.7 also shows comparison of *i*SAFT with the results from the same molecular simulations for the surface tension. The *i*SAFT predictions show very good quantitative agreement in all cases. The study has also been extended to demonstrate how more realistic longer single-tail and more complex double-tail surfactants partition themselves to the interface and what effect this has on the interfacial tension. As a segment-based DFT, *i*SAFT easily tracks the distribution of individual segments at the interface. Density profile distributions of the individual segments suggest the heads and tails of the surfactant tend to curl up near the surface on either side of the interface rather than extend into the solvent as typically depicted.

3.4.3.2 Lipid Molecules and Bilayer Formation

Most biological membranes possess bilayer structures formed by self-assembling of lipid molecules in an aqueous medium. Studies concerning how these membranes react to temperature, concentration, and mechanical changes and how materials are transported through membranes have drawn much attention. To successfully model lipids and bilayer structures, a theory must be capable of explicitly handling chain heterogeneity (i.e., size and chemical difference of individual segments within a single molecule), chain polydispersity, and compressibility effects. Some of these features are typically missed or difficult to handle in molecular-based DFT and SCFT approaches. A segment-based DFT has promise to give greater insight into such systems.

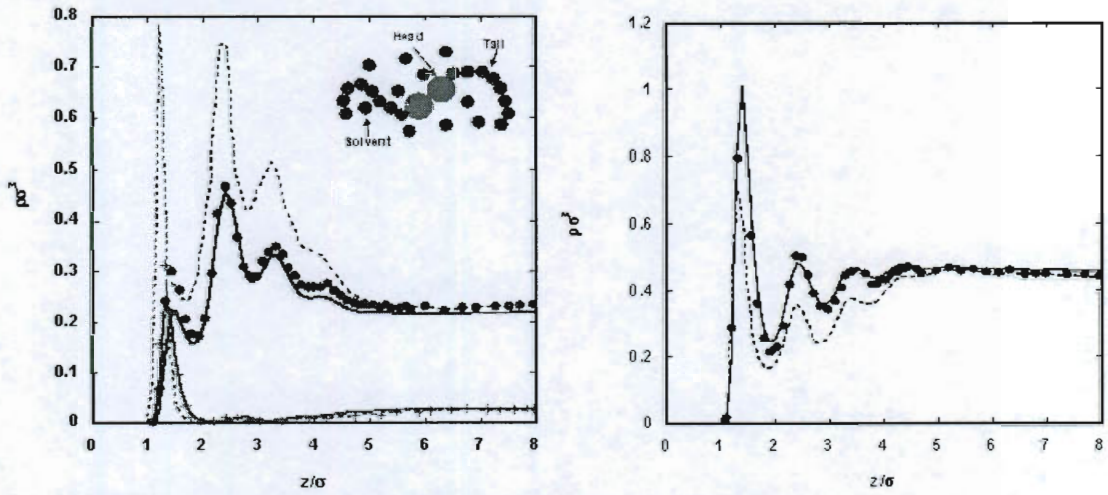

Figure 3.8 Comparison of head segment (light grey), tail segment (black), and solvent (dark grey) density profiles from *i*SAFT[24] (solid), CMS-DFT[226] (dashed), and molecular simulation[226] (symbols) for repulsive chains near a repulsive wall with total bulk density $\rho_b^* = 0.709$ and $x_s = 0.630$.

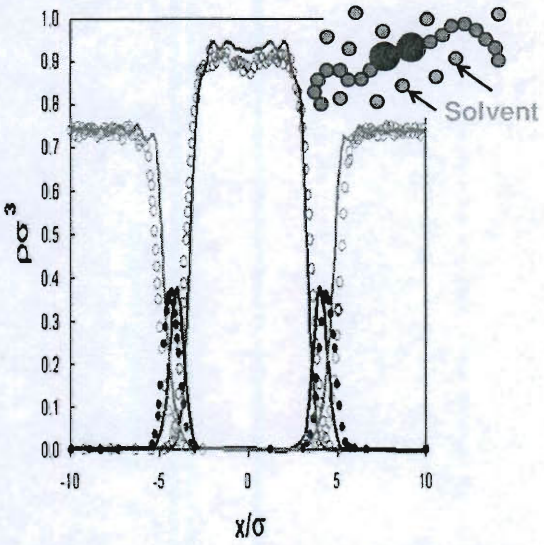

Figure 3.9 Comparison of the density profiles for a bilayer structure from *i*SAFT[24] (curves) and molecular simulation[226] (symbols). Black, dark grey, and light grey represent head, tail, and solvent segments respectively.

The work of Frink and Frischknecht[226,227] showed the great potential of DFT to describe confined lipid structure, bilayer structure, and even mechanical properties of bilayers, such as the lateral stress and area compressibility. However, the predictions of the CMS-DFT were far from quantitatively accurate when compared with the molecular simulations of a model lipid system.[226] Jain *et al.*[24] applied *i*SAFT to the same model system and Figure 3.8 shows the comparison of their results with both the CMS-DFT and molecular simulation for a purely repulsive system. This shows *i*SAFT agrees very well with the simulations and performs much better than the CMS-DFT. *i*SAFT also accurately predicts the bilayer morphology, depicted in Figure 3.9 with the simulation results[226] for the same system, as well as the equilibrium spacing of a zero tension bilayer structure, which is the natural state for bilayers in real biological systems.

3.4.4 Tethered Polymers

Polymers tethered onto material surfaces have found numerous important applications in colloidal stabilization, surface protection, lubrication, microscale delivery and encapsulation, immobilization, and catalysis. The addition of successfully describing tethering to a polyatomic theory could expand the applicability to a much wider range of systems including branched polymers, star polymers, dendrimers, polymer brushes, and surface modifications. Thus, it is appealing for theoreticians to study the stretching, coiling, or collapsing of polymer tethers, forces of interaction between tethered surfaces, and how these attributes are affected by the number of polymer chains per surface area (grafting density), molecular interactions, and solvent quality. Works in this area include the early scaling theories developed by Alexander[228] and de Gennes,[6] SCFT,[229,230] Monte Carlo simulations,[231-233] molecular dynamics,[234-236] Brownian dynamics,[237-239] and DFT.[112,114,176-178,240] With so many great works in this field, the focus here will be on how DFT compares to other methods mentioned in this section.

Figure 3.10 compares the density profiles of polymer brushes tethered on a planar surface in the presence of a free polymer solution from *i*SAFT[112] with the simulation results of Grest.[235] The chain length of the free polymer is eventually reduced to 0 which corresponds to the implicit solvent case. The theory is in good agreement with these simulations by capturing the collapse of the brushes (decrease in brush height) due to the effect of solvent volume

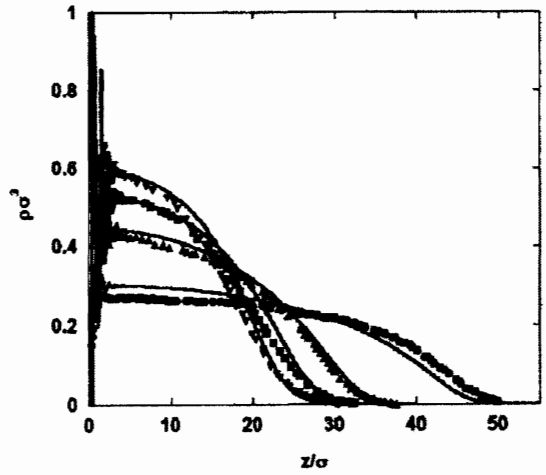

Figure 3.10 Segment density profiles of $N_g = 100$ length hard chains tethered to a hard wall with grafting density $\rho_g \sigma^2 = 0.1$ in the presence of implicit solvent (●) or explicit free polymer solvent with $N_f = 2$ (▲), $N_f = 5$ (■), or $N_f = 10$ (▼) segments. Symbols are the simulation data of Grest[235] and curves are *i*SAFT predictions. Figure taken from Jain *et al.*[112]

exclusions. The effect of grafting density and interaction strength has also been studied using *i*SAFT and compared to molecular simulations. Figure 3.11 shows the density profiles of the grafted chains on opposite surfaces and the free polymers at two bulk free polymer volume fractions from both *i*SAFT[114] and SCFT. The theories agree semi-quantitatively at high free polymer concentration except at the surface where SCFT misses the density fluctuations. As free polymer concentration decreases, SCFT predicts a stronger compression effect from free polymers than *i*SAFT. The forces between grafted surfaces have also been calculated and compared with the scaling theory of Alexander,[228] which states that for good solvent conditions, the interaction force between surfaces should scale as $\rho_g^{3/2}$ where ρ_g is the grafting density. Figure 3.12 shows *i*SAFT

is in agreement with this scaling relationship. The force curves reduced by $\rho_g^{3/2}$ for cases of various grafting density and grafted polymer length overlay each other at the same compression ratio. (The compression ratio is defined as the ratio of half surface separation to unperturbed single brush height).

DFTs have been applied to study a number of other interesting areas concerning tethered polymers. Polyelectrolyte brushes (PEBs) have been investigated extensively[176-178] because they are more realistic descriptions of real tethers. The effects of salt concentration, polymer grafting density, length of the tethered polyelectrolyte, counter ion valence and ionic strength have been examined. The "osmotic brush" regime at low salt concentrations and the "salted brush" regime at high salt concentrations have also been characterized and compared with scaling theories.[241] Moreover, when coupling with trivalent counter ions, the local electrostatic potential exhibits charge inversion. However,

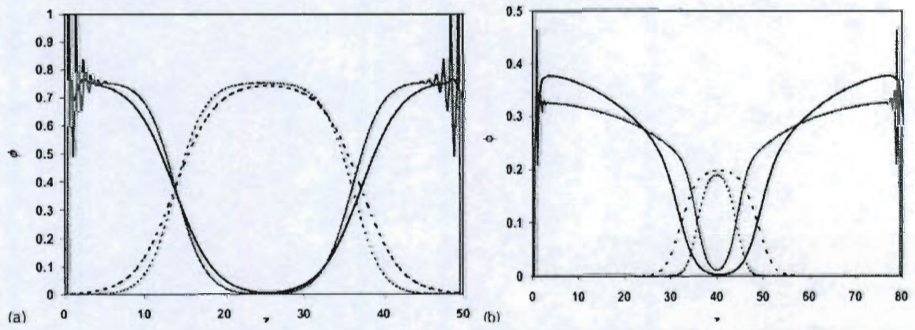

Figure 3.11 Density profiles of $N_g = 101$ length grafted chains (solid lines) and $N_g = 100$ length free polymer chains (dotted lines) between two plates with grafting density $\rho_g \sigma^2 = 0.1$ calculated using *i*SAFT (grey) and SCFT (black). (Left) Free polymer bulk volume fraction $\phi_f^b = 0.75$ and plate separation $H = 50$. (Right) $\phi_f^b = 2$ and $H = 80$. Figure taken from Jain *et al.*[114]

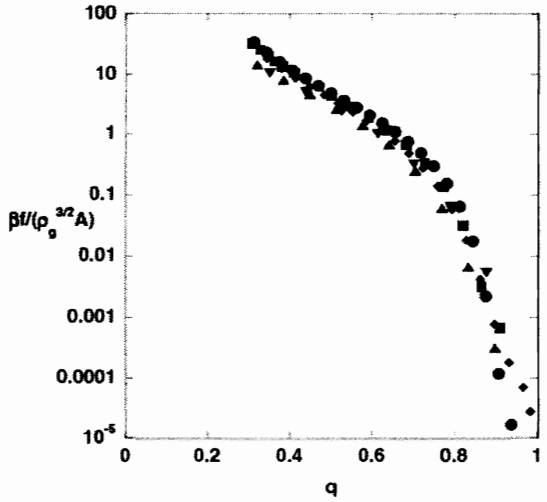

Figure 3.12 Interaction force calculated by iSAFT between the two grafted monolayers in the absence of free polymer scaled by $\rho_g^{3/2}$ as a function of the compression ratio $q = H/2H_0$ where H is the surface separation and H_0 is the unperturbed single brush height for $N_g = 51$ and $\rho_g\sigma^2 = 0.1$ (◆), $N_g = 101$ and $\rho_g\sigma^2 = 0.1$ (■), $N_g = 151$ and $\rho_g\sigma^2 = 0.1$ (●), $N_g = 101$ and $\rho_g\sigma^2 = 0.03$ (▲), and $N_g = 101$ and $\rho_g\sigma^2 = 0.01$ (▼). Figure taken from Jain *et al.*[114]

current PEB studies are limited to planar geometry and the primitive model (neglects the excluded volume of solvent molecules). Another important topic is the adsorption of both simple fluids[242] and macromolecules[240] in polymer brushes. Aside from common parameters that govern these systems like grafting density and tether length, the effect of end architecture of the tethers has also been studied.[243] Depending on whether the end of the tethers mimic a linear, branched, star, or dendritic polymer, the adsorptions of spherical molecules change drastically. This could provide guidelines for applications in surface protection, encapsulation, and microfluidic devices. Since the tethers are described within the same framework as linear chain bonding in DFTs derived

from Wertheim's TPT1, a universal DFT capable of handling different polymer structures has been proposed by introducing a tree-type representation of polymers.[244] Very recently, lipid bilayer structure is proposed to be described by tethered lipid molecules on imaginary surfaces.[131] While the integrity of the bilayer structure could be maintained, the fluidic nature of the bilayers is clearly neglected. Still, this model could be utilized to study transport aspects of components through lipid bilayers.

3.5 Future Direction and Development

This and previous reviews[12,13] have detailed the wide-ranging applicability and impressive versatility of density functional theory to accurately model complex fluids in a self-consistent framework from the bulk to the interface. It has been demonstrated that DFT not only provides a mechanism for predicting challenging phase behavior and interfacial properties, but it also gives valuable insight into the intricate multiscale nuances that govern these types of systems. This provides a very useful tool in the more intelligent design of future materials for both general and very specific purposes. This is especially useful where limitations in solving problems that have previously been unattainable with more conventional theories are encountered. While equations of state and phenomenological theories still have their place within science and engineering, expecting these classical approaches to perform well with the multiscale dynamic and equilibrium problems on the leading edge of technology today is naïve. In many of the applications presented, the performance of DFT has also been compared with other leading theories such as SCFT and molecular simulation.

This is not to suggest DFT should replace these approaches. Rather, it is more attractive to recognize the advantages of these different methodologies and attempt to better integrate them into hybrid techniques. As an example, application of a combined DFT-SCFT approach to the copolymer nanocomposite problem was discussed above, and the belief is similar hybrid methods are the best direction for the field of molecular modeling.

Despite the use of DFT in reproducing the behavior of many diverse systems, it is by no means exhaustive, and the prospective capabilities of its continued extension are directly linked to the development of accurate force models and functionals describing the relevant physics. Many of the currently available extensions have been discussed here; however, certain assumptions are typically attached to the initial justification of any choice for a free energy functional. For this reason, work still needs to be done to relax these assumptions to bring about a more general theory. Specifically, moving away from a mean-field approximation to the molecular interactions allows for the direct connection of more accurate bulk equations of state with the polyatomic DFT. This needs to be done for a segment-based heteronuclear chain rather than assuming a homonuclear chain, where the characteristics of individual functional groups in the chain are averaged into a single set of parameters for the whole molecule. Similarly, extending renormalization group theories and approaches for dealing with charged species for such a system will allow for more accurate studies across all physical conditions including near the critical point and discovery or identification of potential thermodynamically unstable

regions of the phase diagram for both nonionic and ionic polyatomic molecules. Lastly, more effective and efficient numerical techniques must continue to be an emphasis for DFT to maintain its computational advantage. Many of the current studies are done on model systems with the simplification of only a single dimension of inhomogeneity (planar or radial surface). To address even more complex phenomena such as bicontinuous or gyroidal phases, multidimensional aggregation behavior, protein folding, profiles near patterned surfaces, or micelle formation, multiple dimensions of inhomogeneity will have to be considered.

CHAPTER 4 INTERFACIAL STATISTICAL ASSOCIATING FLUID THEORY: APPLICATION TO MICROSTRUCTURE AND INTERFACIAL TENSION OF AN OIL-WATER-SURFACTANT INTERFACE

4.1 Introduction

Surface active agents (surfactants) and their blends have long been used as mechanisms for lowering the surface tension of liquids or interfacial tension between species with low affinities for one another (e.g., oil and water). In such a system, the typically polar head group and hydrocarbon chain serve as the hydrophilic and hydrophobic ends of the amphiphilic surfactant molecule, respectively. This makes it favorable for the partitioning, alignment, and aggregation of the amphiphile at the interface which affects the surface properties of the system (e.g., relative reduction of interfacial tension). As a result, surfactants will also often increase the mutual solubility of chemically dissimilar species and/or lead to the formation of ordered phases such as lamellae and vesicles. Depending on the nature of the system and chemical structure, surfactants can serve as wetting, dispersing, emulsifying, foaming, and antifoaming agents. This has led to widespread use of surfactants in many commercial applications such as detergents, fabric softeners, shampoos, paints, inks, coatings, adhesives, insecticides, pesticides, enhanced oil recovery, fire fighting, and drug delivery. Some of the challenging fundamental phenomena necessary to understand in such applications are surface wetting, colloid stability, mechanical stability, thermal stability, foaming, interaction with biological substances, environmental impact, and toxicity. Thus, understanding the complex thermodynamics of ordered and disordered phase coexistence often

found in these systems and the property effects is of great importance practically and theoretically. It has led to continued extensive experimental studies. However, because of the complex nature of the species and the resulting microstructure, theoretical and simulation based studies have only recently made gains in explaining some of the physical phenomena and finding application in novel surfactant design in industry.[245,246] Some of these complexities can include using salts and ionic surfactants requiring a model for charged species, multiple surfactants complicating the phase behavior and computational tractability, and real oils being hydrocarbon mixtures rather than simplified single components as many modeling studies assume. More recently, simplified models that are computationally tractable due to incorporating only the essential physics have been used to systematically study surfactant behavior. This began with a lattice model proposed by Widom *et al.*,[247,248] which has been the basis for several other lattice approaches.[249-261] A continuum model similar to that of Widom and Wheeler was proposed by Telo da Gama and Gubbins.[222] Other mean-field theories using this continuum model[262,263] have also been applied. The purpose of these different models is to study the relationships between the surfactant chemical structure and thermodynamic properties such as interfacial or surface tension.

The molecular approach applied to this system in this work is classical density functional theory (DFT). Different DFT formalisms as well as self-consistent field theory (SCFT) have been applied to similar problems.[24,264-272] DFT has the advantages of including short and long range molecular structure

and compressibility effects. In recent years, accurate DFT's have been developed for associating molecules (e.g., see Segura, Chapman, and Shukla[21]) as well as polyatomic molecules. Combining the theories of Segura *et al.*[20,21] and Woodward,[273] Yu and Wu[122,123] proposed a DFT for polyatomic homonuclear molecules that reduces to the statistical associating fluid theory (SAFT) equation of state in the homogeneous fluid limit. Based on a separate theory of Segura *et al.*,[20,21] Tripathi and Chapman[25,26] proposed a segment-based DFT using Wertheim's first order thermodynamic perturbation theory[15-18] (TPT1) which is now known as interfacial statistical associating fluid theory (*i*SAFT). This original form of the theory was successfully applied to polymer mixtures, melts, and blends confined in slit-like pores. Dominik *et al.*[151] extended the theory to real systems to study the interfacial properties of *n*-alkanes and polymers. The *i*SAFT approach is appealing because it's TPT1 basis means it also reduces to the SAFT equation of state in the homogeneous limit[19,46-48,53] which has long been established as an accurate and versatile equation of state for polymeric fluids.[274] Approximations made in the derivation of *i*SAFT made it only accurate for homonuclear chains. Thus, the modified *i*SAFT version (hereafter referred to as simply *i*SAFT) was proposed by Jain *et al.*[24] which generalized the theory to be accurate for heteronuclear chains such as lipids, block copolymers, and surfactants. While other DFT approaches have been developed, the focus will be on the *i*SAFT approach because of the accuracy of the predictions, computational efficiency, lack of need for input from other theories or simulation, and the ability to accurately model bulk and inhomogeneous systems within the

same framework. Publications using the Chandler-McCoy-Singer DFT[99-101] (CMS-DFT) discuss the approximations necessary in SCFT approaches that are not necessary in typical DFT formulations.

In this work, the use of the *i*SAFT classical DFT is validated by accurately reproducing simulation results[221,225] of the Telo da Gama and Gubbins model.[222] This will give a better understanding of the molecular level physics that govern the system behavior and provide a basis for future work on a systematic study of surfactant chemical structure impact on the microstructure and interfacial tension. The *i*SAFT model has promise to give greater insight into such behavior because it explicitly accounts for compressibility effects and the differences in individual segments which are typically missed with molecular based DFT and SCFT approaches.

4.2 The *i*SAFT Model

*i*SAFT is a DFT for inhomogeneous fluid mixtures of polyatomic molecules.[24] These molecules are modeled as fully flexible chains of tangentially bonded spherical segments. Classical DFTs are typically formulated for an open system in the grand canonical ensemble. Thus, the system is at a fixed volume (V), temperature (T), and chemical potential (μ) and subject to an external field $V^{ext}(\mathbf{r})$. The appropriate free energy for this ensemble is the grand free energy (Ω). The functional form of the grand free energy for a fluid of chains is related to a functional for the intrinsic Helmholtz free energy (A) according to

$$\Omega\left[\rho_\alpha(\mathbf{r})\right] = A\left[\rho_\alpha(\mathbf{r})\right] - \sum_{\alpha=1}^{m} \int d\mathbf{r}' \rho_\alpha(\mathbf{r}')\left(\mu_\alpha - V_\alpha^{ext}(\mathbf{r}')\right) \tag{4.1}$$

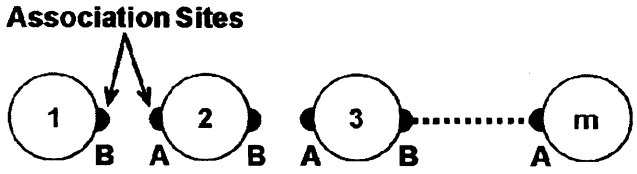

Figure 4.1 Schematic of linear chain formation from m associating spheres using Wertheim's TPT1.

where ρ_α and μ_α are the segment density and chemical potential of the α^{th} segment respectively, V_α^{ext} is the external field acting on that segment, and the summation is over all m segments in the chain. For the system to be at equilibrium, the grand free energy must be minimized. This is expressed mathematically by taking the functional derivative of equation (4.1) with respect to the segment density and setting it equal to zero. This results in a system of variational equations known as the Euler-Lagrange equations given by

$$\frac{\delta A[\rho_\alpha(\mathbf{r})]}{\delta\rho_\alpha(\mathbf{r})} = \mu_\alpha - V_\alpha^{ext}(\mathbf{r}) \quad \forall\alpha = 1,\ldots,m. \tag{4.2}$$

Solving this system of equations gives the equilibrium segment density profiles. The expression for the free energy for chain molecules is derived by taking the complete association limit of Wertheim's theory[19,21,24] for a mixture of atomic molecules (segments) as shown in Figure 4.1. The intrinsic Helmholtz free energy functional is written as a perturbation expansion to a reference fluid as

$$\begin{aligned} A[\rho_\alpha] &= A^{id}[\rho_\alpha] + A^{ex}[\rho_\alpha] \\ &= A^{id}[\rho_\alpha] + A^{ex,hs}[\rho_\alpha] + A^{ex,assoc}[\rho_\alpha] + A^{ex,att}[\rho_\alpha] \end{aligned} \tag{4.3}$$

where $A^{id}[\rho_\alpha]$ is the ideal free energy functional for a mixture from statistical mechanics and $A^{ex}[\rho_\alpha]$ accounts for additional excess perturbations leading to more realistic molecular level physics. DFTs differ on how the intermolecular and intramolecular interactions are split between these terms. Here, the excess free energy functional superscripts are hs for the hard sphere contribution accounting for excluded volume effects, $assoc$ for the TPT1 association used for chain formation, and att for the long range van der Waals type attraction between the segments.

4.2.1 Free Energy Functionals

The ideal free energy functional for nonassociating segments is defined from statistical mechanics as

$$\beta A^{id}[\rho_\alpha] = \int d\mathbf{r} \sum_{\alpha=1}^{m} \rho_\alpha(\mathbf{r})\left[\ln \rho_\alpha(\mathbf{r}) - 1\right] \tag{4.4}$$

where the temperature dependent terms that do not affect the equilibrium structure, properties, or phase behavior have been dropped, $\beta = 1/k_b T$, k_b is Boltzmann's constant, and T is the temperature. The hard sphere term is calculated from Rosenfeld's Fundamental Measure Theory[97] (FMT) for a mixture according to

$$\beta A^{ex,hs}[\rho_\alpha] = \int d\mathbf{r} \Phi\left[n_\alpha(\mathbf{r})\right] \tag{4.5}$$

where $\Phi[n_\alpha]$ is given by

$$\Phi\left[n_\alpha(\mathbf{r})\right] = -n_0 \ln(1-n_3) + \frac{n_1 n_2}{1-n_3} + \frac{n_2^3}{24\pi(1-n_3)^2} - \frac{n_{v1}\cdot n_{v2}}{1-n_3} - \frac{n_2(n_{v1}\cdot n_{v2})}{8\pi(1-n_3)^2} \tag{4.6}$$

and n_α are the weighted densities as defined by Rosenfeld. The long range attractions are accounted for using a mean-field approximation,[275] which neglects pair correlations leading to the form

$$\beta A^{ex,att}[\rho_\alpha] = \frac{1}{2}\sum_{\alpha=1}^{m}\sum_{\gamma=1}^{m}\int_{|\mathbf{r}_2-\mathbf{r}_1|>\sigma_{\alpha\gamma}} d\mathbf{r}_1 d\mathbf{r}_2 \beta u_{\alpha\gamma}^{att}(|\mathbf{r}_2-\mathbf{r}_1|)\rho_\alpha(\mathbf{r}_1)\rho_\alpha(\mathbf{r}_2) \tag{4.7}$$

with $u_{\alpha\gamma}^{att}$ being the attractive part of the pair potential between segments α and γ. The contribution to the free energy functional due to chain formation is developed by first considering a system of associating spheres. For a finite association strength, $A^{ex,assoc}[\rho_\alpha]$ from Wertheim's TPT1 is[19,21]

$$\beta A^{ex,assoc}[\rho_\alpha] = \int d\mathbf{r}_1 \sum_{\alpha=1}^{m}\rho_\alpha(\mathbf{r}_1)\sum_{A\in\Gamma^{(\alpha)}}\left[\ln\chi_A^\alpha(\mathbf{r}_1) - \frac{\chi_A^\alpha(\mathbf{r}_1)}{2} + \frac{1}{2}\right] \tag{4.8}$$

where the inner summation is over the set of all association sites on segment α, $\Gamma^{(\alpha)}$, and $\chi_A^{(\alpha)}$ is the fraction of α segments not bonded at site A. This fraction is defined by the law of mass action as[19,21]

$$\chi_A^\alpha(\mathbf{r}_1) = \frac{1}{1+\int d\mathbf{r}_2 \chi_B^{\alpha'}(\mathbf{r}_2)\Delta^{\alpha\alpha'}(\mathbf{r}_1,\mathbf{r}_2)\rho_{\alpha'}(\mathbf{r}_2)} \tag{4.9}$$

where α' denotes a neighboring segment that bonds at site B to site A on segment α, and

$$\Delta^{\alpha\alpha'}(\mathbf{r}_1,\mathbf{r}_2) = \mathrm{K}\left[\exp(\beta\varepsilon_0)\frac{\delta(|\mathbf{r}_1-\mathbf{r}_2|-\sigma^{\alpha\alpha'})}{4\pi(\sigma^{\alpha\alpha'})^2} - 1\right] y^{\alpha\alpha'}(\mathbf{r}_1,\mathbf{r}_2). \tag{4.10}$$

Here, K is a constant geometric factor representing the volume available for association, ε_0 is the association energy, and $y^{\alpha\alpha'}(\mathbf{r}_1,\mathbf{r}_2)$ is the cavity correlation

function for an inhomogeneous hard sphere reference fluid. This is approximated by averaging the potential of mean force between particles at $\mathbf{r}_1$ and $\mathbf{r}_2$. This is equivalent to the geometric mean of the cavity functions centered at the two positions. The cavity correlation function at each position is approximated by the homogeneous cavity correlation function evaluated at a weighted density according to

$$y^{\alpha\alpha'}(\mathbf{r}_1,\mathbf{r}_2)=\sqrt{y^{\alpha\alpha'}\left[\bar{\rho}_\gamma(\mathbf{r}_1)\right]y^{\alpha\alpha'}\left[\bar{\rho}_\gamma(\mathbf{r}_2)\right]}\,. \tag{4.11}$$

The over-bar denotes the weighted density where the simple weighting implemented here is

$$\bar{\rho}_\gamma(\mathbf{r}_1)=\frac{3}{4\pi\sigma_\gamma^3}\int_{|\mathbf{r}_1-\mathbf{r}_2|<\sigma_\gamma} d\mathbf{r}_2\rho_\gamma(\mathbf{r}_2)\,. \tag{4.12}$$

4.2.2 Functional Derivatives

In order to solve for the equilibrium fluid structure, the functional derivatives of the terms defined in section 4.2.1 are needed in equation (4.2). These expressions are

$$\frac{\delta\beta A^{id}\left[\rho_\gamma\right]}{\delta\rho_\alpha(\mathbf{r})}=\ln\rho_\alpha(\mathbf{r})\,, \tag{4.13}$$

$$\frac{\delta\beta A^{ex,hs}\left[\rho_\gamma\right]}{\delta\rho_\alpha(\mathbf{r})}=\int d\mathbf{r}\,\frac{\delta\Phi\left[n_\alpha(\mathbf{r})\right]}{\delta\rho_\alpha(\mathbf{r})}\,, \tag{4.14}$$

$$\frac{\delta\beta A^{ex,att}\left[\rho_\gamma\right]}{\delta\rho_\alpha(\mathbf{r})}=\sum_{\gamma=1}^{m}\int_{|\mathbf{r}-\mathbf{r}_1|>\sigma_{\alpha\gamma}} d\mathbf{r}_1\beta u_{\alpha\gamma}^{att}\left(|\mathbf{r}-\mathbf{r}_1|\right)\rho_\gamma(\mathbf{r}_1) \tag{4.15}$$

and

$$\frac{\delta\beta A^{ex,assoc}\left[\rho_\gamma\right]}{\delta\rho_\alpha(\mathbf{r})}=\sum_{A\in\Gamma^{(\alpha)}}\left[\ln\chi_A^\alpha(\mathbf{r}_1)-\frac{\chi_A^\alpha(\mathbf{r}_1)}{2}+\frac{1}{2}\right]+\sum_{\gamma=1}^{m}\int d\mathbf{r}_1\rho_\gamma(\mathbf{r}_1)\sum_{A\in\Gamma^{(\gamma)}}\left[1-\frac{\chi_A^\gamma(\mathbf{r}_1)}{2}\right]\frac{\delta\chi_A^\gamma(\mathbf{r}_1)}{\delta\rho_\alpha(\mathbf{r})} \quad (4.16)$$

Jain *et al.*[24] showed that the functional derivative of the association term can be simplified such that it does not involve functional derivatives of $\chi_A^{(\alpha)}$. Furthermore, taking the limit of complete association (i.e., $\varepsilon_0\to\infty$) gives[24]

$$\frac{\delta\beta A^{ex,assoc}\left[\rho_\alpha\right]}{\delta\rho_\alpha(\mathbf{r})}=\sum_{A\in\Gamma^{(\alpha)}}\ln\chi_A^\alpha(\mathbf{r}_1)-\frac{1}{2}\sum_{\gamma=1}^{m}\sum_{\gamma'}^{\{\gamma\}}\int d\mathbf{r}_1\rho_\gamma(\mathbf{r}_1)\frac{\delta\ln y^{\gamma\gamma'}\left[\bar{\rho}_\alpha(\mathbf{r}_1)\right]}{\delta\rho_\alpha(\mathbf{r})} \quad (4.17)$$

where $\{\gamma'\}$ is the set of all segments bonded to segment γ. In this equation, the first term enforces stoichiometry and the cavity function is further approximated using the weighted density.

4.3 Equilibrium Density Profiles and Interfacial Tension

These expressions for the functional derivatives can be substituted back into the Euler-Lagrange equation given in equation (4.2). The set of coupled nonlinear equations (for all m segments) can be solved using equation (4.9) for $\chi_A^{(\alpha)}$; however, Jain *et al.*[24] showed how these equations can be decoupled for systems of linear chains like those in the model system being considered here. For such chains, each terminal segment has a single bonding site, either A or B, while each internal segment has two bonding sites, both A and B. This reduces the expressions for the fraction of segments not bonded at each type of association site to

$$\chi_A^{\alpha}(\mathbf{r}_{\alpha}) = \left[\exp\left(\beta \sum_{i=\alpha+1}^{m} \mu_i \right) \times \right.$$
$$\left. \int \cdots \int d\mathbf{r}_{\alpha+1} \cdots d\mathbf{r}_m \exp\left(\sum_{i=\alpha+1}^{m} \left[D_i(\mathbf{r}_i) - \beta V_i^{ext}(\mathbf{r}_i) \right] \right) \prod_{i=\alpha}^{m-1} \Delta^{(i,i+1)}(\mathbf{r}_i, \mathbf{r}_{i+1}) \right]^{-1} \quad (4.18)$$

and

$$\chi_B^{\alpha}(\mathbf{r}_{\alpha}) = \left[\exp\left(\beta \sum_{i=1}^{\alpha-1} \mu_i \right) \times \right.$$
$$\left. \int \cdots \int d\mathbf{r}_1 \cdots d\mathbf{r}_{\alpha-1} \exp\left(\sum_{i=1}^{\alpha-1} \left[D_i(\mathbf{r}_i) - \beta V_i^{ext}(\mathbf{r}_i) \right] \right) \prod_{i=1}^{\alpha-1} \Delta^{(i,i+1)}(\mathbf{r}_i, \mathbf{r}_{i+1}) \right]^{-1}, \quad (4.19)$$

where $D_{\alpha}(\mathbf{r})$ is given by

$$D_{\alpha}(\mathbf{r}) = \frac{1}{2} \sum_{\gamma=1}^{m} \sum_{\gamma'}^{\{\gamma\}} \int d\mathbf{r}_1 \rho_{\gamma}(\mathbf{r}_1) \frac{\delta \ln y^{\gamma\gamma'}\left[\overline{\rho}_{\alpha}(\mathbf{r}_1) \right]}{\delta \rho_{\alpha}(\mathbf{r})} - \frac{\delta \beta A^{ex,hs}[\rho_{\alpha}]}{\delta \rho_{\alpha}(\mathbf{r})} - \frac{\delta \beta A^{ex,att}[\rho_{\alpha}]}{\delta \rho_{\alpha}(\mathbf{r})}. \quad (4.20)$$

Finally, the expressions for the equilibrium density profiles are given by

$$\rho_{\alpha}(\mathbf{r}_{\alpha}) = \exp(\beta \mu_M) \exp\left[D_{\alpha}(\mathbf{r}_{\alpha}) - \beta V_{\alpha}^{ext}(\mathbf{r}_{\alpha}) \right] I_{1,\alpha}(\mathbf{r}_{\alpha}) I_{2,\alpha}(\mathbf{r}_{\alpha}), \quad (4.21)$$

where $\mu_M = \sum_{i=1}^{m} \mu_i$ is the bulk chemical potential of the chain, $I_{1,\alpha}(\mathbf{r}_{\alpha}) = \left[\exp\left(\beta \sum_{i=1}^{\alpha-1} \mu_i \right) \chi_B^{\alpha}(\mathbf{r}_{\alpha}) \right]^{-1}$, and $I_{2,\alpha}(\mathbf{r}_{\alpha}) = \left[\exp\left(\beta \sum_{\alpha-1}^{m} \mu_i \right) \chi_A^{\alpha}(\mathbf{r}_{\alpha}) \right]^{-1}$. The values of $I_{1,\alpha}$ and $I_{2,\alpha}$ are multiple integrals calculated using the recurrence:

$$I_{1,\alpha}(\mathbf{r}_{\alpha}) = \int d\mathbf{r}_{\alpha-1} I_{1,\alpha-1}(\mathbf{r}_{\alpha-1}) \left[D_{\alpha-1}(\mathbf{r}_{\alpha-1}) - \beta V_{\alpha-1}^{ext}(\mathbf{r}_{\alpha-1}) \right] \Delta^{(\alpha-1,\alpha)}(\mathbf{r}_{\alpha-1}, \mathbf{r}_{\alpha}) \quad (4.22)$$

and

$$I_{2,\alpha}(\mathbf{r}_{\alpha}) = \int d\mathbf{r}_{\alpha+1} I_{2,\alpha+1}(\mathbf{r}_{\alpha+1}) \left[D_{\alpha+1}(\mathbf{r}_{\alpha+1}) - \beta V_{\alpha+1}^{ext}(\mathbf{r}_{\alpha+1}) \right] \Delta^{(\alpha,\alpha+1)}(\mathbf{r}_{\alpha}, \mathbf{r}_{\alpha+1}), \quad (4.23)$$

which are initialized according to

$$I_{1,1}(\mathbf{r}_1) = 1 \quad (4.24)$$

and

$$I_{2,m}(\mathbf{r}_m)=1. \tag{4.25}$$

This produces the grand free energy

$$\beta\Omega[\rho_\alpha]=\sum_{\alpha=1}^{m}\int d\mathbf{r}_\alpha\rho_\alpha(\mathbf{r}_\alpha)\left[D_\alpha(\mathbf{r}_\alpha)+\frac{n\left(\Gamma^{(\alpha)}\right)}{2}-1\right], \tag{4.26}$$

where $n\left(\Gamma^{(\alpha)}\right)$ is the total number of association sites on segment α. Using the grand free energy of the inhomogeneous system, the interfacial or surface tension is defined as the difference between it and the grand free energy of the homogeneous system according to

$$\gamma=\Omega[\rho_\alpha]-\hat{\Omega}\int d\mathbf{r}_\alpha\,, \tag{4.27}$$

where $\hat{\Omega}$ is the bulk (homogeneous) grand free energy.

The *i*SAFT DFT was applied to the model system defined by Telo da Gama and Gubbins,[222] where the oil and water solvent molecules are single spherical segments. A linear single-tail surfactant molecule is constructed by bonding m water-like spherical segments to n oil-like spherical segments to form a chain with a hydrophilic (water-like) head group (H) and hydrophobic (oil-like) tail group (T) to give the desired H_mT_n molecular structure as depicted in Figure 4.2. All segments have the same diameter and like segments have equivalent attraction energy (further details of the potential model are discussed in section 4.4). Assuming a planar oil-water interface, inhomogeneity will only be considered in the dimension normal to the surface of the interface (z). With no

external field acting on the system, the bulk chemical potentials and densities are determined using the homogeneous limit of the model (the SAFT equation of state) to perform a simple flash calculation. To compute the equilibrium density profiles, the domain is divided into equally spaced grid points along the dimension normal to the surface. Infinite bulk boundary conditions are applied at both boundaries with one side arbitrarily chosen as the "oil-rich" phase and the other being the "water-rich" phase. The distance between grid points (0.1σ) and length of the domain (20σ) are chosen such that the converged profiles are smooth and the bulk limit is reached at each boundary. These profiles are solved for using Picard's iteration method. The initial guess for the density profile is a step change from one bulk phase to the other at the middle of the domain. At every iteration, an estimate to the density profile for each segment is calculated using equation (4.21). The calculated density at each grid point is mixed with the old profile to provide the new density profile. Iterations continue until the density profiles do not change appreciably. All of the integrations are done using the composite Simpson's rule.

4.4 Results and Discussion

4.4.1 Microstructure of the Interface

To validate the application of *i*SAFT to such model oil-water-surfactant systems, predictions of the density profiles were compared with the simulation results of Smit.[221] These simulations for the microstructure of the interface were carried out a reduced temperature of $T^* = k_b T/\varepsilon = 1.0$ and a total reduced

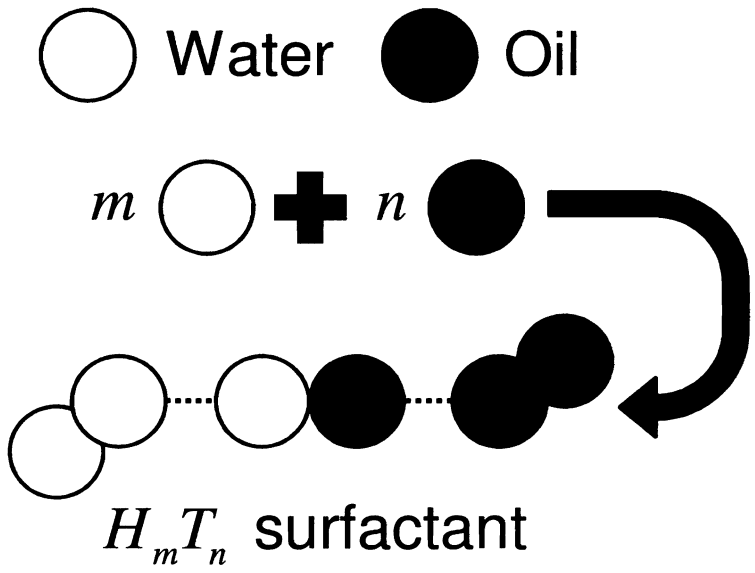

Figure 4.2 Schematic of the model oil-water-surfactant system proposed by Telo da Gama and Gubbins[222] with purely repulsive interactions between unlike segments and LJ type attraction between like segments.

segment density of $\rho^* = \rho\sigma^3 = 0.7$. The full potential is written as an attractive perturbation to a hard sphere reference fluid according to

$$u_{i,j}(r) = u_{i,j}^{ref}(r) + u_{i,j}^{att}(r). \tag{4.28}$$

The reference fluid potential is

$$u_{i,j}^{ref}(r) = \begin{cases} \infty & r \le r_{min} \\ 0 & \text{otherwise} \end{cases}, \tag{4.29}$$

while the attractive part of the potential is a cut and shifted Lenard-Jones (LJ) potential given by

$$u_{i,j}^{att}(r) = \begin{cases} u_{i,j}^{LJ}(r) - u_{i,j}^{LJ}(r_{i,j}^c) & r \le r_{i,j}^c \\ 0 & r > r_{i,j}^c \end{cases}, \tag{4.30}$$

with

$$u_{i,j}^{LJ}(r) = 4\varepsilon_{i,j}\left[\left(\frac{\sigma_{i,j}}{r}\right)^{12} - \left(\frac{\sigma_{i,j}}{r}\right)^{6}\right]. \tag{4.31}$$

The subscripts i and j represent the different segment types in the system (oil, water, head, and tail) and $r_{min} = 2^{1/6}\sigma$ is the minimum in the LJ potential. For simplification, all the segments have the same diameter $\sigma_{i,j} = \sigma$ and the same magnitude of the interaction energy $\varepsilon_{i,j} = \varepsilon$. The difference in interactions between like and unlike segments is in the cutoff radius, $r_{i,j}^{c}$ which is 2.5σ for like segment pairs (i.e., oil-oil, water-water, oil-tail, water-head) and r_{min} for unlike segment pairs (i.e., oil-water, oil-head, water-tail). This means all interactions between unlike pairs are purely repulsive. Within *i*SAFT, the attractions are treated as a perturbation to a hard sphere reference fluid in the spirit of the Weeks-Chandler-Anderson perturbation theory,[223,224] which splits the pair potential as defined in equation (4.29) where the reference and attraction terms are now defined as

$$u_{i,j}^{ref}(r) = \begin{cases} \infty & r \le \sigma_{i,j} \\ 0 & \text{otherwise} \end{cases} \tag{4.32}$$

and

$$u_{i,j}^{att}(r) = \begin{cases} 0 & r \le \sigma_{i,j} \\ u_{i,j}^{LJ}(r_{min}) - u_{i,j}^{LJ}(r_c) & \sigma_{i,j} \le r \le r_{min} \\ u_{i,j}^{LJ}(r) - u_{i,j}^{LJ}(r_c) & r_{min} \le r \le r_c \\ 0 & r_c \le r \end{cases}, \tag{4.33}$$

with $r_c = 2.5\sigma$. This is slightly different from the simulation potential in its inclusion of a small additional attraction between σ and r_{min}.

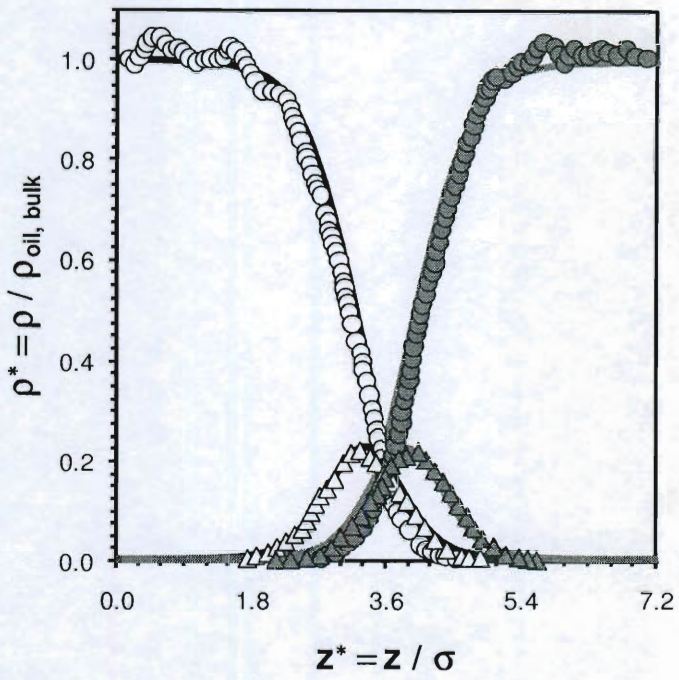

Figure 4.3 Comparison of segment density profile *i*SAFT predictions (solid lines) with the simulation data of Smit[221] (symbols) for 24 H_1T_1 surfactant molecules. Symbols are for oil (white circles), water (grey circles), tail segments (white triangles), and head segments (grey triangles).

As mentioned above, validation of the *i*SAFT approach is done with comparisons to the canonical ensemble molecular simulation work of Smit.[221] Equilibrium density profiles are reported for 24, 48, and 64 H_1T_1 surfactant molecules in the interface using the model described above. For this planar interface, the calculation reduces to a single dimension of inhomogeneity since only the structure normal to the interface is of interest. Figure 4.3, Figure 4.4, and Figure 4.5 show comparisons of the density profiles predicted by the theory with the simulation results for the different interfacial surfactant loadings. Despite the minor difference in the *i*SAFT attractive potential model, the predictions of

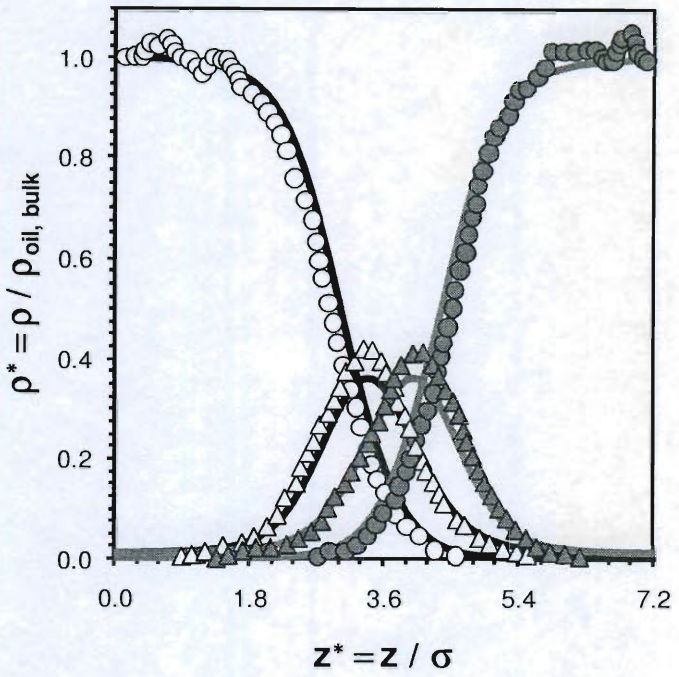

Figure 4.4 Comparison of segment density profile *i*SAFT predictions (solid lines) with the simulation data of Smit[221] (symbols) for 48 H_1T_1 surfactant molecules. Symbols are for oil (white circles), water (grey circles), tail segments (white triangles), and head segments (grey triangles).

*i*SAFT show good quantitative agreement in all cases. As the number of surfactant molecules increases, the agreement remains qualitatively good, but the quantitative agreement decreases. Specifically, the solvent (oil and water) depletion at the interface is less pronounced in the *i*SAFT prediction which leads to slight under predictions of the head and tail peaks of the surfactant. This is likely due to a combination of factors. First, the simulated system was too small to produce a full bulk region particularly at higher surfactant concentrations.[221] One result of this is increased noise in the simulated bulk densities for the solvents which makes the scaling somewhat arbitrary. Second, the simulation

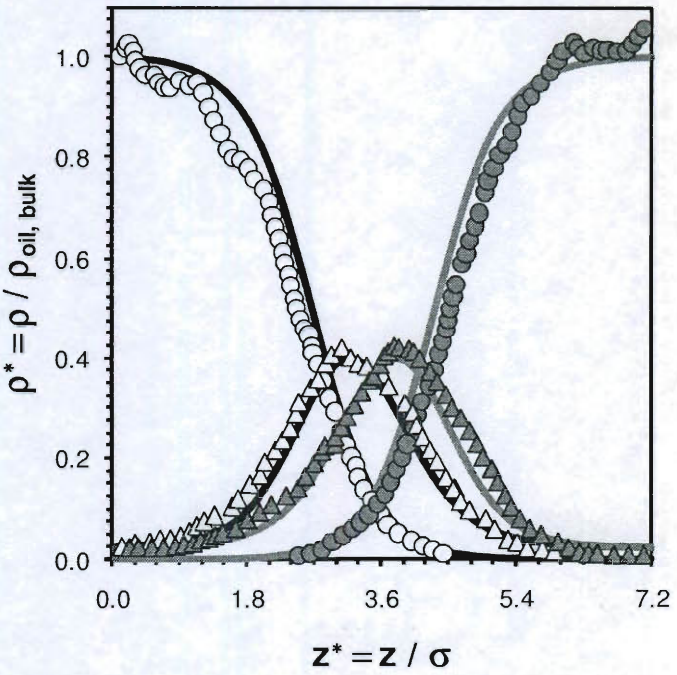

Figure 4.5 Comparison of segment density profile *i*SAFT predictions (solid lines) with the simulation data of Smit[221] (symbols) for 64 H_1T_1 surfactant molecules. Symbols are for oil (white circles), water (grey circles), tail segments (white triangles), and head segments (grey triangles).

results show all of the surfactant molecules exist only at the surface and no mutual solubility of the solvent molecules. However, the *i*SAFT calculations start with a bulk SAFT flash calculation that suggests low solubility of the surfactant in both bulk phases along with limited mutual solubility of the solvents. Additionally, with the definition of the interfacial region being somewhat arbitrary and likely ambiguous, the number of surfactant molecules in the *i*SAFT calculations was determined by integrating the head and tail profiles across the width of the interface to give a surfactant loading per unit area. If this is matched to the equivalent loading from the simulations, there are naturally going to be shorter

peaks right at the interface to compensate for the aforementioned bulk solubility of the surfactant.

4.4.2 Interfacial Tension

Smit *et al.*[221,225] also calculated the interfacial tension as a function of the number of surfactant molecules in the interface. This study was done for the H_1T_3 and H_1T_5 surfactant structures in addition to the H_1T_1 surfactant whose microstructure was addressed in section 4.4.1. Figure 4.6 shows a comparison between the interfacial tension predictions of *i*SAFT and the simulation results as a function of the surfactant loading in the interface. The interfacial tension is scaled by that of the oil-water system (with no surfactant) to yield excellent qualitative agreement. The predictions for the H_1T_1 and H_1T_3 also showed excellent quantitative agreement. Based on the trend, the projection suggests excellent agreement would also be attained for the H_1T_5 system, but greater surface loadings are unattainable at these system conditions due to the lack of coexisting liquid-like phases with high enough bulk surfactant solubility that would result in sufficient partitioning to the interface. In accordance with experimentally based heuristics, notice that a longer hydrophobic tail leads to a smaller amount of surfactant required to achieve a specified interfacial tension. It is also expected that a surfactant with a longer hydrophobic tail will more effectively partition from the bulk to the interface. The affinity the surfactant has for the interface (due to its interaction potential) essentially drives the surfactant to pack there. The improved effectiveness of the longer tails comes from the packing of the tail segments in such a way that the available space for free oil segments is

reduced which also reduces the unfavorable direct contact between oil-like and water-like segments. This improvement in the surfactant effectiveness appears to have a limiting behavior since adding the two tail segments to go from an H_1T_1 structure to an H_1T_3 structure has greater impact than doing the same to go from the H_1T_3 structure to the H_1T_5 structure.

As briefly mentioned, the tail length of the surfactant also affects partitioning between the bulk phase and the interface. The fact that a surfactant is a trace component in the bulk provides a significant challenge for molecular

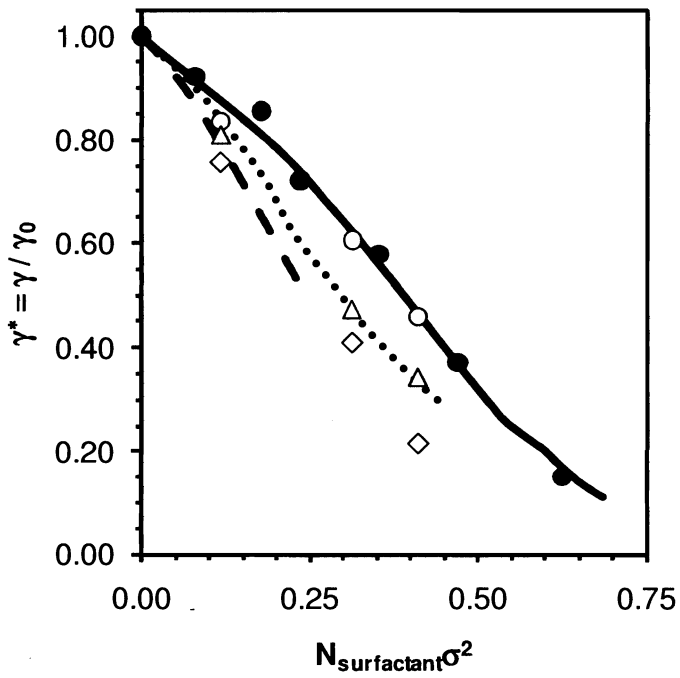

Figure 4.6 Comparison of scaled interfacial tension *i*SAFT predictions (lines) with simulations of Smit[221] (solid symbols) and Smit *et al.*[225] (open symbols) as a function of surfactant surface loading for the H_1T_1 (solid line/circles), H_1T_3 (dotted line/triangles), and H_1T_5 (dashed line/diamonds) surfactant structures. Scaling factor is the interfacial tension of the bare oil-water interface.

simulation as demonstrated here where the size of the simulations were not large enough to address this bulk solubility. The density functional theory has no such limitation. Future studies will consider surfactant partitioning and the affect of molecular structure in more detail.

4.5 Conclusions

The modified *i*SAFT DFT has been applied to study the microstructure and interfacial tension of a model oil-water-surfactant system. Using a simple pair potential that suggests surfactant-like behavior, the model produces excellent qualitative agreement when compared with molecular simulations. The structure at the interface is governed by the structure of the surfactant molecule and the pair potential. A longer hydrophobic tail effectively squeezes out some of the free oil and reduces the unfavorable contact between the dissimilar segment types due to the chain structure. These effects on the microstructure of the interface also affect the interfacial properties—specifically the interfacial tension. The longer tail better reduces the interfacial tension for a given amount of surfactant; however, this behavior appears to have a limit. The application of *i*SAFT to such model oil-water-surfactant systems is the basis for gaining an understanding of the molecular level physics that govern the microstructure and interfacial properties of such systems. This knowledge base will be used to further expand a systematic study to multiple surfactant structures that can serve as a set of heuristics for custom surfactant design. In an age where chemists are capable of devising a scheme for synthesizing any stable molecule we can draw, the use of an accurate theory that can predict such properties becomes a

valuable tool that can guide the experimentalist and tell them what to expect before conducting the experiments.

CHAPTER 5 EXPLORING PARAMETER SPACE EFFECTS ON STRUCTURE-PROPERTY RELATIONSHIPS OF SURFACTANTS AT A LIQUID-LIQUID INTERFACE

5.1 Introduction

Surface active agents (surfactants) and their blends have long been used as mechanisms for chemically modifying the microstructure of the interface between strongly dissimilar species. The effects on the fluid structure can significantly lower the interfacial tension and increase the mutual solubilities of immiscible solvents (e.g., oil and water). In such a system, the amphiphilic nature of the surfactant promotes its partitioning to the interface as the typically polar hydrophilic head group wants to be surrounded with water or other head groups and the lypophillic hydrocarbon chain bonded to this head group is partial to the oil and other tail groups. Depending on the chemical architecture and system conditions, this behavior can also lead to the formation of self-assembled ordered structures such as micelles or vesicles. The tenability of these systems to achieve a set of desired properties has led to the widespread use of surfactants in many commercial, industrial, and consumer goods applications such as detergents, shampoos, inks, paints, coatings, adhesives, enhanced oil recovery, and targeted drug delivery among many others. Some of the many challenging fundamental phenomena to understand in these applications include wetting/drying of surfaces, colloid stability, mechanical stability, thermal stability, foaming, biological substance interactions, environmental impact, and toxicity. This has led to rather consistent and extensive experimental investigation. However, due to the complex molecular physics and resulting microstructure,

theoretical and simulation based studies have only recently made gains in explaining the physical phenomena and predicting the necessary properties for novel surfactant design.[245,246] Some of these complexities can include the use of salts and ionic surfactants, requiring an accurate approach for charged species, multiple surfactants or polydispersity complicating the computational tractability and phase behavior, and real oils being hydrocarbon mixtures rather than simplified coarse-grained single component approximations, as many modeling studies commonly assume. More recently, systematic studies of surfactant behavior have been conducted using simplified reduced models that aim to include only the essential physics, making them computationally tractable. This began with a lattice model proposed by Widom *et al.*[247,248] which has served as the basis for several other lattice model approaches.[249-261] A continuum model similar to that of Widom and Wheeler was proposed by Telo da Gama and Gubbins.[222] Other mean-field theories using this continuum model[262,263] have also been applied. More sophisticated phenomenological and group contribution theories have also been developed. These notably include the work of Blankschtein *et al.*,[276-282] who implemented molecular thermodynamic theory for determining micelle size and shape for mixtures of ionic and/or nonionic surfactants. Coarse-grained mesoscopic scale molecular simulations such as the recent work of Shinoda *et al.*[283-285] have also become popular in this area. The purpose of these different models is to study the effects different tunable parameters such as the surfactant chemical structure and system conditions

have on observable interfacial and thermodynamic properties, such as macrophase and microphase behavior or interfacial tension.

In this work, the molecular level modeling approach applied to this inhomogeneous system of complex fluids is classical density functional theory (DFT). Different DFT formalisms as well as self-consistent field theory (SCFT) have previously been applied to similar problems.[24,264-272] DFT has the advantage of including both short and long range molecular structure along with compressibility effects which are often neglected within SCFT. Works applying the Chandler-McCoy-Singer DFT[99-101] (CMS-DFT) discuss these approximations which are necessary within SCFT but not typically required within DFT.[101,286] In recent years, accurate DFTs have been developed for associating molecules (e.g., see Segura *et al.*[21]) as well as polyatomic molecules. Combining the theories of Segura *et al.*[20,21] and Woodward,[273] Yu and Wu[122,123] proposed a DFT that has the statistical associating fluid theory (SAFT) equation of state[19,46-48,53] as its homogeneous bulk limit. Based on another approach by Segura *et al.*[20,21] Tripathi and Chapman[25,26] proposed a segment-based polyatomic DFT using Wertheim's first-order thermodynamic perturbation theory[15-18] (TPT1) for associating molecules. The DFT of Tripathi and Chapman, now known as interfacial statistical associating fluid theory (*i*SAFT), was successfully applied to polymer mixtures, melts, and blends confined in slit-like pores. Dominik *et al.*[151] extended the application of the theory to real systems in their study of interfacial tension of alkanes and polymers. The *i*SAFT approach is appealing because its TPT1 basis means it also reduces to the SAFT equation of state[19,46-48,53] in its

homogeneous limit which has long been established as an accurate and versatile equation of state — especially for polymeric fluids.[274] Initial approximations in the derivation of *i*SAFT made it only accurate for homonuclear chains. Thus, the modified *i*SAFT version (hereafter referred to as simply *i*SAFT) was proposed by Jain *et al.*[24] which generalized the theory for accurate application to heteronuclear chains such as lipids, block copolymers, and surfactants. While other DFT approaches have been developed (see review of Emborsky *et al.*[14]), the focus here is on *i*SAFT because of the accuracy of its predictions, computational efficiency, lack of necessary input from other theories or simulation, and capability to accurately and self-consistently model both bulk and inhomogeneous systems within a single framework.

In this work, the versatility and capabilities of *i*SAFT are demonstrated for the direct application to surfactant behavior at an oil-water interface. Previous work[111] validated the use of the *i*SAFT DFT with direct comparison of fluid microstructure and interfacial tension *i*SAFT predictions for the H_1T_1 surfactant against the molecular simulations of Smit *et al.*[221,225] using the Telo da Gama and Gubbins model.[222] This is an extension of that work to provide a diverse investigation of part of the vast parameter space available in these systems. Broadening the understanding of the molecular level physics and driving forces behind the self-assembly and corresponding equilibrium properties will continue to provide insight into the performance of real surfactants and guide future studies on structure-property relationships and the exploration of parameter space. The *i*SAFT model has promise to continue to give greater discernment of

such behavior because it explicitly accounts for compressibility effects and the differences of individual segments which are typically missed by the molecular-based DFTs and SCFT approaches.

5.2 Theory and Model

5.2.1 Model System

The oil-water-surfactant system is modeled in the spirit of the Telo da Gama and Gubbins model.[222] In our approach, the solvent molecules are single spheres with a hard core repulsion and a Lennard-Jones (LJ) type attraction. The surfactant molecules are modeled as combinations of tangentially bonded solvent-like spheres (segments) to form freely-jointed chains as depicted in Figure 5.1. As an example, consider m "water-like" segments bonded together to form the hydrophilic head group (H) and n "oil-like" segments bonded together to form the hydrophobic tail group (T). This yields the single-tailed $H_m T_n$ surfactant (Note: this notation is used throughout for differentiating surfactant structures). While all segments in the system have the same hard sphere diameter, σ, they are distinguished by their different long range attractions. These attractions are modeled using the 6-12 LJ potential as a perturbation to a hard sphere reference fluid according to the Weeks-Chandler-Anderson (WCA) perturbation theory.[223,224] This splits the pair potential as

$$u_{\alpha\beta}(r) = u_{\alpha\beta}^{ref}(r) + u_{\alpha\beta}^{att}(r), \tag{5.1}$$

where the hard sphere reference fluid term is

$$u_{\alpha\beta}^{ref}(r) = \begin{cases} \infty & r < \sigma_{\alpha\beta} \\ 0 & \text{otherwise} \end{cases} \tag{5.2}$$

and the attractive perturbation is

$$u_{\alpha\beta}^{att}(r) = \begin{cases} u_{\alpha\beta}^{LJ}(r_{min}) - u_{\alpha\beta}^{LJ}(r_c) & \sigma_{\alpha\beta} \le r < r_{min} \\ u_{\alpha\beta}^{LJ}(r) - u_{\alpha\beta}^{LJ}(r_c) & r_{min} \le r < r_c \\ 0 & \text{otherwise} \end{cases}, \tag{5.3}$$

with the LJ potential defined by

$$u_{\alpha\beta}^{LJ}(r) = 4\varepsilon_{\alpha\beta}\left[\left(\frac{\sigma_{\alpha\beta}}{r}\right)^{12} - \left(\frac{\sigma_{\alpha\beta}}{r}\right)^{6}\right]. \tag{5.4}$$

This makes the minimum in the potential $r_{min} = 2^{1/6}\sigma_{\alpha\beta}$ and the cutoff radius used here is $r_c = 2.5\sigma_{\alpha\beta}$. The energy parameters are $\varepsilon_{oo} = \varepsilon_{ww} = \varepsilon_{tt} = \varepsilon_{hh} = \varepsilon_{ot} = \varepsilon_{wh} = \varepsilon$

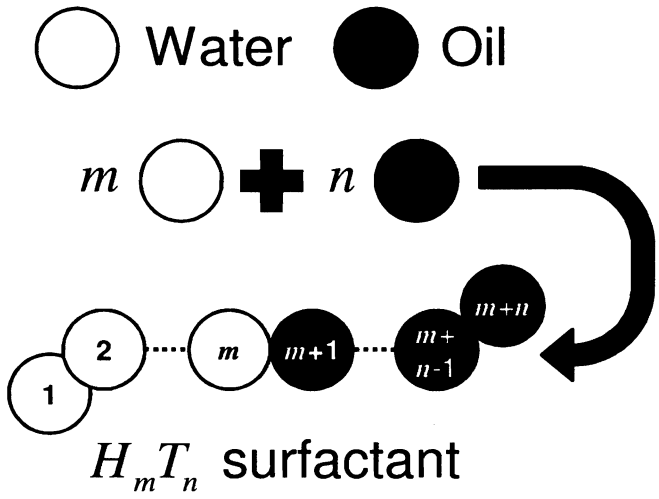

Figure 5.1 Visual representation of spherical solvents and amphiphilic chain construction within the Telo da Gama and Gubbins[222] oil-water-surfactant model.

for the like species and $\varepsilon_{ow} = \varepsilon_{oh} = \varepsilon_{wt} = 0$ for the unlike species with ε defined by the dimensionless temperature $T^* = kT/\varepsilon = 1.0$ where k_b is the Boltzmann constant and T is the temperature. As addressed in our previous work,[111] simulations such as those by Smit *et al.*[221,225] often fall short on their capability to tractably model mutual solubilities of the solvents and the bulk solubility of the surfactant since the presence of trace components require large simulation cells. It will be shown in the following section how these shortcomings are addressed with a simple flash calculation using the homogeneous limit of the theoretical molecular model used in this work. In addition, care must be taken with the boundary conditions used within molecular simulations to assure a full bulk condition is reach which also leads to the necessity of a larger simulation cell. Using infinite bulk boundary conditions and taking advantage of system symmetry allows for a computationally tractable domain size of $L = 20\sigma$ to avoid these same concerns.

5.2.2 Classical Density Functional Theory Formalism

The molecular approach being applied here is density functional theory (DFT). Originally developed for the electronic structure of an inhomogeneous ground state liquid by Hohenberg and Kohn[83] and Kohn and Sham[84] using quantum mechanics, DFT was later adapted to find the equilibrium molecular structure and interfacial properties of a Lennard-Jones fluid using classical mechanics by Ebner *et al.*[85] The specific DFT applied here is interfacial statistical associating fluid theory (*i*SAFT) as initially developed by Tripathi and Chapman[25,26] based on the work by Segura *et al.*[20,21] and later improved by Jain

et al.[24] The *i*SAFT DFT is a segment based approach for inhomogeneous complex polymeric fluids such as the surfactant molecules in this model system. DFTs are typically formulated for an open system in the grand canonical ensemble (fixed volume (V), temperature (T), and chemical potential (μ)). The grand free energy (Ω) for an inhomogeneous system of chains in the absence of an external field is

$$\Omega\left[\rho_\alpha(\mathbf{r})\right] = A\left[\rho_\alpha(\mathbf{r})\right] - \sum_{\alpha=1}^{m} \int d\mathbf{r}' \rho_\alpha(\mathbf{r}') \mu_\alpha \tag{5.5}$$

where ρ_α and μ_α are the density and bulk chemical potential of the α^{th} segment, $A\left[\rho_\alpha(\mathbf{r})\right] \equiv A[\rho_\alpha]$ is the intrinsic Helmholtz free energy functional, and the summation is over all m segments in the chain. The basis of a DFT is the energy minimization principle which is notated mathematically as

$$\left.\frac{\delta\Omega[\rho_\alpha]}{\delta\rho_\alpha}\right|_{\rho_\alpha^{equil}} = 0 \quad \forall\alpha = 1,\ldots,m. \tag{5.6}$$

Using the definition of the grand free energy from equation (5.5), equation (5.6) can be reformulated into a set of Euler-Lagrange variational equations in terms of the intrinsic Helmholtz free energy as

$$\frac{\delta A[\rho_\alpha]}{\delta\rho_\alpha} = \mu_\alpha \quad \forall\alpha = 1,\ldots,m. \tag{5.7}$$

Solving this system of equations gives the equilibrium density profiles of the segments (fluid microstructure). The Helmholtz free energy functional is derived by taking the complete association limit[19,21,24] of Wertheim's TPT1[15-18] for a mixture of atomic associating spheres (segments) as shown in Figure 5.2. The

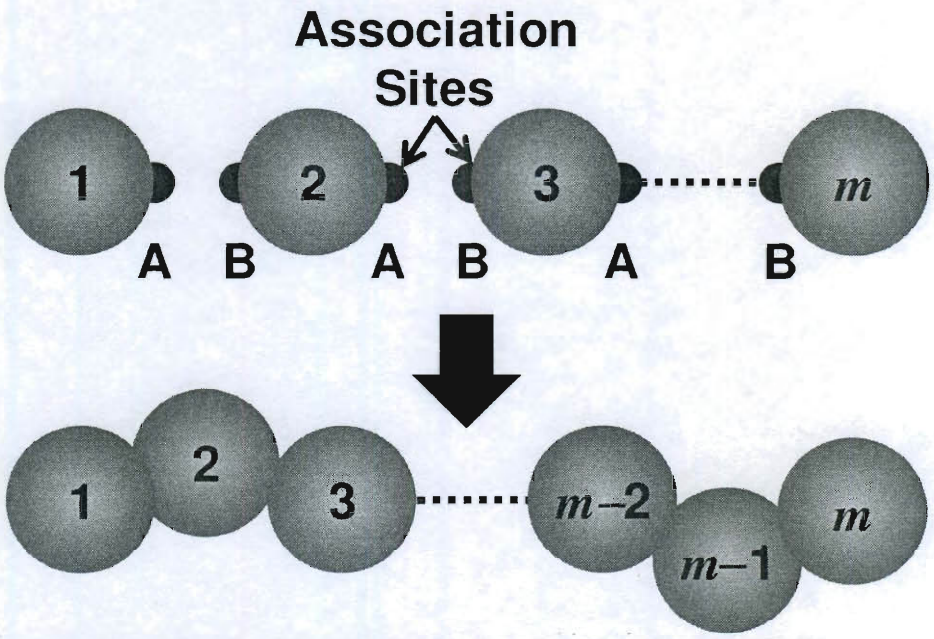

Figure 5.2 Schematic of chain formation from a mixture of associating spheres using Wertheim'sTPT1[15-18] in the complete bonding limit.[19,46]

residual Helmholtz free energy functional of such a system of associating segments is written as a perturbation expansion about a reference fluid to give

$$A[\rho_\alpha] = A^{id}[\rho_\alpha] + A^{ex,hs}[\rho_\alpha] + A^{ex,chain}[\rho_\alpha] + A^{ex,att}[\rho_\alpha] \qquad (5.8)$$

where A^{id} is the ideal free energy of the segments, $A^{ex,hs}$ is the excess free energy due to the excluded volume of the segments (hard sphere repulsions of the reference fluid), $A^{ex,chain}$ is the excess free energy due to chain formation, and $A^{ex,att}$ is the excess free energy due to long-range van der Waals type attraction between the segments.

5.2.2.1 Free Energy Functionals

The exact ideal free energy functional for a system of m non-associating spheres from statistical mechanics is

$$\beta A^{id}[\rho_\alpha] = \int d\mathbf{r} \sum_{\alpha=1}^{m} \rho_\alpha(\mathbf{r}) \left[\ln \rho_\alpha(\mathbf{r}) - 1 \right] \tag{5.9}$$

where the temperature dependent terms that do not affect the fluid microstructure, thermodynamic properties, or phase behavior have been dropped, $\beta = 1/k_b T$, and k_b is the Boltzmann constant. The excluded volume effects are accounted for using Rosenfeld's fundamental measure theory[97] (FMT) for a mixture of hard spheres according to

$$\beta A^{ex,hs}[\rho_\alpha] = \int d\mathbf{r} \Phi\left[n_\alpha(\mathbf{r}) \right] \tag{5.10}$$

and $\Phi[n_\alpha]$ is given by

$$\Phi\left[n_\alpha(\mathbf{r}) \right] = -n_0 \ln(1-n_3) + \frac{n_1 n_2}{1-n_3} + \frac{n_2^3}{24\pi(1-n_3)^2} - \frac{n_{v1} \cdot n_{v2}}{1-n_3} - \frac{n_2 (n_{v1} \cdot n_{v2})}{8\pi(1-n_3)^2}, \tag{5.11}$$

where n_α are the FMT weighted densities. The mean-field approximation,[275] which ignores the correlations between a pair of segments, is used for the long range attractions leading to

$$\beta A^{ex,att}[\rho_\alpha] = \frac{1}{2} \sum_{\alpha=1}^{m} \sum_{\gamma=1}^{m} \int_{|\mathbf{r}_2 - \mathbf{r}_1| > \sigma_{\alpha\gamma}} d\mathbf{r}_1 d\mathbf{r}_2 \beta u_{\alpha\gamma}^{att}\left(|\mathbf{r}_2 - \mathbf{r}_1| \right) \rho_\alpha(\mathbf{r}_1) \rho_\alpha(\mathbf{r}_2), \tag{5.12}$$

where the attractive part of the pair potential is given in equation (5.3). The contribution due to chain formation, $A^{ex.chain}$, is derived from Wertheim's first order thermodynamic perturbation theory[15-18] (TPT1) for finite association $\left(A^{assoc}\right)$ by taking the limit of complete bonding between the associating segments. The TPT1 free energy for finite association is[19,21]

$$\beta A^{ex.assoc}[\rho_\alpha] = \int d\mathbf{r}_1 \sum_{\alpha=1}^{m} \rho_\alpha(\mathbf{r}_1) \sum_{A \in \Gamma^{(\alpha)}} \left[\ln \chi_A^\alpha(\mathbf{r}_1) - \frac{\chi_A^\alpha(\mathbf{r}_1)}{2} + \frac{1}{2} \right] \tag{5.13}$$

where the first summation is over all the segments and the second summation is over the set of all association sites on segment α, $\Gamma^{(\alpha)}$. The fraction of α segments not bonded at association site A is defined by the law of mass action according to

$$\chi_A^{\alpha}(\mathbf{r}_1)=\frac{1}{1+\int d\mathbf{r}_2\chi_B^{\alpha'}(\mathbf{r}_2)\Delta^{\alpha\alpha'}(\mathbf{r}_1,\mathbf{r}_2)\rho_{\alpha'}(\mathbf{r}_2)} \tag{5.14}$$

where α' denotes a neighboring segment whose type B site associates with the type A association site on segment α. The nature of the bond is given by

$$\Delta^{\alpha\alpha'}(\mathbf{r}_1,\mathbf{r}_2)=\mathrm{K}\left[\exp(\beta\varepsilon_0)\frac{\delta\left(|\mathbf{r}_1-\mathbf{r}_2|-\sigma^{\alpha\alpha'}\right)}{4\pi\left(\sigma^{\alpha\alpha'}\right)^2}-1\right]y^{\alpha\alpha'}(\mathbf{r}_1,\mathbf{r}_2) \tag{5.15}$$

where K is a constant geometric factor dependent upon the association volume, ε_0 is the association energy, and $y^{\alpha\alpha'}(\mathbf{r}_1,\mathbf{r}_2)$ is the inhomogeneous cavity correlation function for the hard sphere reference fluid. This cavity correlation function is approximated by averaging the potential of mean force between spheres at positions $\mathbf{r}_1$ and $\mathbf{r}_2$ which is equivalent to the geometric mean of cavity functions centered at these positions in the fluid. The cavity function at each position is approximated by a bulk cavity correlation function evaluated at a weighted density, $\bar{\rho}_\gamma(\mathbf{r}_1)$, according to

$$y^{\alpha\alpha'}(\mathbf{r}_1,\mathbf{r}_2)=\sqrt{y^{\alpha\alpha'}\left[\bar{\rho}_\gamma(\mathbf{r}_1)\right]y^{\alpha\alpha'}\left[\bar{\rho}_\gamma(\mathbf{r}_2)\right]} \tag{5.16}$$

where the simple weighting used in this work is

$$\bar{\rho}_\gamma(\mathbf{r}_1)=\frac{3}{4\pi\sigma_\gamma^3}\int_{|\mathbf{r}_1-\mathbf{r}_2|<\sigma_\gamma} d\mathbf{r}_2\rho_\gamma(\mathbf{r}_2). \tag{5.17}$$

5.2.2.2 Functional Derivatives

To solve equation (5.7) for the equilibrium system fluid structure and its accompanying thermodynamic and interfacial properties, the functional derivatives of the free energy functionals are required. These expressions are given by

$$\frac{\delta\beta A^{id}\left[\rho_\gamma\right]}{\delta\rho_\alpha(\mathbf{r})} = \ln\rho_\alpha(\mathbf{r}), \tag{5.18}$$

$$\frac{\delta\beta A^{ex,hs}\left[\rho_\gamma\right]}{\delta\rho_\alpha(\mathbf{r})} = \int d\mathbf{r}\frac{\delta\Phi\left[n_\alpha(\mathbf{r})\right]}{\delta\rho_\alpha(\mathbf{r})}, \tag{5.19}$$

$$\frac{\delta\beta A^{ex,att}\left[\rho_\gamma\right]}{\delta\rho_\alpha(\mathbf{r})} = \sum_{\gamma=1}^{m}\int_{|\mathbf{r}-\mathbf{r}_1|>\sigma_{\alpha\gamma}} d\mathbf{r}_1\beta u_{\alpha\gamma}^{att}\left(|\mathbf{r}-\mathbf{r}_1|\right)\rho_\gamma(\mathbf{r}_1), \tag{5.20}$$

and

$$\begin{aligned}\frac{\delta\beta A^{ex,assoc}\left[\rho_\gamma\right]}{\delta\rho_\alpha(\mathbf{r})} = &\sum_{A\in\Gamma^{(\alpha)}}\left[\ln\chi_A^\alpha(\mathbf{r}_1) - \frac{\chi_A^\alpha(\mathbf{r}_1)}{2} + \frac{1}{2}\right] + \\ &\sum_{\gamma=1}^{m}\int d\mathbf{r}_1\rho_\gamma(\mathbf{r}_1)\sum_{A\in\Gamma^{(\gamma)}}\left[1-\frac{\chi_A^\gamma(\mathbf{r}_1)}{2}\right]\frac{\delta\chi_A^\gamma(\mathbf{r}_1)}{\delta\rho_\alpha(\mathbf{r})}\end{aligned} \tag{5.21}$$

The functional derivative of the association free energy can be further simplified by manipulating equations (5.14) and (5.21) to eliminate its dependence on the derivative of non-bonded fractions of segments, $\delta\chi_A^\gamma(\mathbf{r}_1)/\delta\rho_\alpha(\mathbf{r})$, as demonstrated by Jain *et al.*[24] Further imposing the limit of complete association ($\varepsilon_0\to\infty$) to form the surfactant chain-like molecules gives[24]

$$\frac{\delta\beta A^{ex,chain}\left[\rho_\alpha\right]}{\delta\rho_\alpha(\mathbf{r})} = \sum_{A\in\Gamma^{(\alpha)}}\ln\chi_A^\alpha(\mathbf{r}) - \frac{1}{2}\sum_{\gamma=1}^{m}\sum_{\gamma'}^{\{\gamma\}}\int d\mathbf{r}_1\rho_\gamma(\mathbf{r}_1)\frac{\delta\ln y^{m'}\left[\bar{\rho}_\alpha(\mathbf{r}_1)\right]}{\delta\rho_\alpha(\mathbf{r})} \tag{5.22}$$

where $\{\gamma'\}$ is the set of all segments bonded to segment γ. The first term in this equation enforces stoichiometry in the chain and the pair cavity correlation function is further approximated by its bulk counterpart evaluated at a weighted density.

5.2.3 Equilibrium fluid structure and interfacial tension

Substituting the expressions for the ideal and chain formation free energy functional derivatives back into the Euler-Lagrange system of equations given in equation (5.7) gives

$$\beta\mu_\alpha = \ln\rho_\alpha(\mathbf{r}) + \sum_{A\in\Gamma^{(\alpha)}} \ln\chi_A^\alpha(\mathbf{r}) - \frac{1}{2}\sum_{\gamma=1}^{m}\sum_{\gamma'}^{\{\gamma'\}}\int d\mathbf{r}_1\rho_\gamma(\mathbf{r}_1)\frac{\delta \ln y^{\gamma\gamma'}\left[\bar{\rho}_\alpha(\mathbf{r}_1)\right]}{\delta\rho_\alpha(\mathbf{r})} + \frac{\delta\beta A^{ex,hs}[\rho_\alpha]}{\delta\rho_\alpha(\mathbf{r})} + \frac{\delta\beta A^{ex,att}[\rho_\alpha]}{\delta\rho_\alpha(\mathbf{r})} \quad (5.23)$$

This system of coupled nonlinear equations (for all m segments) can be solved for the equilibrium fluid structure using equation (5.14) for $\chi_A^{(\alpha)}$. However, the work of Jain *et al.*[24] demonstrated how these equations can be decoupled for a linear chain of m segments like the surfactant structures explored in this work. In these chains, each end segment has a single association site, A or B, and all internal segments have two association sites, both A and B. For such a chain in the absence of an external field, the final expressions for $\chi_A^{(\alpha)}$ and $\chi_B^{(\alpha)}$ reduce to[24]

$$\chi_A^\alpha(\mathbf{r}_\alpha) = \left[\exp\left(\beta\sum_{i=\alpha+1}^{m}\mu_i\right)\int\cdots\int d\mathbf{r}_{\alpha+1}\cdots d\mathbf{r}_m \exp\left(\sum_{i=\alpha+1}^{m} D_i(\mathbf{r}_i)\right)\prod_{i=\alpha}^{m-1}\Delta^{(i,i+1)}(\mathbf{r}_i,\mathbf{r}_{i+1})\right]^{-1} \quad (5.24)$$

and

$$\chi_B^{\alpha}(\mathbf{r}_\alpha)=\left[\exp\left(\beta\sum_{i=1}^{\alpha-1}\mu_i\right)\int\cdots\int d\mathbf{r}_1\cdots d\mathbf{r}_{\alpha-1}\exp\left(\sum_{i=1}^{\alpha-1}D_i(\mathbf{r}_i)\right)\prod_{i=1}^{\alpha-1}\Delta^{(i,i+1)}(\mathbf{r}_i,\mathbf{r}_{i+1})\right]^{-1}, \quad (5.25)$$

where $D_\alpha(\mathbf{r})$ is given by

$$D_\alpha(\mathbf{r})=\frac{1}{2}\sum_{\gamma=1}^{m}\sum_{\gamma'}^{\{\gamma\}}\int d\mathbf{r}_1\rho_\gamma(\mathbf{r}_1)\frac{\delta\ln y^{\gamma\gamma'}\left[\bar{\rho}_\alpha(\mathbf{r}_1)\right]}{\delta\rho_\alpha(\mathbf{r})}-\frac{\delta\beta A^{ex,hs}[\rho_\alpha]}{\delta\rho_\alpha(\mathbf{r})}-\frac{\delta\beta A^{ex,att}[\rho_\alpha]}{\delta\rho_\alpha(\mathbf{r})}. \quad (5.26)$$

Solving for the equilibrium density profile yields[24]

$$\rho_\alpha(\mathbf{r}_\alpha)=\exp(\beta\mu_M)\exp\left(D_\alpha(\mathbf{r}_\alpha)\right)I_{1,\alpha}(\mathbf{r}_\alpha)I_{2,\alpha}(\mathbf{r}_\alpha), \quad (5.27)$$

where $\mu_M=\sum_{i=1}^{m}\mu_i$ is the bulk chemical potential of the chain and the $\mathrm{K}\exp(\beta\varepsilon_0)$ terms in equation (5.15) for $\Delta^{\alpha\alpha'}$ can be eliminated as they cancel with the equivalent terms in μ_M. The expressions $I_{1,\alpha}(\mathbf{r}_\alpha)=\left[\exp\left(\beta\sum_{i=1}^{\alpha-1}\mu_i\right)\chi_B^{\alpha}(\mathbf{r}_\alpha)\right]^{-1}$, and $I_{2,\alpha}(\mathbf{r}_\alpha)=\left[\exp\left(\beta\sum_{\alpha-1}^{m}\mu_i\right)\chi_A^{\alpha}(\mathbf{r}_\alpha)\right]^{-1}$ are multiple integrals that can be evaluated using the recurrence relationships

$$I_{1,\alpha}(\mathbf{r}_\alpha)=\int d\mathbf{r}_{\alpha-1}I_{1,\alpha-1}(\mathbf{r}_{\alpha-1})D_{\alpha-1}(\mathbf{r}_{\alpha-1})\Delta^{(\alpha-1,\alpha)}(\mathbf{r}_{\alpha-1},\mathbf{r}_\alpha) \quad (5.28)$$

and

$$I_{2,\alpha}(\mathbf{r}_\alpha)=\int d\mathbf{r}_{\alpha+1}I_{2,\alpha+1}(\mathbf{r}_{\alpha+1})D_{\alpha+1}(\mathbf{r}_{\alpha+1})\Delta^{(\alpha,\alpha+1)}(\mathbf{r}_\alpha,\mathbf{r}_{\alpha+1}), \quad (5.29)$$

which are initialized with $I_{1,1}(\mathbf{r}_1)=I_{2,m}(\mathbf{r}_m)=1$. Substituting these expressions for the decoupled system back into equation (5.5) for the grand free energy gives

$$\beta\Omega\left[\{\rho_\alpha(\mathbf{r}_\alpha)\}\right]=\sum_{\alpha=1}^{m}\int d\mathbf{r}_\alpha\rho_\alpha(\mathbf{r}_\alpha)\left[D_\alpha(\mathbf{r}_\alpha)+\frac{n\left(\Gamma^{(\alpha)}\right)}{2}-1\right], \quad (5.30)$$

where $n\left(\Gamma^{(\alpha)}\right)$ is the number of association sites on the α^{th} segment. The interfacial tension is then defined as the difference between the inhomogeneous grand free energy and the homogeneous (bulk) grand free energy of the same system under the same conditions according to

$$\gamma = \Omega\left[\{\rho_\alpha(\mathbf{r})\}\right] - \hat{\Omega}\int d\mathbf{r}_\alpha , \tag{5.31}$$

where $\hat{\Omega}$ is the bulk grand free energy.

The *i*SAFT DFT was applied to the model system of Telo da Gama and Gubbins[222] to explore the effects of different system parameters on both the fluid microstructure and interfacial tension. Assuming a planar oil-water interface, the inhomogeneity was considered only in the dimension normal to the surface of the interface (z). With no external field applied to the system, the bulk chemical potentials and densities for the coexisting oil-rich and water-rich phases are determined using the homogeneous limit of the DFT (the SAFT equation of state) to perform a simple flash calculation. To numerically calculate the equilibrium density profiles, the domain is divided into equally spaced grid points along the dimension normal to the surface. As mentioned previously, to allow for sufficient convergence to the bulk limit at each boundary, a domain of $L = 20\sigma$ was used. Additionally, to achieve adequate resolution of the density profiles, all calculations used a discretization size of 0.05σ. Infinite bulk boundary conditions are implemented at both boundaries to avoid potential interaction between the interfaces of neighboring calculation domains that can be encountered with periodic boundary conditions and a minimum image convention. The profiles are

solved for using Picard's iteration method. The initial guess is a step profile from one bulk phase to the other at the middle of the domain. At every iteration, an estimate of the density for every segment is calculated using equation (5.27). The calculated density profile at each grid point is mixed with the old profile to provide a new density profile. Iterations continue until the density profiles no longer change appreciably. All numerical integrations are performed using a composite Simpson's rule.

5.3 Results and Discussion

As discussed above, the phase behavior, microstructure, and interfacial properties of surfactant systems are sensitive to multiple parameters making an extensive study of parameter space by experiments or molecular simulation quite difficult. This study aims to use the *i*SAFT DFT to confirm observed behavior relative to some of these parameters and provide molecular level insight to the physics/thermodynamics governing this behavior. All of the systems studied here approximate the interface between two liquid-like phases as planar.

5.3.1 Effect of Chain Length

In our previous work,[111] the application of *i*SAFT to the model system outlined above was validated against the molecular simulation work of Smit *et al.*[221,225] This demonstrated the capability of *i*SAFT to accurately reproduce the microstructure of an H_1T_1 surfactant at an oil-water interface. Predictions of the interfacial tension behavior as a function of the surface loading for H_1T_1, H_1T_3, and H_1T_5 surfactant structures also showed excellent agreement with their simulation results. When only the structure normal to the interface is of interest, the DFT

calculations are simplified by taking advantage of system symmetry to reduce the problem to a single dimension of inhomogeneity (z). This leads to a significantly easier exploration of parameter space which starts with extending the hydrophobic tail length in both the single head single tail (H_1T_n) and symmetric diblock copolymer (H_mT_m) series of structures. Figure 5.3 and Figure 5.4 show the interfacial tension predictions by the theory as a function of the equilibrium bulk solubility of the surfactant in the aqueous phase for both of these structure types. These results show the additional tail segments improve the effectiveness of the surfactant as less bulk dissolved surfactant is required to achieve the same interfacial tension. This behavior is qualitatively consistent with Traube's rule[287] and experimental observations (e.g., see the work by Smit *et al.*[225] for *p*-(*x*-alkyl)benzene sulfonates) for low to moderate surfactant concentrations. Given the assumption of a planar interface, these calculations are unable to capture any curvature of the interface or formation of more complex structures such as micelles. Thus, these predictions do not exhibit the characteristic break towards limiting behavior consistent with micellization at higher surfactant concentrations. However, the stabilization of a single micelle can be modeled using radial coordinates with the inhomogeneity still in the single dimension normal to the surface (r). With the DFT framework derived generally for multiple dimensions, even more complex fluid architectures are also reproducible since the assumption of system symmetry can be relaxed. These extensions are the focus of potential future work on similar surfactant systems.

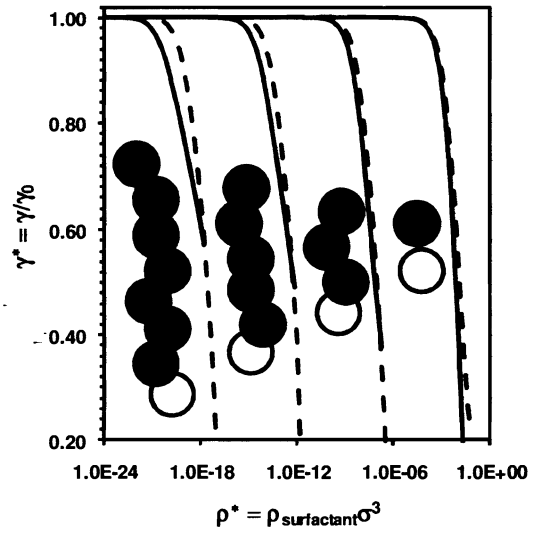

Figure 5.3 Semilog plot for the effect of surfactant structure and bulk aqueous surfactant concentration on the scaled interfacial tension at $P^* = \beta P/\rho = 2.66$ for a series of linear single head single tail surfactants. Predictions made using *i*SAFT for an oil molecule with $m = 1$ (solid curves and $m = 8$ (dashed curves). The scaling factor (γ_0) is the interfacial tension of the bare oil-water interface.

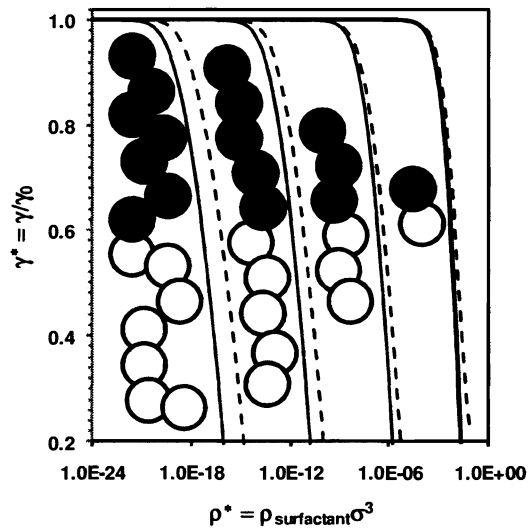

Figure 5.4 Semilog plot for the effect of surfactant structure and bulk aqueous surfactant concentration on the scaled interfacial tension at $P^* = \beta P/\rho = 2.66$ for a series of diblock symmetric surfactants. Predictions made using *i*SAFT for an oil molecule with $m = 1$ (solid curves and $m = 8$ (dashed curves). The scaling factor (γ_0) is the interfacial tension of the bare oil-water interface.

With the bulk chemical potential driving the DFT calculations for the equilibrium fluid microstructure, the equal spacing between the curves for the single head single tail structures in Figure 5.3 suggests the log of the bulk solubility, and consequently bulk chemical potential, is a linear function of the chain length. This linear dependence for a SAFT based equation of state was expected following the theoretical derivations of Ghonasgi *et al.*[154] They showed the log of the solubility of a polyatomic solute in its antisolvent is a linear function of the solute chain length. Other than the presence of the single water-like head segment, the surfactant molecules are essentially oil-like chains, and the potential model being used makes water its antisolvent. Thus, the equal spacing confirms the SAFT equation of state as the *i*SAFT homogeneous limit. The symmetric diblock copolymer surfactants of Figure 5.4 show a similar spacing; however, the addition of a water-like head segment for each additional oil-like tail segment mean the dependence is no longer linear.

While the impacts on observable characteristics or experimentally measurable properties provide connections to applications, it is the equilibrium fluid structure that provides insight into the governing physics. Figure 5.5 shows a series of converged equilibrium density profiles for the H_7T_7 surfactant. As anticipated with such a harsh potential model, increasing the amount of surfactant dissolved in the bulk corresponds to a significant increase in the aggregation of surfactant at the interface. This is because the forced connection between the hydrophilic head group and hydrophobic tail group makes it energetically favorable to partition to the interface. In addition, as surfactant

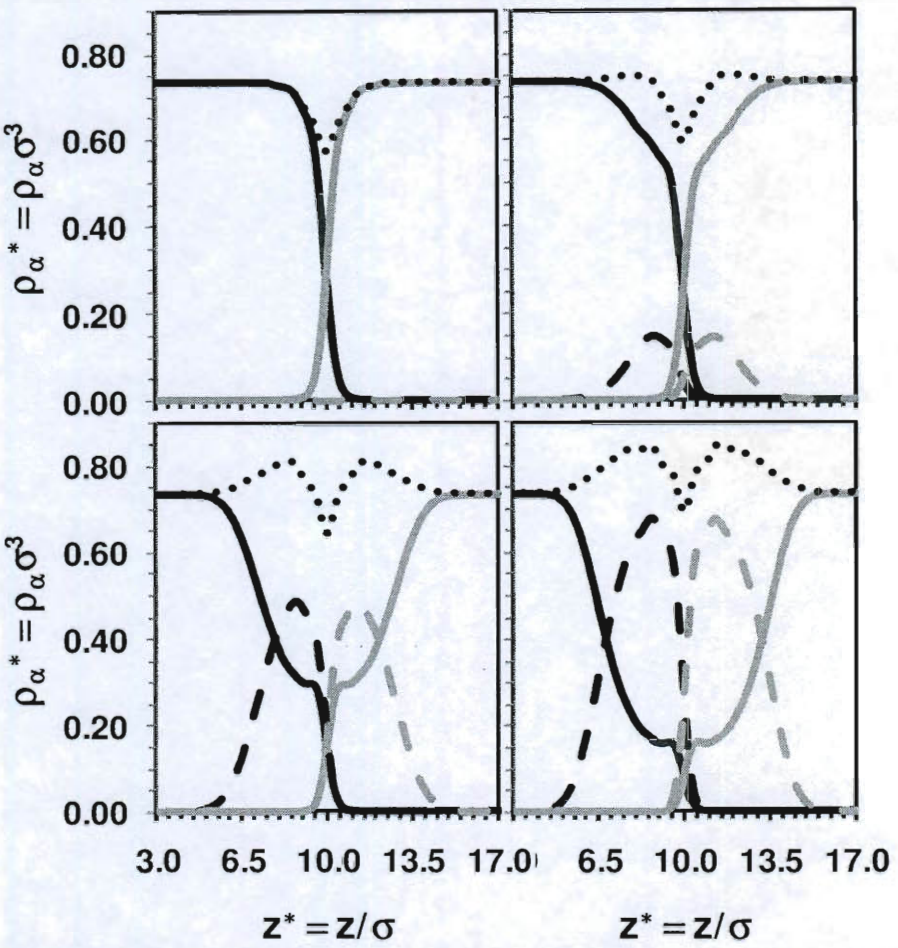

Figure 5.5 Equilibrium fluid microstructure from *i*SAFT for a H_7T_7 surfactant using an $m = 1$ oil molecule with bulk surfactant mole fractions of $x_{H_7T_7}^{H_2O} = 10^{-21}$ (top left), 10^{-18} (top right), 10^{-15} (bottom left), and 10^{-12} (bottom right). Curves are for the oil (solid black), water (solid grey), tail (dashed black), head (dashed grey), and total (dotted black) segment density profiles.

accumulates, solvent molecules are squeezed away from both sides of the interface, forming a large depletion region which reduces the effective contact surface area for unfavorable segment interactions, while increasing preferred segment interactions and reducing the interfacial tension (Figure 5.4).

There are two very interesting observations here. First, with an interface centered at $z^* = z/\sigma = 10.0$ and seven surfactant segments with diameter σ on either side of that interface, full extension of the surfactant would mean the head and tail segment density distribution profiles should extend to $z^* = 16.5$ and $z^* = 3.5$, respectively; however, they are much closer to the interface. Secondly, at the higher surfactant concentrations (bottom row of Figure 5.5), there is a distinct 'kink' in the solvent profiles. Since *i*SAFT is formulated using a segment density basis, profiles for the individual segments in the chain can be separated from the overall density distribution of a specific segment type to gain a better understanding of the behavior. Figure 5.6 shows a more detailed set of density profiles where the terminal and center segment density profiles of the surfactant have been separated from the rest of the chain. As expected from the harsh potential model, the central head and tail segments are pinned to the interface as indicated by their sharp narrow peaks within approximately $\pm 0.5\sigma$ of the interface. On the other hand, the terminal segments show a broad distribution centered near 2.75σ away from the center of the interface. This suggests a collapsed head and tail structuring on either side of the interface which could be qualitatively approximated by a diatomic surfactant molecule with a larger segment diameter similar to the depiction in Figure 5.7. In such a case, the figure also demonstrates how the packing of these larger spheres leaves interstitial spaces large enough to trap solvent molecules near the surface leading to the 'kink' in the oil and water density profiles. The collapsed nature of the surfactant differs from the typically accepted conceptual image of a fully

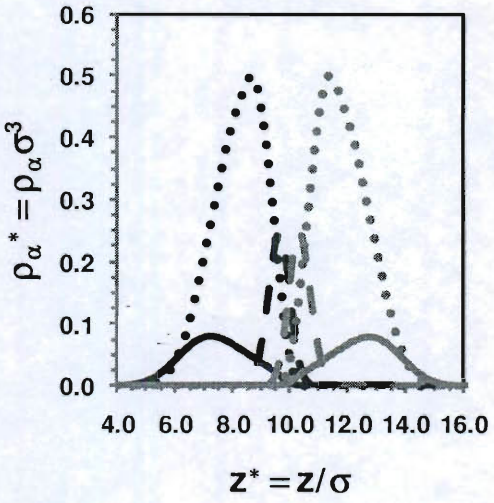

Figure 5.6 Detailed equilibrium segment density profiles for the symmetric diblock H_7T_7 surfactant at bulk mole fraction $x_{H_7T_7}^{H_2O} = 10^{-15}$ (bottom left of Figure 5.5). Curves are the head group (grey) and tail group (black) terminal (solid), central (dashed), and internal (dotted) segment density profiles.

extended surfactant, but it is a result of the thermodynamics at these particular system conditions. The energetically favorable extension of the tail segments into the oil, for example, is enthalpically driven by an increased available surface area for interaction with the solvent. Entropically, however, the more collapsed nature is the preferred conformation and dominates at equilibrium.

5.3.2 Oil Structure

Within the SAFT model, representing both oil and water with single spheres is highly unrealistic. While water is often modeled as a single associating sphere, the many alkanes that typically make up oil mixtures are better represented with chain-like molecules. Thus, the same calculations were done for the series of structures discussed in section 5.3.1 using a more representative eight segment chain for the oil molecule. Figure 5.3 and Figure

5.4 show the affect of this change on the interfacial tension predictions. While the qualitative behavior is very similar, the surfactants have become less effective (i.e., more surfactant is needed to achieve the same interfacial tension).

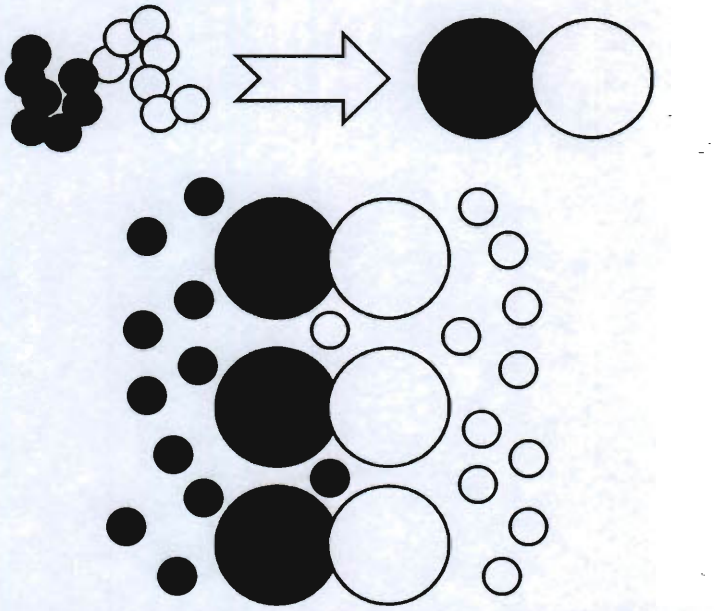

Figure 5.7 Visual representation of the collapse interfacial packing of a chain-like diblock symmetric surfactant approximated by a diatomic molecule with equivalent volume and the resulting "trapped" solvent molecules.

Given the series of equilibrium density profiles in Figure 5.8, the aqueous phase behaves consistent with the profiles where a single sphere oil molecule was used. The additional surfactant leads to a depletion of solvent near the surface and the 'kink' indicative of the collapsed packing of the head group trapping water molecules near the surface is still present. On the other hand, the oil phase is more densely packed and less susceptible to being squeezed away from the interface meaning there is a much narrower depletion region. This leads to a narrower and sharper peak in the tail density profile. With the tail groups packed tightly into such a narrow depletion region, it is more difficult for

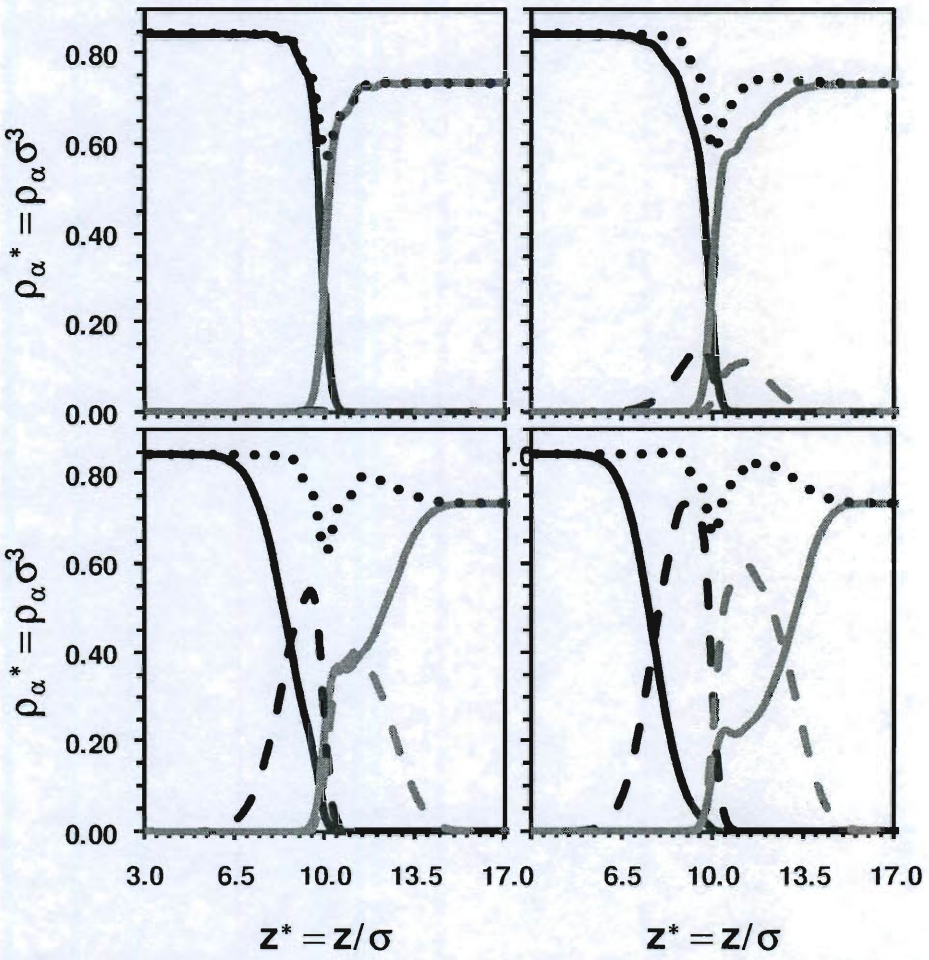

Figure 5.8 Equilibrium fluid microstructure from *i*SAFT for a H_7T_7 surfactant using an $m = 8$ oil molecule with bulk surfactant mole fractions of $x_{H_7T_7}^{H_2O} = 10^{-38}$ (top left), 10^{-36} (top right), 10^{-34} (bottom left), and 10^{-32} (bottom right). Curves are for the oil (solid black), water (solid grey), tail (dashed black), head (dashed grey), and total (dotted black) segment density profiles.

the surfactant molecules to partition to the interface – the packing frustration reduces the favorable energetic benefits leading to the need for more bulk dissolved surfactant to achieve the same interfacial tension. In addition, the larger oil molecule and tightly packed depletion region does not provide adequate interstitial spacing to trap the larger solvent molecules near the surface. Thus,

there is no longer a 'kink' in the oil profile. With this harsh pair potential, these results are qualitatively similar to *i*SAFT predictions for chain confirmations of polymer brushes as a function of grafting density and solvent chain length.[112,114]

5.3.3 Single vs. Double Tail Surfactant Structure

Despite multiple industrial applications of surfactants using branched hydrophobic tail groups, little is understood about the effect branching has on the system microstructure and thermodynamic or interfacial properties. Studies have been done to investigate the effect of branching on interfacial tension by self-consistent field theory and molecular dynamics simulations of model surfactants[288-290] These studies all concluded that the branched tail structures were less effective than their single tail equivalent (more dissolved surfactant in the bulk aqueous phase to achieve the same interfacial tension). Depending on the nature of the setup, experimental studies[290-294] have reported branched surfactants are more, equal, or less efficient. The presumption has been that these differences are due to different packing of branched surfactants in the interface compared to linear ones.[295,296] Rekvig *et al.*[289] used dissipative particle dynamics to investigate the molecular description of branching effects on interfacial tension. They conclude the head group properties, specifically through the packing and ordering of the molecules, are the governing effects on the interfacial tension. In addition, they identify partitioning of the surfactant between the bulk fluid phases and the interface as a significant contributor to the surfactant efficiency. As discussed above, molecular simulations are highly inefficient and often ineffective at modeling such systems with trace components

in an explicit solvent bulk phase in direct contact with an interface highly populated with that same trace component due to the very low bulk concentrations and long diffusion times.[289] DFT approaches, such as *i*SAFT, do not suffer from these same shortcomings. Thus, *i*SAFT has been applied to assess the effects of symmetry using the representative series of model surfactant structures all with six tail segments illustrated in Figure 5.9.

The left plot in Figure 5.10 shows *i*SAFT predictions for the interfacial tension as a function of bulk surfactant density for this series. These results show the single tail structure requires less surfactant in the bulk water phase to achieve the same interfacial tension as the other asymmetric structures meaning it is more effective consistent with the behavior the previous studies. These predictions also show the impact on the effectiveness decreases as the location of the head group is shifted to a more symmetric position. The experimental

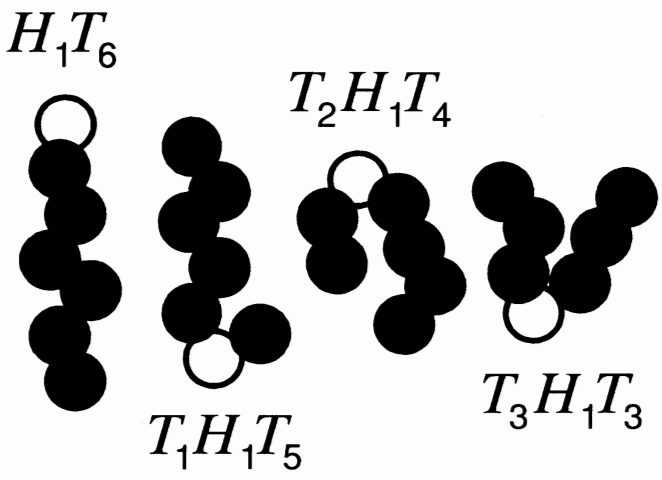

Figure 5.9 Structure permutations containing a single head segment and six tail segments for assessing the shift in head group location.

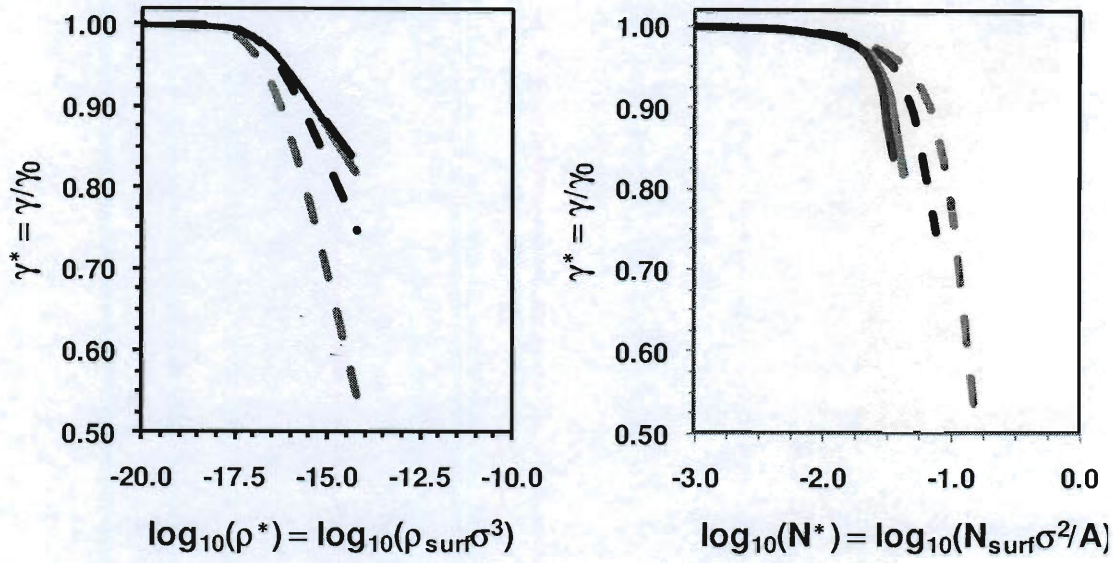

Figure 5.10 Performance effects on the scaled interfacial tension of the bulk surfactant concentration (left) and number of surfactant molecules per unit area in the interface (right) for the structures H_1T_6 (solid black), $T_1H_1T_5$ (solid grey), $T_2H_1T_4$ (dashed black), and $T_3H_1T_3$ (dashed grey).

work of Doe *et al.*[297] and found similar observations. Systematically shifting the benzene sulfonate head group from end to midpoint attachment in a series of alkylbenzene sulfonate surfactants showed less sensitivity to composition and an increase in the interfacial tension for multiple alkyl groups. Adkins *et al.*[298] also showed qualitatively similar behavior for nonionic surfactants at air-water and carbon dioxide-water interfaces. Extension of the current study to all surfactant structure combinations with five, seven, and eight tail segments has also produced results consistent with these experiments.

While effectiveness of a surfactant is a valuable measure, equally important is its efficiency. This is directly connected to its ability to partition from the bulk to the interface and how well it packs once at the interface. With all the

surfactant structures studied here having just a single head segment, integrating the head segment density profile in the interface gives the surface loading $\left(N^* = N_{\text{surfactant}}\sigma^2/A\right)$, or number of surfactant molecules per unit area. The right plot in Figure 5.10 shows how this surface loading affects the interfacial tension and interpretation of surfactant performance. The completely symmetric $T_3H_1T_3$ surfactant actually requires a lower surface concentration of molecules at the interface than its more asymmetric counterparts to achieve the same interfacial tension. Comparing the standard deviation of the peaks in the head density profiles for the different surfactants at the same surface coverage showed increased symmetry leads to narrower peaks (smaller standard deviation). This indicates a tighter ordering of the head groups and a greater excluded volume effect from the two tails whose available conformations are restricted causing them to more efficiently squeeze the solvent away from the interface. As the surfactant becomes more asymmetric, the peaks broaden for the same surface concentration of surfactant molecules suggesting a looser packing or staggering. This relaxes the packing frustrations of the attached fully flexible tail groups allowing them to more easily accommodate additional oil molecules near the surface. Thus, while the symmetric double tail structure is much more efficient in reducing the interfacial tension, its chemical potential at the surface is much higher than the other structures, and this chemical potential decreases by increasing the asymmetry all the way down to the single tail surfactant. Matching this chemical potential in the bulk to achieve equilibrium translates into a higher bulk surfactant concentration. Equivalently, this means the H_1T_6 surfactant

partitions to the interface more readily, but shifting the head group location improves performance provided the surfactant can be pushed into the interface.

5.3.4 Mixed Surfactant Systems

While the results of sections 5.3.1, 5.3.2, and 5.3.3 have demonstrated how the presence of a single surfactant can have a profound effect on the fluid microstructure and interfacial properties of the liquid-liquid interface between distinctly different solvents, many industrial and commercial applications actually employ mixtures of multiple amphiphiles to achieve the desired properties. Whether combinations of anionic/cationic,[299-301] nonionic/anionic,[302-307] or nonionic/cationic[308-311] surfactants, it has been found that using mixtures are often more robust and more capable of optimizing the system for a particular property than the individual surfactants.[312] This enhanced performance through the use of a co-surfactant is known as synergism. With advancements in computing power, there have been a few synergism studies done using molecular simulation[302,312-316] to investigate the molecular level behavior; however, they often have to use significantly coarse-grained models to account for the dilute bulk phases and efficiently access the length and time scales of interest. As an example, the dissipative particle dynamics simulations of Li *et al.*[312] demonstrated synergistic behavior of a mixture of sodium dodecylbenzene sulfonate (SDBS) and Triton X-100 (TX-100) at an oil-water interface where salinity was introduced through affects on the repulsion parameters of a coarse-grained model. By optimizing the mixture, the interfacial tension was lowered at concentrations lower than the critical micelle concentration of either individual

surfactant and an ultra-low interfacial tension was found at an optimal salinity. Consistent with results shown within this work, they found the nonionic TX-100 readily partitioned to the interface. On the other hand, the salinity had to be adjusted to promote SDBS partitioning. Rather than evenly covering the interface, SDBS aggregated into patches leaving cavities which the TX-100 was appropriately sized to fill leading to lower interfacial tension.

Currently, theoretical developments are being explored for implementing charges into *i*SAFT explicitly. Thus, these initial calculations for mixed surfactant systems investigate a mixture of nonionic surfactants. Synergistic behavior similar to the simulation study described above is possible for nonionic mixtures provided the relative difference in partitioning to the interface by the two surfactants is significant enough. Based on the single tail *i*SAFT results and analysis from previous work,[111] the hypothesis was an appropriate mixture of the H_1T_3 and H_1T_7 surfactants would exhibit the behavior of an H_1T_5 surfactant. Figure 5.11 shows how adding H_1T_3 to a system with fixed H_1T_7 bulk aqueous mole fraction affects the interfacial tension with reference curves given for the H_1T_3, H_1T_5, and H_1T_7 surfactants. The left plot shows a systematic shift at low H_1T_3 concentrations as more H_1T_7 is used indicating behavior consistent with only the presence of H_1T_7 as expected. Increasing the amount of H_1T_3 shows its impact on the interfacial tension starts being felt, but all systems appear to converge to the H_1T_3 reference curve. Thus, the results are rescaled by the interfacial tension of a system with only the designated amount of H_1T_7 and Figure 5.11b

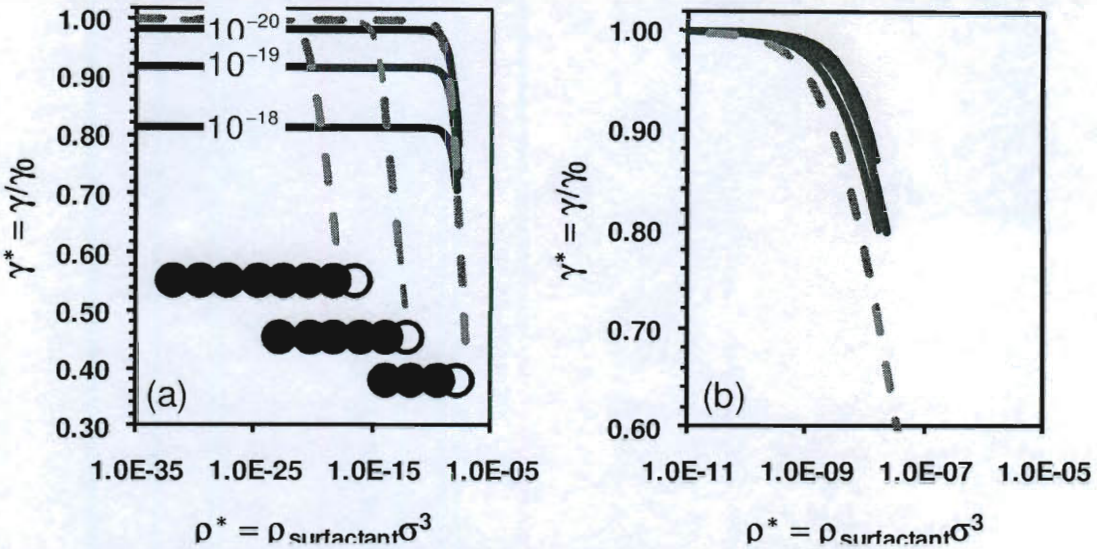

Figure 5.11 Effect of the total bulk aqueous phase surfactant concentration on the scaled interfacial tension. Curves are *i*SAFT predictions for a mixture of H_1T_3 and H_1T_7 (solid black) with the labeled bulk mole fractions $\left(x_{H_1T_7}^{H_2O}\right)$ and the indicated single surfactant systems (dashed grey) for reference. The scaling factors are the interfacial tension of (a) the bare oil-water interface and (b) the H_1T_7 single surfactant system with its corresponding bulk mole fraction.

demonstrates how these curves essentially collapse to the H_1T_3 curve with only a small decrease in the effectiveness for the different mixed systems. These suggest the presence of the second surfactant is negligible with respect to the interfacial tension, but potential changes in the fluid microstructure affecting the efficiency are only discernable with the equilibrium density profiles.

A series of equilibrium density profiles are given in Figure 5.12 to demonstrate the effects adding either surfactant has on the observed fluid behavior. In addition, magnified profiles of only the surfactant head and tail groups for both surfactants are given in Figure 5.13 for clarity. As expected from results in section 5.3.1 for structural changes that occur when longer tail groups

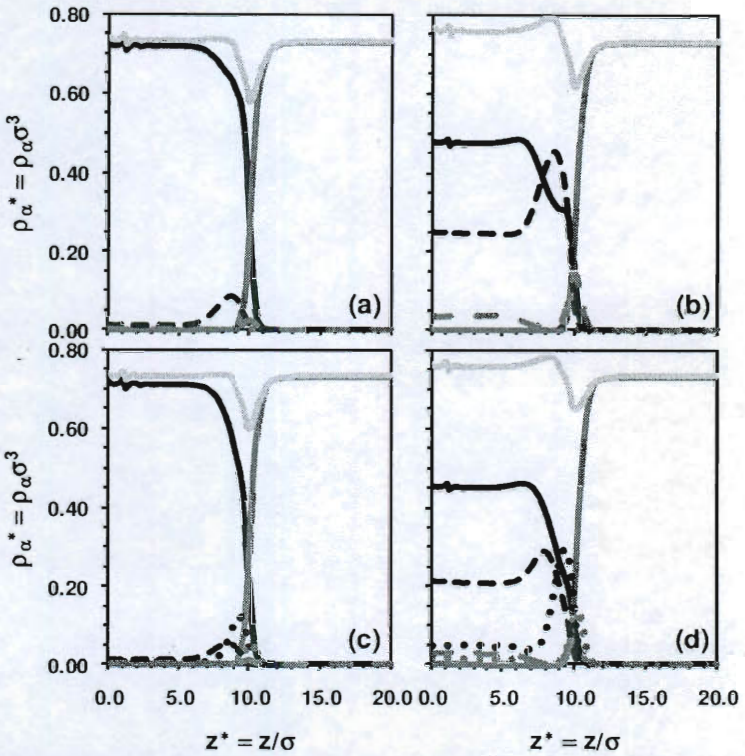

Figure 5.12 Equilibrium density profiles for a mixed surfactant system containing H_1T_3 and H_1T_7 from *i*SAFT. Black curves are oil-like segments, dark grey curves are water-like segments, and light grey curves are total segment density. Solid lines are solvents, dotted lines are for H_1T_3, and dashed lines are for H_1T_7. Fixed bulk mole fractions are $x_{H_1T_3}^{oil} = 10^{-4}$ (a and b), $x_{H_1T_3}^{oil} = 10^{-2}$ (c and d), $x_{H_1T_7}^{H_2O} = 10^{-20}$ (a and c), and $x_{H_1T_7}^{H_2O} = 10^{-18}$ (b and d).

are used in a system with only a single surfactant, the solvent depletion region for oil is wider and more pronounced than that of water. The formation of such a depletion region is a result of the entropic benefit of the chains maintaining their collapsed conformation outweighing any increased enthalpic preference from extending into the solvent, and the larger excluded volume of multiple tail segments exacerbates this. Thus, the solvent molecules are pushed away from the interface leading to a reduced interfacial tension. When increasing the

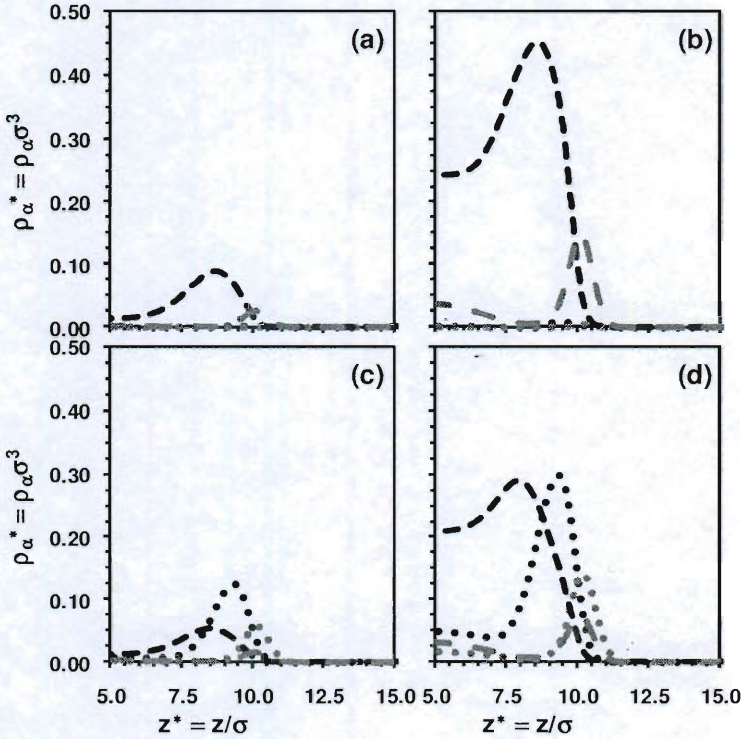

Figure 5.13 Magnified equilibrium density profiles from *i*SAFT for a mixed surfactant system focusing on the head and tail segment profiles. See Figure 5.12 caption for description.

concentration of H_1T_7 in the presence of only dilute amounts of H_1T_3 (frames a and c), this phenomenon appears to be independent of the presence of the cosurfactant. On the other hand, a very small increase in the amount of H_1T_7 dissolved in the bulk aqueous phase (comparing frames a and b) leads to a tremendous increase in its presence at the interface and solubility in oil. At this level of surfactant, the previously identified structuring of the tail segments collapsed near the interface in a longer chain is trapping oil molecules near the surface and causing a 'kink' in the oil density profile. Interestingly, increasing the amount of H_1T_3 in the system (frame d) mitigates this packing effect. Close

inspection of the surfactant profiles shows the head groups of both are still tightly packed near the interface with only a slight broadening for the H_1T_7 head group. However, the tight packing of the H_1T_3 tail segments has shifted and broadened peak for the H_1T_7 tail segments meaning there is now a more organized staggering and structuring right at the interface where the H_1T_3 tail segments have essentially taken the place of previously trapped oil molecules similar to the observed synergistic behavior of the SDBS and TX-100 simulations described above. In addition, this efficiently packed dense layer of oil-like tail segments causes depletion in the water-like head segments before rebounding to the bulk oil-rich phase limit. This suggests the presence of a higher order structure serving as a stabilizing layer between the bulk phase and the interface which would require higher dimension calculations to confirm and characterize.

5.3.5 Temperature Effects

Despite the mitigation of trapped oil molecules near the surface at higher aggregation of H_1T_7 in the interface, there is no observed synergistic effect on the interfacial tension. This is likely because the relative difference in partitioning by the two surfactants is not sufficiently large. There are several other mechanisms for altering how the surfactant partitions including changing the dimensionless temperature. While the previous section discussed the common use of mixed surfactants involving ionic surfactants, it is commonly the behavior of included nonionic surfactants that dominate. Several experimental works (e.g., see Hou and Li[317]) have explored the dependence of these systems on temperature, salt

concentration, and surfactant concentration. Hou and Li[317] showed that although the anionic surfactant becomes more hydrophilic, the increase in the hydrophobicity of the nonionic surfactant is much greater with increasing temperature. In fact, Anton *et al.*[318] quantified the effect as being approximately six times greater on the nonionic surfactant meaning anionic-nonionic surfactant mixtures behave qualitatively similar to single nonionic surfactants.[317] Thus, studying temperature effects on these single nonionic surfactant systems will provide insights into mixed surfactant systems and how to appropriately tune system parameters to find synergistic combinations. As an example, Figure 5.14 shows two perspectives of the same *i*SAFT predicted effects of both temperature and bulk aqueous surfactant concentration on the interfacial tension for an H_1T_5 surfactant. According to these predictions, either increasing the interaction energies or reducing the temperature to achieve an increase in the dimensionless temperature will improve the effectiveness of the surfactant (less surfactant necessary in the equilibrium bulk aqueous phase to achieve a given interfacial tension). Changes in nonionic surfactant performance in response to the thermal energy of the system were attributed to increased tail group salvation by Adkins *et al.* As expected, a certain threshold of surfactant is required before the interfacial tension is affected and this breakpoint depends on the temperature. Interestingly, there is no improvement gained by changing the interaction energies or temperature below a certain amount of surfactant. Also, at a dimensionless temperature of approximately $T^* = 0.525$, no amount of surfactant causes an improvement to the interfacial tension.

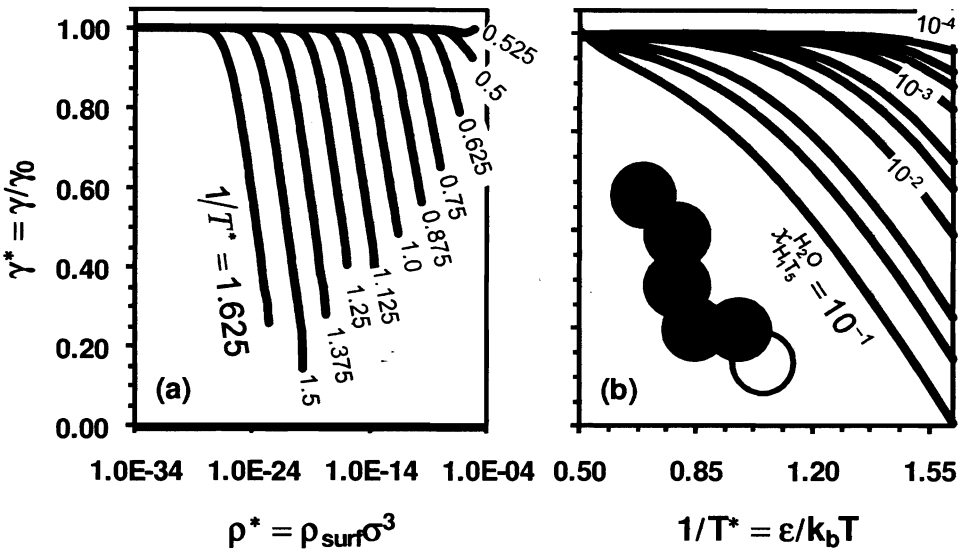

Figure 5.14 Effects on the *i*SAFT predicted scaled interfacial tension for the dimensionless temperature $\left(T^* = k_b T/\varepsilon\right)$ and surfactant concentration in the bulk aqueous phase for an H_1T_5 surfactant. Plots show curves for (a) isotherms and (b) constant bulk compositions.

To better understand these trends, Figure 5.15 shows several equilibrium density profiles for different dimensionless temperature and bulk oil surfactant mole fraction combinations. No matter the temperature, increasing the amount of surfactant in the oil produces changes in structuring consistent with the analysis in section 5.3.1. Additional surfactant in the bulk translates to increased aggregation in the interface which squeezes out solvent molecules creating depletion regions on either side of the interface. Naturally, having more tail segments than head segments creates a larger depletion of oil than water. The characteristic 'kink' in the oil profile consistent with the collapsed tail group trapping some of the solvent molecules can also be seen (especially at higher surfactant concentrations).

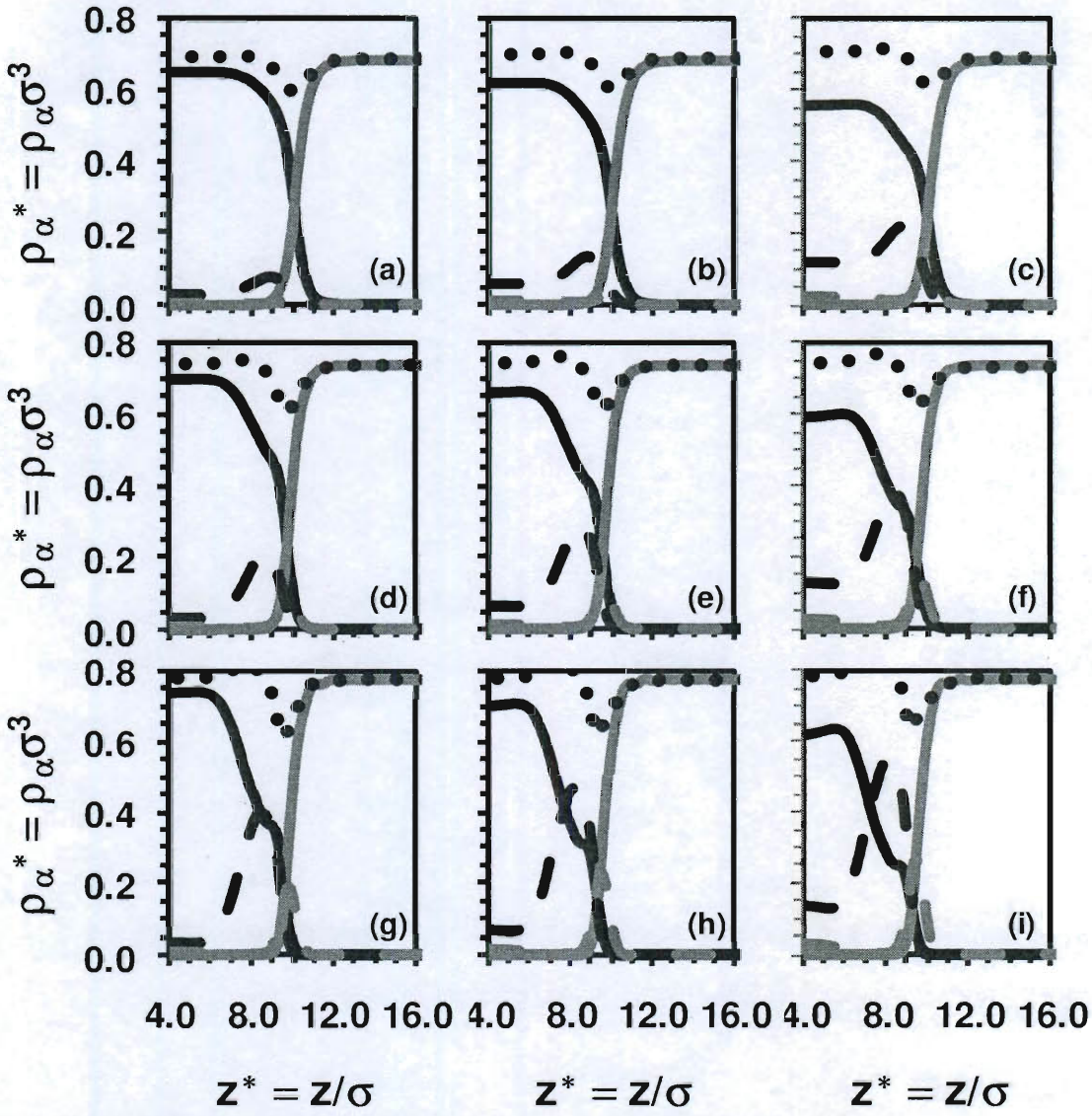

Figure 5.15 Effect of dimensionless temperature (T^*) and bulk oil phase mole fraction of surfactant $\left(x_{H_1T_7}^{oil}\right)$ on the *i*SAFT equilibrium density profiles for an H_1T_5 surfactant. Curves are for oil (solid black), water (solid grey), tail (dashed black), head (dashed grey), and total (dotted black) segment density profiles at the conditions $1/T^* = 0.75$ (a-c), $1/T^* = 1.00$ (d-f), $1/T^* = 1.25$ (g-i), $x_{H_1T_7}^{oil} = 0.05$ (a, d, g), $x_{H_1T_7}^{oil} = 0.10$ (b, e, h), and $x_{H_1T_7}^{oil} = 0.20$ (c, f, i).

More interesting conclusions are found when looking at changes to the fluid microstructure in response to changes in the temperature (or interaction energies). When the temperature is increased (frames a-c), the peaks for the tail segments in the interface get broader and shorter. This indicates greater staggering and looser packing which eliminates the trapping of solvent molecules near the interface. Thus, the relative partitioning of the surfactant is decreasing and the entropic penalty for the chains to extend is reduced relative to the improved enthalpic benefit. The equilibrium structure is also approaching that of the contact between a bulk oil phase and bulk water phase which explains why there is less affect on the interfacial tension. Pushing this to its limit by continuing to increase the temperature reduces the system to the oil-water system no matter how much surfactant is introduced. This was the case with the flat curve for $1/T^* = 0.525$ in Figure 5.14. If the temperature is decreased instead (frames g-i), the tail segment distribution near the interface increases and becomes much narrower indicating the thermodynamics have a much stronger entropic preference. Because of this, the surfactant molecules become highly structured and the trapping of oil molecules occurs at a much lower bulk concentration than seen previously. These equilibrium profiles also indicate the surfactant molecules feel a much stronger preference for the interface than remaining in the bulk disordered phases. It is this change in preference for the interface which can be useful in determining the best cosurfactants to achieve mixed surfactant synergy.

5.4 Conclusions

In this work, a systematic study through part of the vast multidimensional parameter space of an oil-water-surfactant system was done using the *i*SAFT polyatomic segment-based DFT. This molecular model, originally developed by Tripathi and Chapman[25,26] from the work of Segura *et al.*[20,21] and later corrected for stoichiometric consistency of heteronuclear chains by Jain *et al.*,[24] captures the molecular level physics and thermodynamics necessary to describe the equilibrium fluid microstructure and interfacial properties of complex fluids such as surfactants. The DFT is based on Rosenfeld's fundamental measure theory[97] formalism for hard spheres and accounts for chain formation using the complete bonding limit of Wertheim's first-order thermodynamic perturbation theory[15-18] for associating spheres. Attractive interactions between segments are treated using a mean-field approximation.[275]

Based on the original simple pair potential for the continuum model of Telo da Gama and Gubbins,[222] the density functional theory provides insights into the phenomena governing affects on the interfacial tension and fluid microstructure by parameters such as the molecular structure of both the oil and surfactant, presence of cosurfactants, and temperature. From the results of this work and our previous work[111] which validated this approach against the molecular simulations of Smit *et al.*,[221,225] there are several general system behavior observations. The harshness of the pair potential encourages partitioning of the surfactant to the interface. Structuring of the head group and tail group segments on either side of the interface pushes solvent molecules away forming

depletion regions in the oil and water density profiles and a dimple in the total segment density profile consistent with a reduction in the interfacial tension. Based on the equilibrium density profiles, the surfactant molecule tends to collapse on the surface. The nature of this interfacial structure is determined by the system thermodynamics and a competition between enthalpic and entropic driving forces. At high enough aggregation of an amphiphile with a sufficiently long chain length, solvent molecules are small enough to be trapped within interstitial void spaces right at the interface. This comes from a "balled up" collapsed surfactant structure which forms as a result of the entropy dominating any enthalpic improvements to the free energy through increased attraction between the segments in an extended chain conformation. This is schematically approximated by a diatomic surfactant with an equivalent excluded volume.

One of the more intuitive ways to affect the observed properties is through the structure of the surfactant. Increasing the tail length of the single head single tail or diblock symmetric molecular architecture increased the effectiveness of the surfactant through an exaggeration of the effects described above where the effectiveness is defined by the obtainable interfacial tension for a given amount of surfactant dissolved in the bulk aqueous phase at equilibrium. However, as demonstrated with a comparison of head group location in double-tail structures, improved effectiveness does not imply more efficiency. While a lower interfacial tension at a given bulk aqueous phase concentration is obtained using the completely asymmetric single head single tail structure, packing effects lead to the need of fewer surfactant molecules in the interface to achieve a particular

interfacial tension when the head group is shifted to the midpoint making the symmetric structure more efficient. Thus, the single tail isomers more readily partition to the interface, but branching (at least into two tails) leads to better performance per molecule in the interface.

The surfactant partitioning and fluid structure were also shown to be significantly impacted by the oil structure, presence of a cosurfactant, and temperature. A more realistic chain-like oil molecule produces a much denser bulk oil phase that is more difficult for the surfactant to penetrate or squeeze away from the interface. As a result, there is a much narrower depletion region for the tail groups to pack into leading to decreased partitioning and lower effectiveness. However, this oil molecule is no longer capable of fitting into any of the void spaces created by the collapsed amphiphilic chains. The theory also showed how the trapping of solvent molecules near the surface can be mitigated through the use of a cosurfactant or changes in the temperature. The mutual structuring of two single tailed collapsed surfactant molecules with different tail lengths showed how the longer tailed surfactant reorients itself to make room for the shorter chain surfactant near the surface which leaves no room for the solvent. While this had no discernable impact on the interfacial tension of the model system at an assumed planar interface, it is believed this will affect higher order structuring and/or micellization. On the other hand, increasing the temperature (or decreasing the interaction energies) showed a decrease in the harshness of the pair potential leading to increased probability of more extended chain conformations. When taken to its limit, the system exhibits no discernable

difference when compared with an oil-water system which means there is much lower partitioning to the interface no matter how much surfactant is added. However, decreasing the temperature (or increasing the interaction energies) has the opposite effect. There is a dramatic increase in the preference for the interface leading to significant reductions in the interfacial tension.

This study has not only demonstrated the capability of at least qualitatively reproducing experimentally observed behavior, but it has also shown the ability of the *i*SAFT density functional theory to serve as a tool for assisting in the exploration of potential surfactant systems. Such a tool could streamline the time-consuming laboratory investigations looking for specific performance characteristics. Combinations of the structure-property relationships studied here along with continued theoretical development will serve as guides for continued exploration of these complex systems using the *i*SAFT DFT. Continued development will produce improvements in the tool's capability of identifying promising systems with greatest potential that can be further refined through laboratory studies.

5.5 Future Work

Throughout this work, the assumption was that calculations for all systems in all parts of phase space were in the stable liquid-liquid region and could be adequately approximated with a planar interface. However, experimental studies for several nonionic surfactants, such as the series of polyoxyethylene alcohols $\left(C_iE_j = \mathrm{H(CH_2)_i(OC_2H_4)_jOH}\right)$, have shown that liquid-liquid-liquid equilibrium with the potential for Windsor type phase behavior is present under the

appropriate thermodynamic conditions. In this region of phase space, the middle surfactant-rich phase will either wet or dewet the interface between the upper oil-rich phase and lower water-rich phase. When this middle phase completely wets that interface, the interfacial tensions obey Antonow's rule;[319] however, when that interface is only partially wet by the surfactant-rich phase, the interfacial tensions are related through Neumann's inequality.[320] It has been shown experimentally that the surfactant chain length is a key feature in determining the wetting behavior of the oil-water interface. Systems with short chain surfactants such as C_4E_1 and C_4E_1 exhibit wetting middle phases at all temperatures.[321,322] On the other hand, longer chain surfactants like C_9E_3 have demonstrated non-wetting behavior at all temperatures.[323,324] Perhaps more interestingly, surfactants with intermediate chain lengths can have a wetting transition where they transition from non-wetting behavior to completely wetting.[325-327] Extending the current work for model systems to first perform a flash calculation for such a three liquid phase system and then correlate this with an appropriate set of initial guess density profiles within the *i*SAFT DFT could provide some significant insight. The flexibility and robustness of *i*SAFT would allow for a detailed study of multiple structures to define heuristics for the minimum chain length necessary for complete wetting behavior and the maximum chain length for completely non-wetting behavior. It would also allow for the investigation of correlations between surfactant structure, oil structure, and the wetting transition temperature. Finally, this extension would allow for the investigation of Windsor type phase behavior where, for example, the interfacial tension is the same between the middle

surfactant-rich phase and both the upper oil-rich and lower water-rich phases in Windsor type III behavior.

As mentioned above, approximating the interface as planar has neglected any curvature of the interface and the potential for higher order microstructures. This does not allow for the determination of relevant system properties such as the critical micelle concentration, the phase diagram, and the characteristic curvature of the interface. In order to continue to take advantage of the segment-based free energy functionals and specifically characterize individual segments, these become increasingly important. As an example, consider using a larger segment diameter for the typically bulkier head group. This molecule will naturally pack differently in the interface and the appropriate system conditions would promote this interface to curve. This could allow the tail segments to more effectively push oil molecules away from the interface by not forming the larger collapsed structures that trap the solvent near the surface as described above. These effects can be investigated by moving to multiple dimensions of inhomogeneity or adopting different coordinate systems based on the assumed system symmetry. As outlined in section 5.3.1, the stability of individual spherical micelles could be studied by adopting a spherical coordinate system with a single dimension of inhomogeneity in the radial dimension. Similar to the approach used for determining the equilibrium lamellar spacing of symmetric diblock copolymers outlined by Jain *et al.*,[113] the most stable size of the micelle could be correlated to the surfactant structure and compared with other approaches such as the model of Blankschtein *et al.*[276-282] The stability of even more complex

multidimensional structures such as cylindrical micelles could be studied by yet again using system symmetry assumptions and a cylindrical coordinate system. Going to the complete three dimensional form of the functionals can be used to identify the specific spatial distribution of all the molecules. A full description of the fluid structure allows for the study of not only microphase behavior but also bulk and surface aggregation of the surfactant which was identified as an important characteristic of the mixed surfactant systems for instance. Naturally, with increased detail and complexity in the model comes increased computational cost. Thus, there is great value in pursuing the use of more sophisticated numerical integration techniques, numerical solvers, and streamlined coding possibly within either a parallel computing environment or conversion to the CUDA programming language to execute code on the much faster GPUs rather than CPUs. These technical developments are crucial if density functional theory is going to maintain its computational advantage over molecular simulation.

Lastly, this study has been carried out using adaptations of the basic continuum oil-water-surfactant model system proposed by Telo da Gama and Gubbins.[222] While this has served well for qualitatively reproducing observations from both molecular simulation and experiments, the eventual goal of this research is to quantitatively reproduce the properties of real systems with an interest in serving as a predictive tool for the targeted design of novel systems that take advantage of specific properties. To make this transition from investigating the molecular level physics of model systems to the specifics of real

systems, free energy functionals must continue to be developed to increase the physical descriptions of realistic behavior. Some of these include, among others, a theory for handling charged species or restricting the orientation of segments through intramolecular bonding. These and other developments are described in greater detail in section 3.5.

CHAPTER 6 CONCLUDING REMARKS

The work of this thesis has been focused on the extension and application of molecular models with an emphasis on the statistical thermodynamics of complex fluids. The statistical associating fluid theory (SAFT) equation of state for bulk fluids and interfacial SAFT (*i*SAFT) density functional theory (DFT) for inhomogeneous fluids were applied to complex systems with an emphasis on the phase behavior, thermodynamic properties, and fluid microstructure of mixtures involving dilute or trace components. Highlights of the important developments and key conclusions from these different applications are outlined below.

- A strategy was presented for determining the intrinsic perturbed-chain SAFT (PC-SAFT) parameters of complex species that exhibit interactions on multiple length scales (e.g., hydrogen bonding and polar substances). By considering dilute mixtures, it was demonstrated how the dimensionality of the nonlinear parameter fitting problem can be reduced using reasonable physical arguments for the negligibility of any anisotropic contributions. The resulting parameter set for water was used to reproduce experimental data for the vapor-liquid, liquid-liquid and vapor-liquid-liquid equilibrium of water with multiple alkanes across a myriad of physical conditions. These studies produced excellent qualitative and reasonably good to excellent quantitative agreement without employing a binary interaction parameter. Due to the limited availability of credible recommended mutual solubility experimental measurements, an accurate model for the phase behavior can be used to check the consistency of future reported data. With the acceptance of PC-

SAFT as an exceptionally accurate approach for modeling hydrocarbons (especially longer chain molecules), these parameters can be used to extend solubility predictions to branched and polymeric molecules or physical conditions where experimental data is either unavailable or difficult to obtain. In addition, the remaining polar and hydrogen bonding parameters could be fit using the commonly accepted technique and subsequently tested for performance in multiple mixture environments. Lastly, with a dispersion energy nearly twice what is commonly used in molecular simulation, it would be interesting to perform comparisons between current accepted simulation parameter sets and those reported here.

- Using the *i*SAFT DFT, the structure and interfacial properties of the model oil-water-surfactant system of Telo da Gama and Gubbins[222] was investigated. Within the model, oil and water are single spherical hard core segments that exhibit long-range attraction through a cut and shifted Lennard-Jones pair potential. These attractions were accounted for using a mean-field approximation within the theory. Surfactant-like molecules are created by bonding a specified number of oil-like and water-like segments into chains to form the desired topographical structure. From the DFT, the expected partitioning to the interface of surfactant molecules and its affect on the interfacial tension was captured. Comparisons of the equilibrium fluid microstructure for a fixed number of H_1T_1 molecules in the interface were compared with the molecular simulations of Smit,[221] and *i*SAFT showed excellent agreement. In addition, predictions of the corresponding interfacial

tension for H_1T_1, H_1T_3, and H_1T_5 structures as a function of the number of surfactant molecules in the interface demonstrated the capability of the theory to accurately capture the properties of the inhomogeneous system. The advantage of having a computationally efficient and self-consistent molecular theory that reduces to an accurate equation of state in the homogeneous limit was demonstrated through the direct determination of the trace component concentrations in the bulk. These validations for applying *i*SAFT to such a system were the basis for the extended study of parameter space.

- Based on quantitatively accurate reproduction of molecular simulations, application of *i*SAFT to a model oil-water-surfactant system similar to that of Telo da Gama and Gubbins[222] was extended to do a systematic study of several parameters affecting the structure and properties of an assumed planar interface.
    - Chain length

Increasing the tail length of a series of single head single tail and diblock symmetric surfactant structures accurately captured the improved effectiveness. As the surfactant partitions to the interface, it is unable to overcome the strong entropic preference to remain in a collapsed conformation. This structuring pushes solvent away from the interface, causing a depletion region and reduces the surface area available for unfavorable interactions. When the chain length is long enough and enough surfactant has accumulated, solvent molecules get trapped near the interface in the void spaces created by the packing of neighboring collapsed structures. While these predictions are consistent with

molecular simulations and experimental observations, the assumption of a planar interface does not allow for determination of the critical micelle concentration and the characteristic break towards limiting behavior of the interfacial tension at the onset of micellization.

- Oil structure

The same qualitative behavior was observed for the series of surfactant structures when adopting a more realistic chain-like oil molecule, although the effectiveness was slightly reduced. This comes about from increased packing frustration and greater resistance to partitioning to the interface. A denser oil phase produces a sharper and narrower depletion region indicative of less penetration by the tail segments. Rather than adopt the more restrictive conformation necessary to pack in the interface, the surfactant prefers to remain in the aqueous phase despite the energetic penalty associated with increased interactions between the water molecules and tail segments.

- Double Tail Asymmetry

The theory was also capable of capturing the experimentally observed changes in surfactant effectiveness as the head group is shifted from end to midpoint attachment for a fixed number of tail segments. While attachment at the end produced the most effective behavior, using the equilibrium density profiles demonstrated how the midpoint attachment of a symmetric structure gives more efficient behavior. This means fewer surfactant molecules are needed in the interface to achieve a desired interfacial tension with a symmetric structure, but it is more difficult to get this surfactant to partition to the interface.

- Mixed Surfactant Synergism

Although the mixed nonionic surfactant system did not demonstrate typical synergistic behavior, it did produce interesting changes to the fluid structure. For a fixed amount of the longer tailed surfactant, increasing the amount of a shorter tail surfactant mitigates the trapping of solvent molecules near the interface. This pushes the tail segments of the longer chain molecule further into the oil. Eventually, as the amount of shorter tailed surfactant continues to be increased, this shorter tailed surfactant begins to dominate the observed behavior with only small decreases in effectiveness due to the presence of the longer tailed surfactant. Since synergistic effects on observable properties are dependent on a significant difference in the partitioning of the two surfactants, it is concluded that adjusting the tail length in a mixture of two oil-like surfactants is insufficient at these conditions. However, in applications where solvent recuperation is pertinent (e.g., enhanced oil recovery), the demonstrated capability of nonionic cosurfactant mixtures to mediate or even completely eliminate the trapping of solvent molecules near the surface that result from interfacial packing effects provides promise. While the chosen cosurfactants do not produce any improvements over the use of the individual surfactants, these results do demonstrate the functionality of *i*SAFT as a tool for investigating surfactant combinations and identifying those that are most promising. These identified systems can be further refined in the laboratory without requiring time-consuming experimental searches through the parameter space.

- Temperature

Changing the temperature proved to greatly affect both the equilibrium microstructure and interfacial tension. Increasing the temperature (decreasing the dispersion energy) reduces the strength of the entropic penalty of chain extension while increasing the enthalpic benefit of the long-range pair interactions. This leads to a broader and shallower depletion region consistent with the approach to a disordered phase. At its limit, it was shown that system conditions exist where there is no net effect on the interfacial tension for any amount of added surfactant. It is believed these affects on structuring in the interface can be coupled with the presence of a cosurfactant to produce observed synergistic behavior.

While the past several years have seen significant development and advancement of both density functional theory in general and *i*SAFT specifically, this approach to the molecular modeling of inhomogeneous complex fluids is relatively young. As discussed in the detailed review of Chapter 3, its gained momentum through broad diversification of its demonstrated success in many important applications – especially with those that are intractable by other approaches. To maintain this momentum, the advantage in computational efficiency must be maintained, as fluids with inhomogeneities in two and three dimensions such as bicontinuous or gyroidal phases are explored. This will require continued development of numerical methods and algorithms which are specifically designed for the DFT framework similar to how advancements in the field of molecular simulation have occurred.[328] A brief summary of some

potential future theoretical directions of the field, described in more detail in the review of Chapter 3, are given below.

Improving Long-Range Dispersion

As outlined in Chapter 3, most density functional theory implementations, including *i*SAFT, use the mean-field approximation for long-range interactions which neglects pair correlations within the fluid. While effective in at least qualitatively reproducing fluid microstructure, it is still desirable to develop a more sophisticated mechanism for handling these correlations within a DFT. Specifically, a dispersion term that reduces to the corresponding dispersion term of an accurate equation of state (e.g., PC-SAFT) in the homogeneous limit of a segment based DFT such as *i*SAFT is of high interest. Many of the local density approximation approaches and applications to molecular based density functional theories are outlined in the comprehensive review of Chapter 3, and they have demonstrated significant improvements in property predictions for real systems. Dominik *et al.*[151] did demonstrate an effective mapping of the PC-SAFT dispersion energies to corresponding mean-field SAFT dispersion energies for the *n*-alkanes to accurately reproduce the bulk and interfacial properties. Ideally, however, no mapping would be necessary to determine the inhomogeneous pair correlation function.

Chain Stiffness and Bond Flexibility

As described in the theoretical development and background of the TPT1 basis of both SAFT and *i*SAFT, the orientation (angular) dependence is integrated out when considering chain formation to produce a fully-flexible

approximation. As indicated by the successful application to many diverse systems, this is adequate for at least qualitatively capturing the essential physics of many polyatomic systems. However, there are some polyatomic systems where the chain flexibility or stiffness is important in determining both the structure and properties. Some of these include polymer blends, liquid crystals, and surfactant/lipid molecules. Some early developments of a more generalized approach to the free energy functional form from Wertheim's theory are part of ongoing work within this research group, including the effects of using more restricted surfactant molecular structures as an extension of the work presented here. This approach is capable of multiple permutations of first and second order thermodynamic perturbation theory, which allows for regions of rigidity and full flexibility on the same molecule. Initial results for rigid triatomic chains with different bond angles show excellent agreement with molecular simulation. In addition, molecules of varying shapes and sizes can be accommodated through more sophisticated reference fluid structures (e.g., rods, discs, or spheroids), which can be implemented within the density functional theory using alternative formulations of the fundamental measure theory.[329-333]

Dynamic Density Functional Theory

The applications detailed within this thesis have looked at the equilibrium (time invariant) structure and properties of inhomogeneous systems. Development of a time-dependent version of *i*SAFT would extend the range of applicability to include access to non-equilibrium states, dynamic behavior, and transport properties.[334-338] Potential applications would include super-cooled

liquids, self-healing materials, time-dependent mesostructures, and shear induced behavior.

REFERENCES

(1) Redlich, O.; Kwong, J. N. S. *Chem. Rev.* **1949**, *44*, 233.
(2) Peng, D.-Y.; Robinson, D. B. *Ind. Eng. Chem. Fundam.* **1976**, *15*, 59.
(3) Wei, Y. S.; Sadus, R. J. *AIChE J.* **2000**, *46*, 169.
(4) Bymaster, A.; Emborsky, C.; Dominik, A.; Chapman, W. G. *Ind. Eng. Chem. Res.* **2008**, *47*, 6264.
(5) Evans, R. In *Fundamentals of Inhomogeneous Fluids*; Henderson, D., Ed.; Marcel-Dekker: New York, 1992, p 85.
(6) de Gennes, P. G. *Macromolecules* **1980**, *13*, 1069.
(7) Asakura, S.; Oosawa, F. *J. Chem. Phys.* **1954**, *22*, 1255.
(8) Asakura, S.; Oosawa, F. *J. Polym. Sci.* **1958**, *33*, 183.
(9) Yang, S. A.; Yan, D. D.; Tan, H. G.; Shi, A. C. *Phys. Rev. E* **2006**, *74*, 041808.
(10) Geisinger, T.; Muller, M.; Binder, K. *J. Chem. Phys.* **1999**, *111*, 5241.
(11) Geisinger, T.; Muller, M.; Binder, K. *J. Chem. Phys.* **1999**, *111*, 5251.
(12) Wu, J. *AIChE J.* **2006**, *52*, 1169.
(13) Wu, J.; Li, Z. *Annu. Rev. Phys. Chem.* **2007**, *58*, 85.
(14) Emborsky, C. P.; Feng, Z.; Cox, K. R.; Chapman, W. G. *Fluid Phase Equilib.* **2011**, *In Press*.
(15) Wertheim, M. S. *J. Stat. Phys.* **1984**, *35*, 19.
(16) Wertheim, M. S. *J. Stat. Phys.* **1984**, *35*, 35.
(17) Wertheim, M. S. *J. Stat. Phys.* **1986**, *42*, 459.
(18) Wertheim, M. S. *J. Stat. Phys.* **1986**, *42*, 477.
(19) Chapman, W. G., Cornell University, 1988.
(20) Segura, C. J.; Chapman, W. G. *Mol. Phys.* **1995**, *86*, 415.
(21) Segura, C. J.; Chapman, W. G.; Shukla, K. P. *Mol. Phys.* **1997**, *90*, 759.
(22) Segura, C. J.; Vakarin, E. V.; Chapman, W. G.; Holovko, M. F. *J. Chem. Phys.* **1998**, *108*, 4837.
(23) Segura, C. J.; Jie, Z.; Chapman, W. G. *Mol. Phys.* **2001**, *99*, 1.
(24) Jain, S.; Dominik, A.; Chapman, W. G. *J. Chem. Phys.* **2007**, *127*.
(25) Tripathi, S.; Chapman, W. G. *J. Chem. Phys.* **2005**, *122*, 094506.
(26) Tripathi, S.; Chapman, W. G. *Phys. Rev. Lett.* **2005**, *94*, 087801.
(27) Gubkina, G. F.; Lotter, Y. G.; Skripka, V. G. *Chem. Technol. Fuels Oils* **1974**, *10*, 441.
(28) Namiot, A. Y.; Skripka, V. G.; Lotter, Y. G. *Zh. Fiz. Khim.* **1976**, *50*, 2718.
(29) Olds, R. H.; Sage, B. H.; Lacey, W. N. *Ind. Eng. Chem.* **1942**, *34*, 1223.
(30) Reamer, H. H.; Olds, R. H.; Sage, B. H.; Lacey, W. N. *Ind. Eng. Chem.* **1943**, *35*, 790.
(31) Rigby, M.; Prausnitz, J. M. *J. Phys. Chem.* **1968**, *72*, 330.
(32) Sultanov, R. G.; Skripka, V. G. *Zh. Fiz. Khim.* **1973**, *47*, 1035.
(33) Yarrison, M.; Cox, K. R.; Chapman, W. G. *Ind. Eng. Chem. Res.* **2006**, *45*, 6770.
(34) Song, K. Y.; Yarrison, M.; Chapman, W. G. *Fluid Phase Equilib.* **2004**, *224*, 271.

(35) NIST Measurement Services Division: 2003.
(36) Brunner, E. *J. Chem. Thermodyn.* **1990**, *22*, 335.
(37) Economou, I. G.; Tsonopoulos, C. *Chem. Eng. Sci.* **1997**, *52*, 511.
(38) Economou, I. G.; Donohue, M. D. *Fluid Phase Equilib.* **1996**, *116*, 518.
(39) Tsonopoulos, C.; Heidman, J. L. *Fluid Phase Equilib.* **1986**, *29*, 391.
(40) Mathias, P. M.; Copeman, T. W. Callaway Gardens, GA, USA, 1983; Vol. 13, p 91.
(41) Michel, S.; Hooper, H. H.; Prausnitz, J. M. *Fluid Phase Equilib.* **1989**, *45*, 173.
(42) Gross, J.; Sadowski, G. *Fluid Phase Equilib.* **2000**, *168*, 183.
(43) Gross, J.; Sadowski, G. *J. Chem. Phys.* **2001**, *40*, 1244.
(44) Banaszak, M.; Chiew, Y. C.; O'Lenick, R.; Radosz, M. *J. Chem. Phys.* **1994**, *100*, 3803.
(45) Blas, F. J.; Vega, L. F. *Mol. Phys.* **1997**, *92*, 135.
(46) Chapman, W. G.; Jackson, G.; Gubbins, K. E. *Mol. Phys.* **1988**, *65*, 1057.
(47) Chapman, W. G. *J. Chem. Phys.* **1990**, *93*, 4299.
(48) Chapman, W. G.; Gubbins, K. E.; Jackson, G.; Radosz, M. *Ind. Eng. Chem. Res.* **1990**, *29*, 1709.
(49) Chen, S. S.; Kreglewski, A.; 10 ed. Braunschweig, West Germany, 1977; Vol. 81, p 1048.
(50) Ghonasgi, D.; Chapman, W. G. *AIChE J.* **1994**, *40*, 878.
(51) Ghonasgi, D.; Perez, V.; Chapman, W. G. *Int. J. Thermophys.* **1995**, *16*, 715.
(52) Ghosh, A.; Blaesing, J.; Jog, P. K.; Chapman, W. G. *Macromolecules* **2005**, *38*, 1025.
(53) Jackson, G.; Chapman, W. G.; Gubbins, K. E. *Mol. Phys.* **1988**, *65*, 1.
(54) Jog, P. K.; Sauer, S. G.; Blaesing, J.; Chapman, W. G. *Ind. Eng. Chem. Res.* **2001**, *40*, 4641.
(55) Sauer, S. G.; Chapman, W. G. *Ind. Eng. Chem. Res.* **2003**, *42*, 5687.
(56) Gil-Villegas, A.; Galindo, A.; Jackson, G. *Mol. Phys.* **2001**, *99*, 531.
(57) Tsivintzelis, I.; Grenner, A.; Economou, I. G.; Kontogeorgis, G. M. *Ind. Eng. Chem. Res.* **2008**, *47*, 5651.
(58) Vega, L. F.; Llovell, F.; Blas, F. J. *J. Phys. Chem. B* **2009**, *113*, 7621.
(59) Voutsas, E. C.; Boulougouris, G. C.; Economou, I. G.; Tassios, D. P. *Ind. Eng. Chem. Res.* **2000**, *39*, 797.
(60) Saul, A.; Wagner, W. *J. Phys. Chem. Ref. Data* **1987**, *16*, 893.
(61) Wagner, W.; Saul, A.; Pruss, A. *J. Phys. Chem. Ref. Data* **1994**, *23*, 515.
(62) Barker, J. A.; Henderson, D. *J. Chem. Phys.* **1967**, *47*, 4714.
(63) Barker, J. A.; Henderson, D. *J. Chem. Phys.* **1967**, *47*, 2856.
(64) Carnahan, N. F.; Starling, K. E. *J. Chem. Phys.* **1969**, *51*, 635.
(65) Boublik, T. *J. Chem. Phys.* **1970**, *53*, 471.
(66) Mansoori, G. A.; Carnahan, N. F.; Starling, K. E.; Leland, T. W., Jr. *J. Chem. Phys.* **1971**, *54*, 1523.
(67) Berendsen, H. J. C.; Postma, J. M. P.; van Gunsteren, W. F.; Hermans, J. In *Molecular Forces*; Pullman, B., Ed.; D. Reidell: Dordrecht, 1981, p 331.

(68) Berendsen, H. J. C.; Grigera, J. R.; Straatsma, T. P. *J. Phys. Chem.* **1987**, *91*, 6269.
(69) Berendsen, H. J. C.; Grigera, J. R.; Straatsma, T. P. *J. Phys. Chem.* **2002**, *91*, 6269.
(70) Tsonopoulos, C. *Fluid Phase Equilib.* **1999**, *156*, 21.
(71) Wagner, J. *Revitalization and Maintenance: Water-Hydrocarbon Mutual Solubility Data*, Gas Processors Association (GPA), 1999.
(72) Song, K. Y.; Kobayashi, R. *Fluid Phase Equilib.* **1994**, *95*, 281.
(73) Kobayashi, R.; Katz, D. L. *Ind. Eng. Chem. Fundam.* **1953**, *45*, 440.
(74) Frank, H. S.; Wen, W. Y. *Disc. Farad. Soc.* **1957**, *24*, 133.
(75) Luck, W. A. P.; 2-3 ed.; Elsevier: Niederoblarn, Austria, 1998; Vol. 448, p 131.
(76) Dill, K. A.; Truskett, T. M.; Vlachy, V.; Hribar-Lee, B. *Annu. Rev. Biophys. Biomol. Struct.* **2005**, *34*, 173.
(77) Truskett, T. M.; Debenedetti, P. G.; Sastry, S.; Torquato, S. *J. Chem. Phys.* **1999**, *111*, 2647.
(78) Truskett, T. M.; Dill, K. A. *J. Chem. Phys.* **2002**, *117*, 5101.
(79) Truskett, T. M.; Dill, K. A. *J. Phys. Chem. B* **2002**, *106*, 11829.
(80) Sear, R. P.; Jackson, G. *J. Chem. Phys.* **1996**, *105*, 1113.
(81) Glover, F. *Comp. Ops. Res.* **1986**, *5*, 533.
(82) Glover, F.; Laguna, M. *Tabu Search*; Kluwer Academic Publishers: Boston, 1997.
(83) Hohenberg, P.; Kohn, W. *Phys. Rev.* **1964**, *136*, B864.
(84) Kohn, W.; Sham, L. J. *Phys. Rev.* **1965**, *140*, A1133.
(85) Ebner, C.; Saam, W. F.; Stroud, D. *Phys. Rev. A* **1976**, *14*, 2264.
(86) McQuarrie, D. A. *Statistical Mechanics*; University Science Books: Sausalito, CA, 2000.
(87) Huang, K. *Statistical Mechanics*; John Wiley & Sons: New York, NY, 1987.
(88) Evans, R. *Adv. Phys.* **1979**, *28*, 143.
(89) McMullen, W. E.; Freed, K. F. *J. Chem. Phys.* **1990**, *92*, 1413.
(90) Chandler, D.; Andersen, H. C. *J. Chem. Phys.* **1972**, *57*, 1930.
(91) Schweizer, K. S.; Curro, J. G. *Phys. Rev. Lett.* **1988**, *60*, 809.
(92) Cummings, P. T.; Stell, G. *Mol. Phys.* **1982**, *46*, 383.
(93) Vanderlick, T. K.; Scriven, L. E.; Davis, H. T. *J. Chem. Phys.* **1989**, *90*, 2422.
(94) Tarazona, P. *Phys. Rev. A* **1985**, *31*, 2672.
(95) Tarazona, P. *Phys. Rev. A* **1985**, *32*, 3148.
(96) Curtin, W. A.; Ashcroft, N. W. *Phys. Rev. Lett.* **1986**, *56*, 2775.
(97) Rosenfeld, Y. *Phys. Rev. Lett.* **1989**, *63*, 980.
(98) Meister, T. F.; Kroll, D. M. *Phys. Rev. A* **1985**, *31*, 4055.
(99) Chandler, D.; McCoy, J. D.; Singer, S. J. *J. Chem. Phys.* **1986**, *85*, 5977.
(100) Chandler, D.; McCoy, J. D.; Singer, S. J. *J. Chem. Phys.* **1986**, *85*, 5971.
(101) McCoy, J. D.; Singer, S. J.; Chandler, D. *J. Chem. Phys.* **1987**, *87*, 4853.
(102) Tripathi, S. PhD Thesis, Rice University, 2004.
(103) Yethiraj, A.; Woodward, C. E. *J. Chem. Phys.* **1995**, *102*, 5499.
(104) Kierlik, E.; Rosinberg, M. L. *J. Chem. Phys.* **1992**, *97*, 9222.

(105) Kierlik, E.; Rosinberg, M. L. *J. Chem. Phys.* **1993**, *99*, 3950.
(106) Kierlik, E.; Rosinberg, M. L. *J. Chem. Phys.* **1994**, *100*, 1716.
(107) Bymaster, A.; Dominik, A.; Chapman, W. G. *J. Phys. Chem. C* **2007**, *111*, 15823.
(108) Bymaster, A.; Jain, S.; Chapman, W. G. *J. Chem. Phys.* **2008**, *128*, 164910.
(109) Bymaster, A., Rice University, 2009.
(110) Bymaster, A.; Chapman, W. G. *J. Phys. Chem. B* **2010**, *114*, 12298.
(111) Emborsky, C. P.; Jain, S.; Cox, K. R.; Chapman, W. G.; Rice University: Houston, TX, 2010, p 23.
(112) Jain, S.; Jog, P. K.; Weinhold, J. D.; Srivastava, R.; Chapman, W. G. *J. Chem. Phys.* **2008**, *128*, 154910.
(113) Jain, S.; Chapman, W. G. *Mol. Phys.* **2009**, *107*, 1.
(114) Jain, S.; Ginzburg, V. V.; Jog, P. K.; Weinhold, J. D.; Srivastava, R.; Chapman, W. G. *J. Chem. Phys.* **2009**, *131*.
(115) Tripathi, S.; Chapman, W. G. *J. Chem. Phys.* **2003**, *118*, 7993.
(116) Tripathi, S.; Chapman, W. G. *J. Chem. Phys.* **2003**, *119*, 12611.
(117) Tripathi, S.; Chapman, W. G. *Condens. Matter Phys.* **2003**, *6*, 523.
(118) Cao, D.; Wu, J. *J. Chem. Phys.* **2004**, *121*, 4210.
(119) Cao, D.; Wu, J. *Macromolecules* **2005**, *38*, 971.
(120) Cao, D.; Cheng, L.; Wang, W. *Chin. Phys.* **2007**, *16*, 2296.
(121) Fu, D.; Wu, J. *Ind. Eng. Chem. Res.* **2005**, *44*, 1120.
(122) Yu, Y.-X.; Wu, J. *J. Chem. Phys.* **2002**, *116*, 7094.
(123) Yu, Y.-X.; Wu, J. *J. Chem. Phys.* **2002**, *117*, 2368.
(124) Bryk, P.; Sokolowski, S. *J. Chem. Phys.* **2004**, *121*, 11314.
(125) Bryk, P.; Bucior, K.; Sokolowski, S.; Zukocinski, G. *J. Phys. Chem. B* **2005**, *109*, 2977.
(126) Bryk, P.; Pizio, O.; Sokolowski, S. *J. Chem. Phys.* **2005**, *122*, 1.
(127) Bryk, P.; Pizio, O.; Sokolowski, S. *J. Chem. Phys.* **2005**, *122*, 174906.
(128) Bryk, P.; Sokolowski, S.; Pizio, O. *J. Chem. Phys.* **2006**, *125*.
(129) Malijevsky, A.; Bryk, P.; Sokolowski, S. *Phys. Rev. E* **2005**, *72*, 032801.
(130) Patrykiejew, A.; Sokolowski, S.; Henderson, D. *Mol. Phys.* **1998**, *95*, 211.
(131) Patrykiejew, A.; Sokolowski, S.; Ilnyskyi, J.; Sokolowska, Z. *J. Chem. Phys.* **2010**, *132*, 244704.
(132) Pizio, O.; Patrykiejew, A.; Sokolowski, S. *J. Chem. Phys.* **2000**, *113*, 10761.
(133) Pizio, O.; Patrykiejew, A.; Sokolowski, S. *J. Chem. Phys.* **2004**, *121*, 11957.
(134) Pizio, O.; Bucior, K.; Patrykiejew, A.; Sokolowski, S. *J. Chem. Phys.* **2005**, *123*, 214902.
(135) Blas, F. J.; del Rio, E. M.; de Miguel, E.; Jackson, G. *Mol. Phys.* **2001**, *99*, 1851.
(136) Gloor, G. J.; Blas, F. J.; del Rio, E. M.; de Miguel, E.; Jackson, G. *Fluid Phase Equilib.* **2002**, *194-197*, 521.
(137) Gloor, G.; Jackson, G.; Blas, F. J.; Del Rio, E. M.; De Miguel, E. *J. Chem. Phys.* **2004**, *121*, 12740.

(138) Gloor, G. J.; Jackson, G.; Blas, F. J.; del Rio, E. M.; de Miguel, E. *J. Phys. Chem. C* **2007**, *111*, 15513.
(139) Llovell, F.; Galindo, A.; Blas, F. J.; Jackson, G. *J. Chem. Phys.* **2010**, *133*, 024704.
(140) Gonzalez, A.; Telo da Gama, M. M. *Phys. Rev. E* **2000**, *62*, 6571.
(141) Osipov, M. A.; Teixeira, P. I. C.; Telo da Gama, M. M. *J. Phys. A: Math. Gen.* **1997**, *30*, 1953.
(142) Teixeira, P. I.; Telo da Gama, M. M. *J. Phys.: Condens. Matter* **1991**, *3*, 111.
(143) Teixeira, P. I. C.; Telo da Gama, M. M. *J. Phys.: Condens. Matter* **2002**, *14*, 12159.
(144) Duque, D.; Pamies, J. C.; Vega, L. F. *J. Chem. Phys.* **2004**, *121*, 11395.
(145) Mejia, A.; Pamies, J. C.; Duque, D.; Segura, H.; Vega, L. F. *J. Chem. Phys.* **2005**, *123*, 1.
(146) Rosenfeld, Y. *Phys. Rev. A* **1990**, *42*, 5978.
(147) Sullivan, D. E. *Phys. Rev. A* **1982**, *25*, 1669.
(148) Honnell, K. G.; Hall, C. K. *J. Chem. Phys.* **1991**, *95*, 4481.
(149) Yethiraj, A.; Hall, C. K. *Macromolecules* **1990**, *23*, 1865.
(150) Rosenfeld, Y. *J. Chem. Phys.* **1993**, *98*, 8126.
(151) Dominik, A.; Tripathi, S.; Chapman, W. G. *Ind. Eng. Chem. Res.* **2006**, *45*, 6785.
(152) Huang, S. H.; Radosz, M. *Ind. Eng. Chem. Res.* **1990**, *29*, 2284.
(153) Huang, S. H.; Radosz, M. *Ind. Eng. Chem. Res.* **1991**, *30*, 1994.
(154) Ghonasgi, D.; Llano-Restrepo, M.; Chapman, W. G. *J. Chem. Phys.* **1993**, *98*, 5662.
(155) Galindo, A.; Davies, L. A.; Gil-Villegas, A.; Jackson, G. *Mol. Phys.* **1998**, *93*, 241.
(156) Gil-Villegas, A.; Galindo, A.; Whitehead, P. J.; Jackson, G.; Burgess, A. N. *J. Chem. Phys.* **1997**, *106*, 4168.
(157) Toxvaerd, S. *J. Chem. Phys.* **1971**, *55*, 3116.
(158) Toxvaerd, S. *Mol. Phys.* **1973**, *26*, 91.
(159) Toxvaerd, S. *J. Chem. Phys.* **1976**, *64*, 2863.
(160) Kahl, H.; Winkelmann, J. *Fluid Phase Equilib.* **2008**, *270*, 50.
(161) Wadewitz, T.; Winkelmann, J. *J. Chem. Phys.* **2000**, *113*, 2447.
(162) Winkelmann, J. *J. Phys.: Condens. Matter* **2001**, *13*, 4739.
(163) Gross, J. *J. Chem. Phys.* **2009**, *131*.
(164) Tang, X.; Gross, J. *J. Supercrit. Fluids* **2010**, *55*, 735.
(165) Forsman, J.; Woodward, C. E. *Macromolecules* **2006**, *39*, 1261.
(166) Woodward, C. E.; Forsman, J. *Macromolecules* **2009**, *42*, 7563.
(167) Yethiraj, A.; Hall, C. K. *J. Chem. Phys.* **1991**, *94*, 3943.
(168) Bucior, K.; Fischer, J.; Patrykiejew, A.; Tscheliessnig, R.; Sokolowski, S. *J. Chem. Phys.* **2007**, *126*, 094704.
(169) Tang, Z. X.; Scriven, L. E.; Davis, H. T. *J. Chem. Phys.* **1992**, *97*, 494.
(170) Tang, Z. X.; Scriven, L. E.; Davis, H. T. *J. Chem. Phys.* **1992**, *97*, 9258.
(171) Blum, L. *Mol. Phys.* **1975**, *30*, 1529.
(172) Blum, L.; Hoye, J. S. *J. Phys. Chem.* **1977**, *81*, 1311.

(173) Waisman, E.; Lebowitz, J. L. *J. Chem. Phys.* **1970**, *52*, 4307.
(174) Waisman, E.; Lebowitz, J. L. *J. Chem. Phys.* **1972**, *56*, 3086.
(175) Waisman, E.; Lebowitz, J. L. *J. Chem. Phys.* **1972**, *56*, 3093.
(176) Jiang, T.; Li, Z. D.; Wu, J. Z. *Macromolecules* **2007**, *40*, 334.
(177) Jiang, T.; Wu, J. Z. *J. Phys. Chem. B* **2008**, *112*, 7713.
(178) Jiang, T.; Wu, J. Z. *J. Chem. Phys.* **2008**, *129*, 084903.
(179) Smagala, T. G.; Patrykiejew, A.; Sokolowski, S.; Pizio, O.; Fawcett, W. R. *J. Chem. Phys.* **2008**, *128*, 024907.
(180) Chan, G. K.-L.; Finken, R. *Phys. Rev. Lett.* **2005**, *94*, 1.
(181) Marques, M. A. L.; Gross, E. K. U. *Annu. Rev. Phys. Chem.* **2004**, *55*, 427.
(182) Lee, J. Y.; Buxton, G. A.; Balazs, A. C. *J. Chem. Phys.* **2004**, *121*, 5531.
(183) Sinani, V. A.; Koktysh, D. S.; Yun, B. G.; Matts, R. L.; Pappas, T. C.; Motamedi, M.; Thomas, S. N.; Kotov, N. A. *Nano Lett.* **2003**, *3*, 1177.
(184) Smith, K. A.; Tyagi, S.; Balazs, A. C. *Macromolecules* **2005**, *38*, 10138.
(185) Pusey, P. N.; Vanmegen, W. *Nature* **1986**, *320*, 340.
(186) Aarts, D.; van der Wiel, J. H.; Lekkerkerker, H. N. W. *J. Phys.: Condens. Matter* **2003**, *15*, S245.
(187) Aarts, D.; Schmidt, M.; Lekkerkerker, H. N. W. *Science* **2004**, *304*, 847.
(188) Blokhuis, E. M.; Kuipers, J.; Vink, R. L. C. *Phys. Rev. Lett.* **2008**, *101*, 086101.
(189) Hennequin, Y.; Aarts, D. G. A. L.; Indekeu, J. O.; Lekkerkerker, H. N. W.; Bonn, D. *Phys Rev Lett* **2008**, *100*, 178305.
(190) Poon, W. C. K. *J. Phys.: Condens. Matter* **2002**, *14*, R859.
(191) Curro, J. G.; Schweizer, K. S. *J. Chem. Phys.* **1987**, *87*, 1842.
(192) Schweizer, K. S.; Curro, J. G. *Phys. Rev. Lett.* **1987**, *58*, 246.
(193) Thompson, R. B.; Ginzburg, V. V.; Matsen, M. W.; Balazs, A. C. *Science* **2001**, *292*, 2469.
(194) Thompson, R. B.; Ginzburg, V. V.; Matsen, M. W.; Balazs, A. C. *Macromolecules* **2002**, *35*, 1060.
(195) Sides, S. W.; Kim, B. J.; Kramer, E. J.; Fredrickson, G. H. *Phys. Rev. Lett.* **2006**, *96*, 250601.
(196) Fuchs, M.; Schweizer, K. S. *Phys. Rev. E* **2001**, *64*, 021514.
(197) Fuchs, M.; Schweizer, K. S. *J. Phys.: Condens. Matter* **2002**, *14*, R239.
(198) Chatterjee, A. P.; Schweizer, K. S. *J. Chem. Phys.* **1998**, *109*, 10464.
(199) Chatterjee, A. P.; Schweizer, K. S. *J. Chem. Phys.* **1998**, *109*, 10477.
(200) Patel, N.; Egorov, S. A. *J. Chem. Phys.* **2004**, *121*, 4987.
(201) Gupta, S.; Zhang, Q. L.; Emrick, T.; Balazs, A. C.; Russell, T. P. *Nature Materials* **2006**, *5*, 229.
(202) Krishnan, R. S.; Mackay, M. E.; Hawker, C. J.; Van Horn, B. *Langmuir* **2005**, *21*, 5770.
(203) Tyagi, S.; Lee, J. Y.; Buxton, G. A.; Balazs, A. C. *Macromolecules* **2004**, *37*, 9160.
(204) McGarrity, E. S.; Frischknecht, A. L.; Frink, L. J. D.; MacKay, M. E. *Phys. Rev. Lett.* **2007**, *99*, 238302.

(205) McGarrity, E. S.; Frischknecht, A. L.; MacKay, M. E. *J. Chem. Phys.* **2008**, *128*, 154904.
(206) Kang, H.; Detcheverry, F. A.; Mangham, A. N.; Stoykovich, M. P.; Daoulas, K. C.; Hamers, R. J.; Muller, M.; de Pablo, J. J.; Nealey, P. F. *Phys. Rev. Lett.* **2008**, *100*, 148303.
(207) Chen, H. Y.; Ruckenstein, E. *J. Chem. Phys.* **2009**, *131*, 244904.
(208) Detcheverry, F. A.; Kang, H. M.; Daoulas, K. C.; Muller, M.; Nealey, P. F.; de Pablo, J. J. *Macromolecules* **2008**, *41*, 4989.
(209) He, L. L.; Zhang, L. X.; Liang, H. J. *J. Phys. Chem. B* **2008**, *112*, 4194.
(210) Schultz, A. J.; Hall, C. K.; Genzer, J. *Macromolecules* **2005**, *38*, 3007.
(211) Schultz, A. J.; Hall, C. K.; Genzer, J. *J. Chem. Phys.* **2002**, *117*, 10329.
(212) Matsen, M. W.; Thompson, R. B. *Macromolecules* **2008**, *41*, 1853.
(213) Yang, Q. H.; Li, M.; Tong, C. H.; Zhu, Y. J. *J. Chem. Phys.* **2009**, *130*, 094903.
(214) Jin, J. Z.; Wu, J. Z. *J. Chem. Phys.* **2008**, *128*, 074901.
(215) Jin, J. Z.; Wu, J. Z.; Frischknecht, A. L. *Macromolecules* **2009**, *42*, 7537.
(216) Li, J.; Li, X.; Ni, X. P.; Wang, X.; Li, H. Z.; Leong, K. W. *Biomaterials* **2006**, *27*, 4132.
(217) Sijbesma, R. P.; Beijer, F. H.; Brunsveld, L.; Folmer, B. J. B.; Hirschberg, J.; Lange, R. F. M.; Lowe, J. K. L.; Meijer, E. W. *Science* **1997**, *278*, 1601.
(218) Asari, T.; Matsuo, S.; Takano, A.; Matsushita, Y. *Macromolecules* **2005**, *38*, 8811.
(219) Asari, T.; Arai, S.; Takano, A.; Matsushita, Y. *Macromolecules* **2006**, *39*, 2232.
(220) Ruokolainen, J.; Makinen, R.; Torkkeli, M.; Makela, T.; Serimaa, R.; ten Brinke, G.; Ikkala, O. *Science* **1998**, *280*, 557.
(221) Smit, B. *Phys. Rev. A* **1988**, *37*, 3431.
(222) Telo da Gama, M. M.; Gubbins, K. E. *Mol. Phys.* **1986**, *59*, 227.
(223) Chandler, D.; Weeks, J. D. *Phys. Rev. Lett.* **1970**, *25*, 149.
(224) Weeks, J. D.; Chandler, D.; Anderson, H. C. *J. Chem. Phys.* **1971**, *54*, 5237.
(225) Smit, B.; Schlijper, A. G.; Rupert, L. A. M.; Vanos, N. M. *J. Phys. Chem.* **1990**, *94*, 6933.
(226) Frischknecht, A. L.; Frink, L. J. D. *Phys. Rev. E* **2005**, *72*, 041924.
(227) Frink, L. J. D.; Frischknecht, A. L. *Phys. Rev. E* **2005**, *72*, 041923.
(228) Alexander, S. *J. De Physique* **1977**, *38*, 983.
(229) Milner, S. T.; Witten, T. A.; Cates, M. E. *Macromolecules* **1988**, *21*, 2610.
(230) Milner, S. T. *Science* **1991**, *251*, 905.
(231) Chakrabarti, A.; Nelson, P.; Toral, R. *Phys. Rev. A* **1992**, *46*, 4930.
(232) Dickman, R.; Hong, D. C. *J. Chem. Phys.* **1991**, *95*, 4650.
(233) Lai, P. Y.; Binder, K. *J. Chem. Phys.* **1991**, *95*, 9288.
(234) Grest, G. S.; Murat, M. *Macromolecules* **1993**, *26*, 3108.
(235) Grest, G. S. *J. Chem. Phys.* **1996**, *105*, 5532.
(236) Murat, M.; Grest, G. S. *Macromolecules* **1989**, *22*, 4054.
(237) Glotzer, S. C.; Horsch, M. A.; Iacovella, C. R.; Zhang, Z. L.; Chan, E. R.; Zhang, X. *Curr. Opin. Colloid Interface Sci.* **2005**, *10*, 287.

(238) Iacovella, C. R.; Keys, A. S.; Horsch, M. A.; Glotzer, S. C. *Phys. Rev. E* **2007**, *75*, 040801.
(239) Iacovella, C. R.; Horsch, M. A.; Glotzer, S. C. *J. Chem. Phys.* **2008**, *129*, 044902.
(240) Milchev, A.; Egorov, S. A.; Binder, K. *J. Chem. Phys.* **2010**, *132*, 184905.
(241) Pincus, P. *Macromolecules* **1991**, *24*, 2912.
(242) Borowko, M.; Rzysko, W.; Sokolowski, S.; Staszewski, T. *J. Phys. Chem. B* **2009**, *113*, 4763.
(243) Xu, X. F.; Cao, D. P. *J. Chem. Phys.* **2009**, *130*, 164901.
(244) Xu, X. F.; Cao, D. P.; Zhang, X. R.; Wang, W. C. *Phys. Rev. E* **2009**, *79*, 021805.
(245) Shelley, J. C.; Shelley, M. Y. *Curr. Opin. Colloid Interface Sci.* **2000**, *5*, 101.
(246) van Helden, A. K. *Progress in Colloid & Polymer Science* **1996**, *100*, 48.
(247) Wheeler, J. C.; Widom, B. *J. Am. Chem. Soc.* **1968**, *90*, 3064.
(248) Widom, B. *J. Phys. Chem.* **1984**, *88*, 6508.
(249) Alexander, S. *J. de Physique Lett.* **1978**, *39*, 1.
(250) Brindle, D.; Care, C. M.; 1 ed. Singapore, 1991; Vol. 2, p 284.
(251) Ciach, A.; Hoye, J. S.; Stell, G. *J. Phys. A: Math. Gen.* **1988**, *21*, 777.
(252) Dill, K. A.; Cantor, R. S. *Macromolecules* **1984**, *17*, 380.
(253) Gompper, G.; Schick, M. *Phys. Rev. Lett.* **1989**, *62*, 1647.
(254) Gompper, G.; Schick, M. *Phys. Rev. B* **1990**, *41*, 9148.
(255) Gompper, G.; Schick, M. *Phys. Rev. Lett.* **1990**, *65*, 1116.
(256) Gompper, G.; Schick, M. *Phys. Rev. A* **1990**, *42*, 2137.
(257) Gompper, G.; Holyst, R.; Schick, M. *Phys. Rev. A* **1991**, *43*, 3157.
(258) Halley, J. W.; Kolan, A. J. *J. Chem. Phys.* **1988**, *88*, 3313.
(259) Leermakers, F. A. M.; Scheutjens, J. M. H. M.; Gaylord, R. J. *Polymer* **1984**, *25*, 1577.
(260) Schick, M.; Wei-Heng, S. *Phys. Rev. B* **1986**, *34*, 1797.
(261) Schick, M.; Wei-Heng, S. *Phys. Rev. Lett.* **1987**, *59*, 1205.
(262) Gruen, D. W. R. *J. Phys. Chem.* **1985**, *89*, 146.
(263) Szleifer, I.; Ben-Shaul, A.; Gelbart, W. M. *J. Chem. Phys.* **1987**, *86*, 7094.
(264) Chang, K.; Morse, D. C. *Macromolecules* **2006**, *39*, 7746.
(265) Chang, K.; Morse, D. C. *Macromolecules* **2006**, *39*, 7397.
(266) Chang, K.; Macosko, C. W.; Morse, D. C. *Macromolecules* **2007**, *40*, 3819.
(267) Dai, K. H.; Norton, L. J.; Kramer, E. J. *Macromolecules* **1994**, *27*, 1949.
(268) Fu, D.; Liang, L.; American Institute of Chemical Engineers: New York, NY 10016-5991, United States, 2005, p 4671.
(269) Shull, K. R.; Kramer, E. J. *Macromolecules* **1990**, *23*, 4769.
(270) Stoyanov, S. D.; Rehage, H.; Paunov, V. N. *Phys. Rev. Lett.* **2003**, *91*, 86102.
(271) Uneyama, T.; Doi, M. *Macromolecules* **2005**, *38*, 5817.
(272) Yeh, M.-C.; Chen, C.-M.; Chen, L.-J. *J. Phys. Chem. B* **2004**, *108*, 7271.
(273) Woodward, C. E. *J. Chem. Phys.* **1991**, *94*, 3183.
(274) Müller, E. A.; Gubbins, K. E. *Ind. Eng. Chem. Res.* **2001**, *40*, 2193.

(275) Hansen, J. P.; McDonald, I. R. *Theory of Simple Liquids*; Academic Publishing: San Diego, 1986.
(276) Blankschtein, D.; Thurston, G. M.; Benedek, G. B. *Phys. Rev. Lett.* **1985**, *54*, 955.
(277) Blankschtein, D.; Thurston, G. M.; Benedek, G. B. *J. Chem. Phys.* **1986**, *85*, 7268.
(278) Goldsipe, A.; Blankschtein, D. *Langmuir* **2007**, *23*, 5953.
(279) Goldsipe, A.; Blankschtein, D. *Langmuir* **2007**, *23*, 5942.
(280) Puvvada, S.; Blankschtein, D. *J. Chem. Phys.* **1990**, *92*, 3710.
(281) Stephenson, B. C.; Goldsipe, A.; Beers, K. J.; Blankschtein, D. *J. Phys. Chem. B* **2007**, *111*, 1025.
(282) Stephenson, B. C.; Goldsipe, A.; Beers, K. J.; Blankschtein, D. *J. Phys. Chem. B* **2007**, *111*, 1045.
(283) Shinoda, W.; Devane, R.; Klein, M. L.; 1-2 ed.; Taylor and Francis Ltd.: 4 Park Square, Milton Park, Abingdon, Oxfordshire, OX14 4RN, United Kingdom, 2007; Vol. 33, p 27.
(284) Shinoda, W.; Devane, R.; Klein, M. L. *Soft Matter* **2008**, *4*, 2454.
(285) Xibing, H.; Shinoda, W.; DeVane, R.; Anderson, K. L.; Klein, M. L. *Chem. Phys. Lett.* **2010**, *487*, 71.
(286) Ye, Y.; McCoy, J. D.; Curro, J. G. *J. Chem. Phys.* **2003**, *119*, 555.
(287) Traube, J. *Samml. Chem. Vortr.* **1899**, *4*, 255.
(288) Klopfer, K. J.; Vanderlick, T. K. *Colloids Surf. A* **1995**, *96*, 171.
(289) Rekvig, L.; Kranenburg, M.; Vreede, J.; Hafskjold, B.; Smit, B. *Langmuir* **2003**, *19*, 8195.
(290) van Os, N. M.; Rupert, L. A. M.; Smit, B.; Hilbers, P. A. J.; Esselink, K.; Boehmer, M. R.; Koopal, L. K. *Colloids Surf. A* **1993**, *81*, 217.
(291) Aspée, A.; Lisi, E. *J. Colloid Interface Sci.* **1996**, *178*, 298.
(292) Pitt, A. R.; Morley, S. D.; Burbidge, N. J.; Quickenden, E. L.; Elsevier Science B.V.: Empoli, Italy, 1996; Vol. 114, p 321.
(293) Varadaraj, R.; Bock, J.; Valint jr., P.; Zushma, S.; Thomas, R. *J. Phys. Chem.* **1991**, *95*, 1671.
(294) Wormuth, K. R.; Zushma, S. *Langmuir* **1991**, *7*, 2048.
(295) Ghaïcha, L.; Leblanc, R. M.; Chattopadhyay, A. K. *J. Phys. Chem.* **1992**, *96*, 10948.
(296) Green, S. R.; Su, T. J.; Lu, J. R.; Penfold, J. *J. Phys. Chem. B* **2000**, *104*, 1507.
(297) Doe, P. H.; Wade, W. H.; Schechter, R. S. *J. Colloid Interface Sci.* **1977**, *59*, 525.
(298) Adkins, S. S.; Chen, X.; Nguyen, Q. P.; Sanders, A. W.; Johnston, K. P. *J. Colloid Interface Sci.* **2010**, *346*, 455.
(299) Chen, L.; Xiao, J.-X.; Ruan, K.; Ma, J. *Langmuir* **2002**, *18*, 7250.
(300) Raghavan, S. R.; Fritz, G.; Kaler, E. W. *Langmuir* **2002**, *18*, 3797.
(301) Wu, Y.; Rosen, M. J. *Langmuir* **2005**, *21*, 2342.
(302) Dominguez, H. *J. Colloid Interface Sci.* **2004**, *274*, 665.
(303) Magnus Bergström, L. *J. Phys. Chem. B* **2005**, *109*, 12387.
(304) Rosen, M. J.; Zhu, Z. H.; Gao, T. *J. Colloid Interface Sci.* **1993**, *157*, 254.

(305) Theander, K.; Pugh, R. J. *J. Colloid Interface Sci.* **2003**, *267*, 9.
(306) Werts, K. M.; Grady, B. P. *J. Surf. Det.*, *14*, 77.
(307) Wojciechowski, K.; Buffle, J. *Colloids Surf. A* **2005**, *257*, 385.
(308) Bumajdad, A.; Eastoe, J.; Griffiths, P.; Steytler, D. C.; Heenan, R. K.; Lu, J. R.; Timmins, P. *Langmuir* **1999**, *15*, 5271.
(309) Bumajdad, A.; Eastoe, J. *J. Colloid Interface Sci.* **2004**, *274*, 268.
(310) Zhang, L.; Zhang, R.; Somasundaran, P. *J. Colloid Interface Sci.* **2006**, *302*, 25.
(311) Zhou, Q.; Somasundaran, P. *J. Colloid Interface Sci.* **2009**, *331*, 288.
(312) Li, Y.; He, X.; Cao, X.; Zhao, G.; Tian, X.; Cui, X. *J. Colloid Interface Sci.* **2007**, *307*, 215.
(313) Dominguez, H. *J. Phys. Chem. B* **2002**, *106*, 5915.
(314) Dominguez, H.; Rivera, M. *Langmuir* **2005**, *21*, 7257.
(315) Fainerman, V. B.; Vollhardt, D.; Emrich, G. *J. Phys. Chem. B* **2001**, *105*, 4324.
(316) Li, Y.; Xu, G.; Luan, Y.; Yuan, S.; Zhang, Z. L.; Elsevier: 2005; Vol. 257-258, p 385.
(317) Hou, Z.; Li, Z.; Wang, H. *J. Dispersion Sci. Technol.* **2001**, *22*, 255.
(318) Anton, R. E.; Castillo, P.; Salager, J. L. *J. Dispersion Sci. Technol.* **1986**, *7*, 319.
(319) Rowlingson, J. S.; Widom, B. *Molecular Theory of Capillarity*; Oxford University Press: Oxford, 1982.
(320) Buff, F.-P. In *The Encyclopedia of Physics*; Flugge, S., Ed.; Springer: Berlin, 1960; Vol. 10, p 298.
(321) Lang, J. C., Jr.; Widom, B. *Physica A* **1975**, *81A*, 190.
(322) Seeto, Y.; Puig, J. E.; Scriven, L. E.; Davis, H. T. *J. Colloid Interface Sci.* **1983**, *96*, 360.
(323) Kahlweit, M.; Stray, R.; Fit-man, P.; Haase, D.; Jen, J.; Schomacker, R. *Langmuir* **1988**, *4*, 499.
(324) Kahlweit, M.; Busse, G. *J. Chem. Phys.* **1989**, *91*, 1339.
(325) Chen, L. J.; Feng, J. F.; Robert, M.; Shukla, K. P. *Phys. Rev. A* **1990**, *42*, 4716.
(326) Robert, M.; Jeng, J. F. *J. De Physique* **1988**, *49*, 1821.
(327) Robert, M.; Shukla, K. P. *Fluid Phase Equilib.* **1992**, *79*, 241.
(328) Frink, L. J. D.; Salinger, A. G.; Sears, M. P.; Weinhold, J. D.; Frischknecht, A. L. *J. Phys.: Condens. Matter* **2002**, *14*, 12167.
(329) Bryk, P. *Phys. Rev. E* **2003**, *68*, 625011.
(330) Esztermann, A.; Schmidt, M. *Phys. Rev. E* **2004**, *70*, 022501.
(331) Esztermann, A.; Reich, H.; Schmidt, M. *Phys. Rev. E* **2006**, *73*.
(332) Hansen-Goos, H.; Mecke, K. *Phys. Rev. Lett.* **2009**, *102*.
(333) Schmidt, M. *Phys. Rev. E* **2001**, *63*, 502011.
(334) Matuszak, D.; Aranovich, G. L.; Donohue, M. D. *J. Non-Equilib. Thermodyn.* **2006**, *31*, 355.
(335) Morita, H.; Kawakatsu, T.; Doi, M.; Yamaguchi, D.; Takenaka, M.; Hashimoto, T. *Macromolecules* **2002**, *35*, 7473.

(336) Zvelindovsky, A. V. M.; van Vlimmeren, B. A. C.; Sevink, G. J. A.; Maurits, N. M.; Fraaije, J. G. E. M. *J. Chem. Phys.* **1998**, *109*, 8751.
(337) Zvelindovsky, A. V.; Sevink, G. J. A.; Fraaije, J. G. E. M. *Phys. Rev. E* **2000**, *62*, R3063.
(338) Zvelindovsky, A. V.; Sevink, G. J. A.; Lyakhova, K. S.; Altevogt, P. *Macromol. Theory Simul.* **2004**, *13*, 140.